# Material Characterization of Timber Utility Poles using Experimental Approaches

by

**Roman Elsener**

A thesis presented to the

University of Technology Sydney

in fulfilment of the
thesis requirement for the
degree

Master of Engineering

Sydney, Australia in March 2014

| | |
|---|---|
| Course: | C03017 |
| Principal Supervisor: | A/Prof Dr Jianchun Li |
| Second Supervisor: | Dr Ulrike Dackermann |

University of Technology Sydney
Faculty of Engineering
Centre for Built Infrastructure Research
15 Broadway
Ultimo, NSW 2007
Australia

**Certificate of Original Authorship**

I certify that the work in this thesis has not previously been submitted for a degree nor has it been submitted as part of requirements for a degree except as fully acknowledged within the text.

I also certify that the thesis has been written by me. Any help that I have received in my research work and the preparation of the thesis itself has been acknowledged. In addition, I certify that all information sources and literature used are indicated in the thesis.

22/03/2014 Production Note: Signature removed prior to publication.

Date and Signature of Student

# ACKNOWLEDGMENT

I would like to express my appreciation to my principal supervisor A/Professor Jianchun Li who was very supportive and motivating throughout my degree. He was an excellent advisor in technical questions and always inspired me in achieving my goals.

I would like to express my gratitude to my second supervisor Dr. Ulrike Dackermann who was a great support in technical as well as practical matters. She always assisted very professionally with words and deeds and it was a pleasure working with her.

The laboratory staff, notably Peter Brown, David Hooper, Mulgheta Hailu, David Dicker, Rami Haddad, Laurence Stonard and Scott Graham were extremely helpful and supportive, everyone in their particular area. I would like to thank them all very much; it was fantastic working with you.

I would also like to thank my fellow students and colleagues, Saad Subhani, Ning Yan and Bahram Jozi. Working together with you was a great pleasure for me since we were a real team in supporting and helping each other in many aspects of our work.

I gratefully acknowledge the collaboration with our industrial partner Ausgrid, in particular Terry Westlake and Bob White whom it was a pleasure working with. They were very supportive in helping us preparing and conducting field tests.

Sincere thanks also to the various academic staff members from UTS and BUAS who assisted with their knowledge in specific questions. Many thanks Keith Crews, Christophe Sigrist, Bijan Samali and Christof Wüthrich.

# ABSTRACT

Utility poles made of timber are a significant part of Australia's infrastructure for power distribution and communication networks. Wood as a natural material deteriorates under the influence of environmental conditions such as weathering, fungus and insect attack which results in a reduction of the strength of the poles. Determining soundness and the remaining strength of timber utility poles in service is crucial in order to maintain a reliable and secure power network.

This thesis presents an investigation of using static and dynamic material testing approaches to determine material properties and detecting internal damage of timber utility poles from two hardwood eucalyptus tree species, i.e. Spotted Gum and Tallowwood. The comparative study of static and dynamic tests based on the wave transmission time or time of flight (TOF) is necessary for the development of novel non-destructive testing (NDT) techniques for the health assessment of in-situ utility poles. In order to develop accurate non-destructive models, knowledge of the orthotropic material properties is necessary.

In open literatures, comparative studies on orthotropic material properties are scarce to find for most eucalyptus species used for utility poles. Typically, material properties are only available in the longitudinal (i.e. along main wood fibre) direction, and most international standards cover only details on material testing in such direction with no coherent or comprehensive guidelines being given for the testing of the other two secondary directions (radial and tangential) of timber. TOF measurements were conducted by several researchers for a number of timber species, however non on high density woods

such as the investigated eucalyptus species.

Based the full set of material properties (Modulus of Elasticity and Poisson's ratios) of two new utility poles determined with static tests in all three orthotropic directions (longitudinally, radially and tangentially), the dynamic tests were calibrated and used for the non-destructive material characterization and internal damage detection. The tests were also conducted taking into account varying moisture contents and different grain angles as they occur in the field. Ultimately, an orthotropic numerical model was created to simulate the experimental damage detection case which could be used to simulate further damage cases. The results revealed that the formulas used for the dynamic material characterization must be adjusted for the investigated species. The numerical model was capable of simulating the experimental case and predicting the TOF for damaged poles. The method has potential for the prediction of internal damage of eucalyptus timber poles in the field.

*Keywords: Timber Properties, Material Testing, Damage Detection, Eucalyptus*

# TABLE OF CONTENTS

# NOMENCLATURE

| | |
|---|---|
| *AT* | Acoustic tomography |
| *CS* | Compression strength |
| *COV* | Coefficient of variation |
| *FE* | Finite element |
| *FSP* | Fibre saturation point |
| *LVDT* | Linear variable differential transducer |
| *MAE* | Mean absolute error |
| *MAPE* | Mean absolute percentage error |
| *MC* | Moisture content |
| *MFA* | Micro fibril angle |
| $MOE_l$ | Modulus of elasticity in longitudinal direction |
| $MOE_r$ | Modulus of elasticity in radial direction |
| $MOE_t$ | Modulus of elasticity in tangential direction |
| *MOR* | Modulus of rupture |
| *NDE* | Non-destructive evaluation |
| *NDT* | Non-destructive testing |
| *P-wave* | Compressional or longitudinal wave |
| *S-wave* | Shear or transversal wave |
| *TOF* | Time of flight |
| *TS* | Tensile strength |

| | |
|---|---|
| *WTT* | Wave transmission time |
| *WSP* | Water saturation point |

## Symbols

| | |
|---|---|
| $c_{LL}$ | P-wave in longitudinal direction |
| $c_{RR}$ | P-wave in radial direction |
| $c_{TT}$ | P-wave in tangential direction |
| $c_{LR.RL}$ | S-wave in longitudinal radial plane |
| $c_{LT,TL}$ | S-wave in longitudinal tangential plane |
| $c_{RT,TR}$ | S-wave in radial tangential plane |
| $\varepsilon$ | Strain |
| $\sigma$ | Stress |
| $f$ | Frequency |
| $G$ | Shear modulus |
| $\lambda$ | Wavelength |
| $\bar{x}$ | Mean value |
| $v$ | Poisson's ratio |
| $V$ | Wave velocity |
| $V_L$ | Longitudinal wave velocity |

# 1 INTRODUCTION

## 1.1 Problem Statement

Utility poles made of timber are traditionally used all over the world as they are relatively low in cost and environmentally friendly. Especially in Australia, utility timber poles represent a significant part of the country's infrastructure for power distribution and communication networks. There are nearly 7 million timber poles in the current network in Australia, and among them, 5 million poles are used for power and communications supply (Nguyen et al. 2004). $40-$50 millions are spent annually on maintenance and asset management to prevent utility lines from failure. The lack of reliable tools for assessing the condition of in-situ poles seriously jeopardizes the maintenance and asset management. For example, in the Eastern States of Australia, about 300,000 electricity poles are replaced every year. However, up to 80% of them are still in very good and serviceable conditions, causing a large waste of natural resources and money (Nguyen et al. 2004). To address the needs of the utility pole asset management industry, a cost-effective and reliable non-destructive testing (NDT) method needs to be developed that is able to identify and separate healthy from unhealthy poles. In the last 20 years, various NDT techniques have been developed to evaluate the conditions and integrity of pile/foundation structures. Among those methods/techniques, visual inspection, sounding and stress wave methods remain the most widely used techniques in practice (Tanasoiu et al. 2002). Visual inspection is undoubtedly one of the oldest

methods used in practice but suffers a major drawback on reliability and accuracy of its results since the method relies on the experience of the operator and accessibility of the structure. Dynamic methods based on stress wave propagation, on the other hand, can offer simple and cost-effective tools for identifying the in-service condition as well as the embedment length of timber poles/piles. However, due to a lack in understanding of stress wave propagation in pole structures, especially with the effect of soil embedment coupled with unknown pole conditions below ground line (such as deterioration, rot, termite attack, etc.), the results rely heavily on experience and interpretations from individual operators. Another issue influencing the testing accuracy is related to the complexity of the timber material with anisotropic and heterogeneous material characteristics. As a matter of fact, the material properties of timber are considerably affected by environmental factors such as temperature and moisture changes. As a result, current dynamic-based methods often fail to produce reliable results, which are vital for the utility pole management industry.

## 1.2 Aim and Scope

The presented research is part of a larger industry supported research project that involves three PhD and one Master student and aims at developing accurate and reliable non-destructive assessment tools for timber poles based on stress wave techniques. The students assigned to the project are working in four different areas to tackle the problem, i.e. first, stress wave theory applied to pole structures including wavelet analysis; second, finite element analysis to simulate and investigate ideal stress wave behaviour in numerical pole structures; third, data post processing and data fusion; and fourth, laboratory and field work to verify stress wave propagation characteristics in timber poles and to determine material properties of timber using static and dynamic testing approaches. The aims of the larger research project can be divided into four stages which are shown in Figure 1-1.

In order to achieve these goals in depth, numerical studies need to be undertaken to investigate and understand the wave propagation in timber poles. To be able to develop accurate models, correct values on various orthotropic material properties need to be available such as the modulus of elasticity (MOE) and the Poisson's ratios. For certain

timber species, however, those values are very rare in literature and can also heavily fluctuate between, but also within the same tree species. Literature values are often only available for the primary longitudinal direction and sometimes date back to the beginning or middle of the last century.

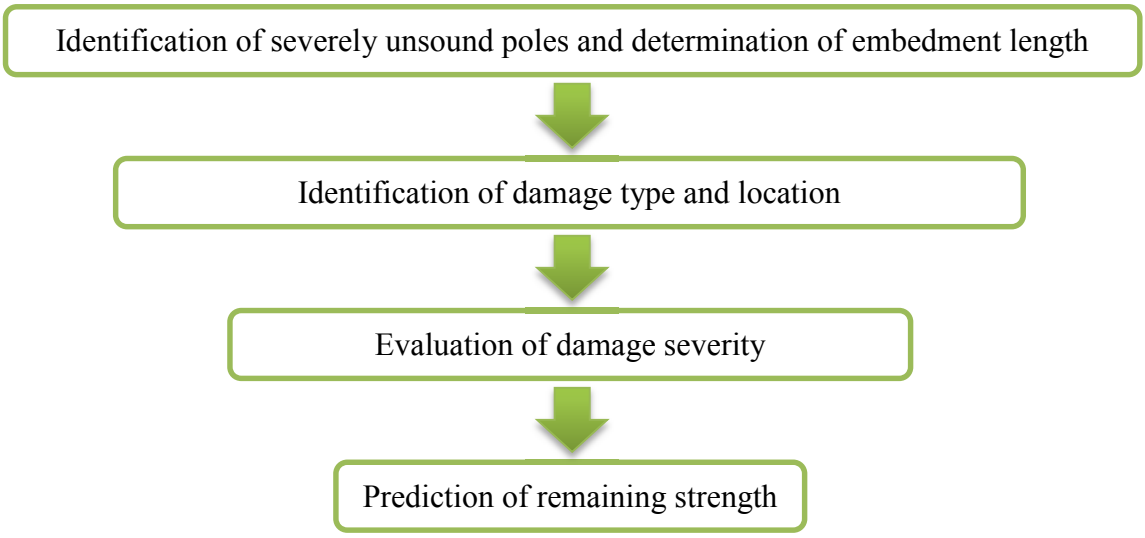


Figure 1-1:Aims of the NDT techniques to be developed for timber poles

The aim of this research work is twofold: At first, the goal is to be able to apply the dynamic testing method for reasonably accurate material characterization and secondly, to apply the acoustic tomography method in order to find and locate internal pole damage.

When timber is used for construction purposes, mainly the *MOE* in longitudinal direction is of interest due to the superior characteristics of wood parallel to the grain. Hence, *MOE* values in radial and tangential direction are scarce in literature. However, to numerically model the orthotropic material characteristics of timber, the elastic properties need to be known. Numerical models require the full set of orthotropic material properties of timber in order to accurately simulate the real structure. The main focus of the presented research work, is concerned with static and dynamic laboratory testing for the determination of various material properties, which will provide the project with benchmark to verify numerical and analytical findings. The dynamic tests based on sonic and ultrasonic waves firstly aim at the non/destructive determination of the timber material characteristics and secondly aim at detecting damage in transversal direction of a timber pole. The following list summarises the aims set for this work:

- Providing a full set of elastic material properties for two hardwood species Spotted Gum and Tallowwood through static and dynamic tests.
- Comparative analysis of different static material testing methods for the determination of the MOE values.
- Comparative study of elastic material properties derived from static and dynamic testing.
- Assessment of current non-destructive testing methods based on wave transmission time for the detection of internal damage of a timber pole.

A comprehensive list of the research goals with detailed explanations can be found in Chapter 3 *Research Methodology*.

## 1.3 Thesis Overview

This thesis is structured into four main parts: 'Introduction', 'Background and Literature Review', 'Methodology' and three 'Testing and Results' chapters presenting the execution, results and discussion of the different series of tests performed, while the last chapter, 'Synthesis', summarizes and reflects the findings.

In the 'Background and Literature Review' Chapter an overview of the general timber characteristics and their mechanical properties are presented, which are important indicators that have to be considered when working with timber. In the Chapter 'Research Methodology', an overview of the methodology applied to the presented research project is given, while the detailed testing methodology for the individual tests are described in the corresponding 'Testing and Results' Chapters. The three 'Testing and Results' Chapters are divided into the three groups of tests that were performed: Static Material Tests, Dynamic Material Tests and Damage Detection. Each 'Testing and Results' Chapters consists of the sections testing execution, results and discussion and conclusion. In the last, Chapter, 'Synthesis' discussions and conclusions over the entire research work are presented.

### 1.3.1 Published Work

The following lists, the already published papers based on this research:

1) Elsener, R., Dackermann, U., Li, J., Samali, B., & Crews, K., (2013) Experimental Investigations of Material Properties of Timber Utility Poles using various Material Testing Approaches, *Advanced Materials Research, 778, 265–272*

This paper was presented at the International Conference on Structural Health Assessment of Timber Structures (SHATIS'13) in Trento, Italy, September 4-6, 2013. It largely presents the findings presented in chapter *4 Static Material Tests*.

2) Elsener, R., Dackermann, U., & Li, J., (2013) Experimental Characterization of the Modulus of Elasticity of Timber Utility Poles Using Static and Dynamic Material Testing Approaches, *Proceedings of the International Conference on Structural Health Monitoring of Intelligent Infrastructure (SHMII-6),* Hong Kong, China, December 9-11, 2013

This paper were presented at the International Conference on Structural Health Monitoring of Intelligent Infrastructure (SHMII-6) in Hong Kong, China, December 9-11, 2013. It comprises the findings of the comparison of static and dynamic MOE's as presented in chapter *5 Ultrasonic Material Tests*.

**The following papers are currently in the process of writing:**

3) Elsener, R., Subhani, M., Li, J. & Dackermann, U. (2014) Ultrasonic and Combined Ultrasonic-mechanical Determination of Poisson's Ratios of Eucalyptus Utility Poles
4) Nguyen, V., Elsener, R., Li, J. & Dackermann, U. (2014) Material Propertiy Evaluation and Damage Assessment of Timber Poles Using Ultrasonic Wave Propagation Techniques

These papers were submitted to the 23rd Australasian Conference on the Mechanics of Structures and Materials ACMSM23, taking place in Byron Bay, Australia on the 9-12 December 2014.

# 2 BACKGROUND AND LITERATURE REVIEW

## 2.1 Chapter Overview

This chapter presents the background and literature review on general wood characteristics, mechanical properties of wood and non-destructive technologies, based on stress waves, to assess wood members. Knowing the wood characteristics and its unique directional, heterogeneous and hygroscopic properties is essential to understand the wave propagation in timber and therefore the underlying operational principals of non-destructive methods based on stress waves. The current theory on stress wave propagation in wood is discussed and the state-of-the-art of non-destructive methods used to assess timber beams, piles, poles or standing trees, is presented.

## 2.2 Characteristics of Wood

Wood is characterized by its anisotropic and hygroscopic behaviour and its heterogeneous structure. From a mechanical point of view, wood is a porous composite material made up of single fibres and rays as a matrix. It is a naturally grown material and has, through its organic nature, different properties which vary from species to species but also within the same tree species. As a rough estimate the coefficient of variation (COV) of the density within the same species can be assumed with 10% where a COV of 22% for the MOE is reasonable (Holzlexikon, 2003). A trees characteristics depend

on the location where it grew, soil quality, water availability and other environmental influences. This is the reason why the values given in this chapter are always average values and are not to be understood as exact values.

### 2.2.1 Anisotropy

As an orthotropic material, wood has three main directions: longitudinal (along the fibre) and radial and tangential (across the fibre) as shown in Figure 2-1, with different characteristics in each of the three directions. For example, the elastic and strength properties as well as the swelling and shrinking behaviour are different depending on the grain direction. Furthermore, the thermal conductivity, the stress wave transmission and the electric resistance also vary depending on the grain direction.

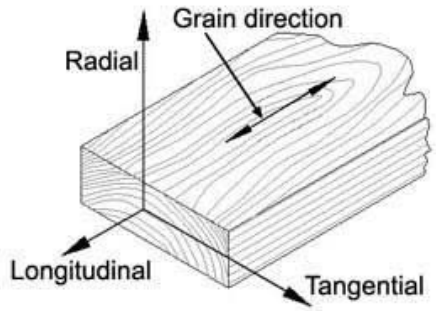


Figure 2-1: The three principal axes of wood with respect to the direction of grain (Kyaw n.d.)

The MOE is a good indicator to demonstrate these differences. When comparing the MOE of all three directions it is noticeable that the MOE in longitudinal direction is about one order of magnitude bigger than the radial MOE while the tangential MOE is the smallest. For construction purposes it is therefore always the longitudinal direction which is being considered. Since the wood fibres are aligned longitudinally and the rays run in radial direction, wood is also anisotropic in a macroscopic and microscopic level.

### 2.2.2 Heterogeneity

From the outside to the inside, a tree consists of the following main parts as shown in Figure 2-2: bark, cambium, sapwood and heartwood. Each section has its specific functions. The bark is the outermost layer which acts as the protection against physical damage, insect attack and fire. The cambium, a very thin layer between the bark and the sapwood and not visible to the naked eye, is the growth zone of a tree which produces all different wood cells and builds one new growth ring each year. The sapwood is the

outer and younger wood layer and its functions are to provide water and nutrition transport up and down the trunk as well as providing stability for the tree. It consists from fibres which are mainly aligned longitudinally. Heartwood is former sapwood and only serves structural purposes. It is not involved in the transport of water or the storage of nutrients anymore. The process when sapwood is converted into heartwood is called heartwood formation and happens when the tree starts to store extractives in the cell walls which makes the wood more durable and resistant against decay. Generally can be said that a big difference in colour between heartwood and sapwood also implies a big difference in density between the two wood layers (Niemz 1993). The pith is in the centre of the trunk and is the juvenile wood which usually has less strength than the heartwood.

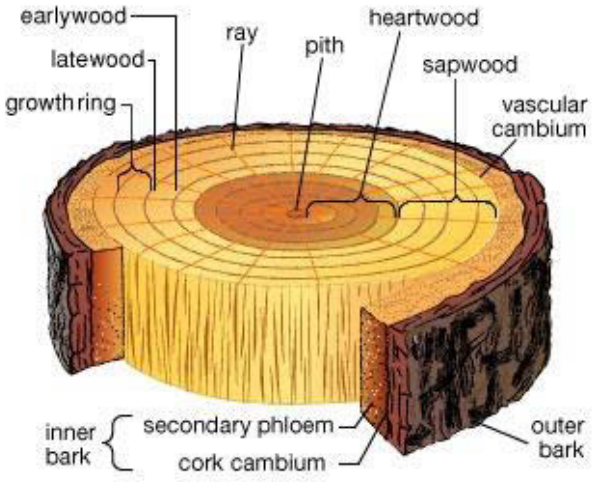


Figure 2-2: Cross section of a tree trunk, displaying its structure and composition (Webster 2006)

Each year a tree adds an additional growth ring on the outside of the trunk which causes it to grow in diameter. An annual growth ring consists of early wood, which is built during a fast growing phase in the beginning of the year (May to July), followed by a phase of slower growth where the late wood is built (August to October). Early and late wood vary in density which is one source for the heterogeneous nature of wood.

When looking at wood in a macroscopic level, a tree trunk is composed of millions of individual cells. The principal components of the cell wall are cellulose (50%), hemicellulose (25%), lignin (20-25%), and extractives (1-5%) (Fengel & Wegener 1983). These percentages have to be understood as approximate values since the proportions of the constituents vary between tree species as well as within the same species and even with-

in a single tree. Figure 2-3 displays photographs at a microscopic level (approximately tenfold magnification) of the cross sections of Spotted Gum and Tallowwood. Both species are diffused-porous which indicates that pores are present in the early as well as in the latewood and are evenly distributed.

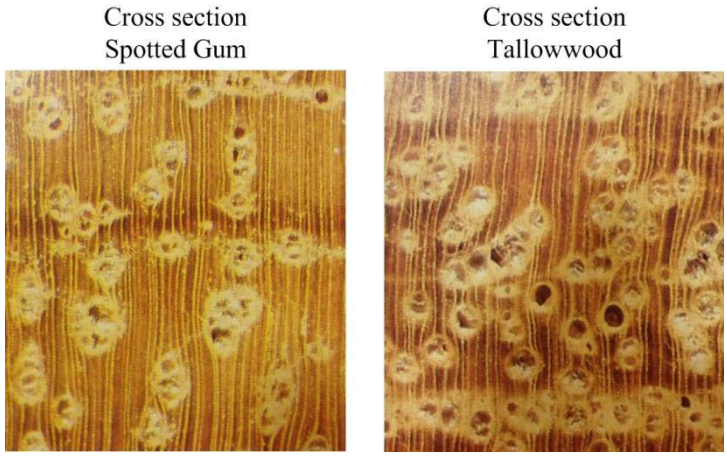


Figure 2-3: Cross sections of Spotted Gum and Tallowwood in a macroscopic scale Ilic et al. (1991)

In the microscopic level, one can distinguish between the main anatomical elements of wood: tracheids, fibres, vessels, rays and parenchyma cells. Tracheids only appear in softwoods and fibres and vessels in hardwoods, but both groups have parenchyma cells and rays. In softwoods, the tracheids serve a mechanical and conducting purpose, while the resin canals and parenchyma cells serve to store nutrition. In hardwoods, the fibres are responsible for the mechanical support of the tree, while the vessels serve a conducting purpose and the rays and parenchyma cells have the storage function. In Figure 2-4 microscopic pictures (approximately fiftyfold magnification) of all three wood sections are shown and display the hardwood's different cell types. In the cross sectional picture, the larger vessels and smaller fibres can be distinguished while in the radial section the rays can be seen. The tangential section shows a section through a vessel, rays and cells. Parenchyma cells cannot be clearly distinguished in the photographs.

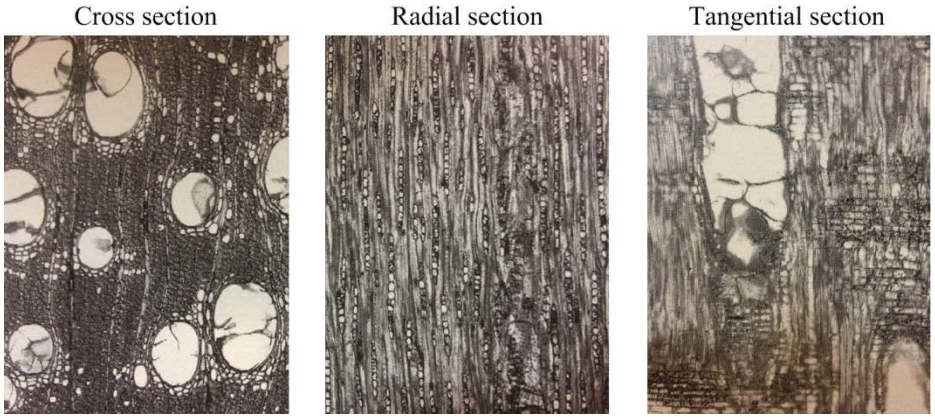


Figure 2-4: Different sections of Tallowwood in a microscopic scale Ilic et al. (1991)

An individual wood fibre is a complex structural element. Figure 2-5 displays a model of the different layers of a woody plant fibre. The cell walls are made up of a network of microfibrils, which are impregnated with lignin.

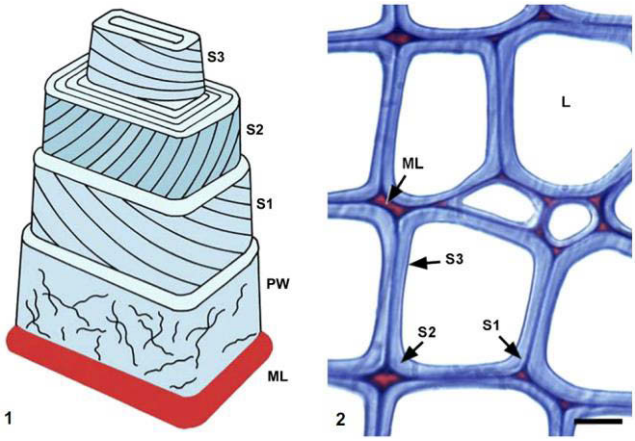


Figure 2-5: (1) Conventional cell wall model which distinguishes five wall layers. (2) Transverse section of early wood cells. With the middle lamella (ML), primary wall (PW), the three secondary wall layers (S1, S2, $S_3$), and lumen (L). (Schwarze 2007)

Also at the microscopic level, the high variability and heterogeneity of the woods constituents is obvious. It is the different types of cells, their proportions, numbers and distribution which make each tree species unique. Even the chemical composition of the cell walls and the organization at the molecular level is highly variable.

#### 2.2.2.1 Special Growth Characteristics and Wood Defects

A further source of heterogeneity in wood are wood defects or special wood characteristics due to specific growth conditions. Juvenile wood and reaction wood are two key examples of the biology of the tree affecting the quality of wood. Juvenile wood is the first grown wood in the centre (pith) of the tree. Its characteristics are usually inferior

compared to the heart and sapwood. Reaction wood is produced when the tree is deflected from the vertical axis to keep it upright. Softwoods produce compression wood on the underside of the trunk or branch and hardwoods produce tension wood on the upside to support the trunk or branches. The characteristics of reaction wood also vary from the regular wood regarding many properties such as swelling and shrinking behaviour as well as the mechanical properties.

Common wood characteristics such as knots, resin and cracks are another source of variability in the wood and are being considered as defects when material testing of timber is performed with small clear specimens. Depending on the tree species and the growth conditions, these attributes can be more or less frequent.

### 2.2.3 Hygroscopicity

Wood is a porous material with the ability to take up and emit water from the air. With changing ambient humidity the dimensional stability of wood is smaller compared to other materials due to its hygroscopic behaviour. Moisture absorbed from the air is bound in the cell wall. The fibre saturation point (FSP) is the condition where the fibre is fully saturated with water, which only happens if the wood is exposed to fully steam saturated air. This point lies, depending on the tree species, between 22% to 30% moisture content. Above this point the water is stored in the cell cavities and spaces and is called free water, while the water stored in the cell walls is referred to as bound water (shown in Figure 2-6).

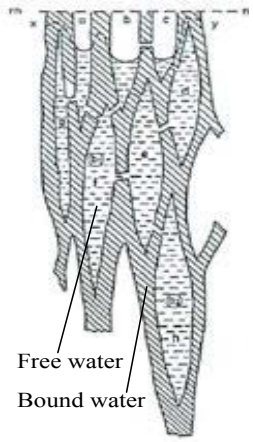


Figure 2-6: Bound and free water in wood

Below the fibre saturation point, water has a significant impact on the wood properties

and also causes it to swell or shrink. The swelling and shrinkage behaviour when wood dries or gets wet is different in all three wood directions. In longitudinal direction the maximum shrinkage is only about 0.3% while in radial direction it can be up to 5% and tangentially 10%. Above fibre saturation the water only influences the density but not the volume anymore. The strength values given in reference books are usually quoted for a moisture content of 12%. With an increase in moisture content, the properties drop with every 1 % moisture change around 2% for the MOE or 4% for the MOR for small clear specimen (Bootle 2005). The moisture content can be calculated with the following equation.

$$u = \frac{m_u - m_d}{m_d} \cdot 100(\%) \qquad (2\text{-}1)$$

where $u$ is the moisture content, $m_u$ the mass of the wet wood and $m_d$ the mass of the dry wood (no water). The woods density is one of the most important properties and varies with changing moisture content. The following formula is used to calculate the density

$$\rho = \frac{m}{V} \qquad (2\text{-}2)$$

where $\rho$ is the density, $m$ is the mass and $V$ is the volume. When density values are given in literature, the moisture content must also be noted which is usually 12%.

### 2.2.4 Wood Pests

Wood is biodegradable and therefore vulnerable to biotic pests. The wood moisture content plays a vital role because it does not only affect the wood properties but also makes wood more vulnerable for fungi and insect attacks once it exceeds around 20% moisture content. The temperature also needs to be in a favourable range for fungi and insects to propagate which lies between 10 ºC and 35 ºC. Above or under this temperature range the activity ceases to a large extent.

Decay producing fungi can attack the sapwood but also the heartwood of almost all wood species which results in decay or rot. It uses cellulose and/or lignin as food source

and penetrates the wood with its microscopic threadlike strands, called hyphae. The two most common wood destroying fungi are brown rot and white rot as illustrated in Figure 2-7. While brown rot fungi mainly feeds on the cellulose, white rot fungi removes both, the cellulose as well as the lignin, and the wood may appear whiter (Eidg. Forschungsanstalt WSL 2012).

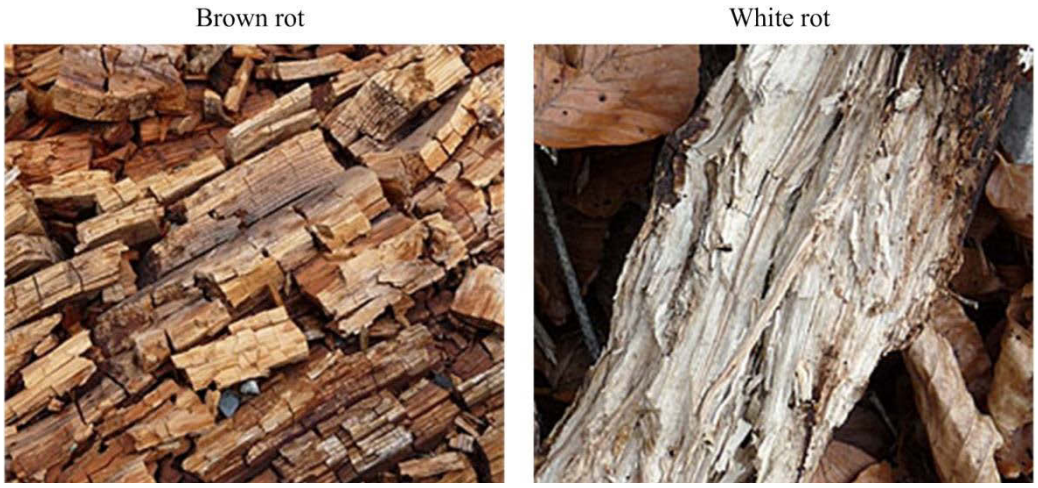


Figure 2-7: Brown rot and white rot fungi Eidg. Forschungsanstalt WSL (2012)

The insect that causes the most damage to wood in service in New South Wales is the subterranean termite *'coptotermes acinaciformis'*. The bodies of the workers are light skinned and very sensitive to sunlight. That's why these termites live underground and dig their way into timber from the ground where they start feeding on the woods cellulose. This species hollows out the centre of trees and sometimes only leave a thin layer of wood on the outside, considerably reducing the trees strength (Figure 2-8).

Figure 2-8:Subterranean termite nest in below ground portion of hardwood pole (Forest Research Institute NZ 1976)

The pole in Figure 2-8 was in service for about 30 years before the nest was discovered.

*C acinaciformis* are known to attack 25 species of eucalyptus, northern kauri pine, hoop pine, cypress pine, sheoke, and silky oak Forest Research Institute NZ (1976).

### 2.2.5 Treatment of Wood

The purpose of preservation of timber is to extend the service life by protecting it against insect and fungi attack as well as to protect it against decay. The increase of the service life of timber makes it more sought after for construction purposes especially for outdoor applications. The service life of timber depends on various factors such as the natural durability of wood, the environmental influences and the type of preservation. For all wood species used for timber poles, the sapwood can be considered non-durable if it is untreated. With the correct treatment, however, it can be made as durable as the heartwood of the most durable wood species. In Australia, the treatment of wood is regulated in Australian Standard 1604.1 (Australian Standard 2012).

Copper chromium arsenic (*CCA*) and Creosote are commonly used especially for outdoor applications on poles and piles (Ausgrid 2011). *CCA* is Australia's most widely used timber preservative and is appreciated for its relatively low cost and its effective protection against termites, fungi and moisture damages. The ingredients have the following roles: copper to control the fungi, arsenic to control termites and chromium to help to fix the copper and arsenic in the wood (www.csiro.au). Creosote also is a fungicide and insecticide but also a natural water repellent which is primarily used on timber poles and railroad ties. It is a greasy liquid which is applied by pressure methods. In NSW, all new utility poles that are being installed are full length copper chromium arsenic impregnated.

Table 2-1: Compilation of durability classes and strength groups of some common wood species used for utility poles in NSW

| ***Species*** | ***Durability Class*** | ***Strength Group*** |
|---|---|---|
| Blackbutt *(Eucalyptus pilularis)* | Class 2 | S2, SD2 |
| Box, grey *(Eucalyptus microcarpa)* | Class 1 | S2, SD2 |
| Gum, grey *(Eucalyptus punctata)* | Class 2 | S1, SD2 |
| Gum, spotted *(Eucalyptus maculata)* | Class 2 | S2, SD2 |
| Ironbark, grey *(Eucalyptus paniculata)* | Class 1 | S1, SD1 |
| Tallowwood *(Eucalyptus microcorys)* | Class 1 | S2, SD2 |

Table 2-1 shows the natural durability ratings of some common utility pole timber species which are listed in the Australian Standard 5604 (Australian Standard 2005) and the strength groups according to Australian/New Zealand Standard 2078 (Australian/New Zealand Standard 2000). The durability classes are divided into four classes whereof Class 1 is the highest (highly durable) with an expected service life of more than 25 years. Class 2 classified timbers are considered durable and have an expected service life of 15-20 years. The strength groups are divided into six groups and unseasoned (S) and dry (SD) ratings. Here again, in group 1 are the timbers with the highest strength ratings. It is obvious, that for utility poles, where high demands on durability and strength are made, only species with strength and durability ratings of the two highest classes are considered.

### 2.2.6 Specific Eucalyptus Characteristics

In Table 2-2, the wood characteristics of Blue Gum (from Wagenführ 2007), Spotted Gum and Tallowwood are presented. The characteristics are divided into physical, mechanical, microscopic and chemical properties. The data of Blue Gum is used to complement, or rather give an idea of the order of magnitude, the values of the two species investigated in this research.

Table 2-2: Summary of physical, mechanical, microscopic and chemical wood characteristics of Blue Gum, Spotted Gum and Tallowwood

| **Wood characteristics** | | | | |
|---|---|---|---|---|
| | | ***Blue Gum*** [1)] | ***Spotted Gum*** | ***Tallowwood*** |
| physical | Density at 12% MC [kg/m$^3$] | 660 ... 790 | 1060 | 1090 |
| | Pores percentage [%] | ~52 | | |
| | Shrinkage radial [%] | ~9.8 | | |
| | Shrinkage tangential [%] | ~20.6 | | |
| mechanical | MOE [N/mm$^2$] | 12,000 | 23,000 | 18,000 |
| | Bending strength [N/mm$^2$] | 75 … 104 | 142 | 134 |
| | Tensile strength [N/mm$^2$] | 90 | 159 | 107 |
| | Compressive strength [N/mm$^2$] | 37 … 51 | 76 | 77 |
| microscopic | Vessels diameter [µm] | 80 ... 110 ... 150 | | |
| | Vessels percentage [%] | ~21 | | |
| | Parenchyma percentage [%] | ~16 | | |
| | Ray height [µm] | 90 ... 160 ... 230 | | |
| | Ray width [µm] | 8 ... 12 ... 22<br>single-layer | single and<br>multi-layer | single-layer |
| | Fibres length [µm] | 1000 ... 1210 ... 1480 | | |
| | Fibres wall thickness [µm] | 4.2 ... 5.6 ... 7.5 | | |
| | Fibres lumen [µm] | 4.4 ... 8.7 ... 13.2 | | |
| | Fibres percentage [%] | ~49 | | |
| chemical | Ethanol benzene solubility [%] | ~3.4 | | |
| | Hot water solubility [%] | 6.2 ... 7 | | |
| | Ether solubility [%] | 0.6 ... 1.3 | | |

1) Data from Wagenführ (2007)

For Spotted Gum and Tallowwood, detailed data is not available in the literature. In the Wood Atlas, however, Wagenführ (2007) presents the entire set of wood characteristics of Blue Gum and lists both, Spotted Gum and Tallowwood, as similar species. Factors such as the fibre length, the number of wood rays and the amount of extractives have an important influence on the stress wave propagation. Information about the microscopic and chemical composition of wood is therefore necessary to make conclusions about certain behaviour of stress waves in wood.

## 2.3 Mechanical Properties of Wood

The mechanical properties of wood are usually determined from so called ‘small clear

specimens' who are free of any faults such as knots, splits or cross grain. The values derived from those tests are often used in literature but cannot be used for design purposes because the values are higher than the ones derived from full scale tests. Literature values for timber are usually averaged data of test series including as many trees as possible due to the high deviations within a wood species but also within a single tree. Even with clear wood specimen, the variability of the timber properties are high because wood is a naturally grown, heterogeneous material.

### 2.3.1 Elastic Properties

Elasticity is the characteristic of a material to fully restore its original state after it was deformed due to an external force. In order to describe the elastic behaviour of wood, twelve constants (whereof nine are independent), are needed. They are three moduli of elasticity E or MOE, three moduli of rigidity G and six Poison's ratios ν. According to the generalized Hooke's law, orthotropic materials can be characterized by the following compliance matrix

$$\begin{bmatrix} \varepsilon_{LL} \\ \varepsilon_{RR} \\ \varepsilon_{TT} \\ \gamma_{LR} \\ \gamma_{LT} \\ \gamma_{RT} \end{bmatrix} = \begin{bmatrix} \frac{1}{E_L} & -\frac{\nu_{RL}}{E_R} & -\frac{\nu_{TL}}{E_T} & 0 & 0 & 0 \\ -\frac{\nu_{LR}}{E_L} & \frac{1}{E_R} & -\frac{\nu_{TR}}{E_T} & 0 & 0 & 0 \\ -\frac{\nu_{LT}}{E_L} & -\frac{\nu_{RT}}{E_R} & \frac{1}{E_T} & 0 & 0 & 0 \\ 0 & 0 & 0 & \frac{1}{G_{LR}} & 0 & 0 \\ 0 & 0 & 0 & 0 & \frac{1}{G_{LT}} & 0 \\ 0 & 0 & 0 & 0 & 0 & \frac{1}{G_{RT}} \end{bmatrix} \times \begin{bmatrix} \sigma_{LL} \\ \sigma_{RR} \\ \sigma_{TT} \\ \sigma_{LR} \\ \sigma_{LT} \\ \sigma_{RT} \end{bmatrix} \quad (2\text{-}3)$$

where $\varepsilon$ is the elastic strain vector, $\sigma$ the stress vector, $E$ the modulus of elastic MOE, $G$ the shear modulus and $v$ the Poisson's ratio. The subscripts $L$, $R$ and $T$ stand for the longitudinal, radial and tangential direction in wood. The matrix can be simplified by the following equation

$$[\varepsilon] = [C] \times [\sigma] \quad (2\text{-}4)$$

where $\varepsilon$ is the strain tensor, $\sigma$ is the stress tensor and $C$ is the orthotropic elastic matrix.

#### 2.3.1.1 Modulus of Elasticity

Due to the three different grain directions, wood has three different MOEs in longitudinal, radial and tangential direction, usually stated as $MOE_L$, $MOE_R$, $MOE_T$. Literature values for the MOE in radial and tangential direction are scarce and values given for $MOE_L$ are most commonly derived from bending tests. $MOE_L$ always has the highest value, followed by $MOE_R$ and $MOE_T$. As a general rule of thumb the ratio for $MOE_R/MOE_L$ can be assumed as 0.1 and for $MOE_T/MOE_L$ as 0.05.

Table 2-3: Compilation of values for the density and MOE of typical wood species used for utility poles in NSW (Bootle 2005)

| ***Species*** | ***Density at 12% MC*** *[kg/m³]* | ***MOE at 12% MC*** *[N/mm²]* |
|---|---|---|
| Blackbutt *(Eucalyptus pilularis)* | 900 | 19,000 |
| Box, grey *(Eucalyptus microcarpa)* | 1120 | 20,000 |
| Gum, grey *(Eucalyptus punctata)* | 1080 | 18,000 |
| Gum, spotted *(Eucalyptus maculata)* | 950 | 23,000 |
| Ironbark, grey *(Eucalyptus paniculata)* | 1120 | 24,000 |
| Tallowwood *(Eucalyptus microcorys)* | 990 | 18,000 |

Table 2-3 shows a compilation of the density and MOE values of some commonly used timber species for utility poles, according to Bootle (2005).

Furthermore, the MOE derived from bending, tension and compression testing can be different from each other. Schneider et al. (1990) investigated the variations between MOE's derived from bending, tension and compression test on sugar maple at 12% moisture content. The researchers found that the determined values ranged from 15.1 GPa for the MOE in compression up to 16.5 GPa for the MOE in tension. Wangaard (1950) compared the MOE's derived from bending and compression tests of several wood species and found that the values computed from compression tests were slightly higher than the ones derived from bending tests.

#### 2.3.1.2 Poisson's Ratio

When an object is stretched it contracts in the perpendicular direction to the applied load. The Poisson's ratio is the ratio of transverse to axial strain. Wood has six Poisson's ratios which are denoted by $\nu_{LR}$, $\nu_{RL}$, $\nu_{LT}$, $\nu_{TL}$, $\nu_{RT}$, and $\nu_{TR}$, where the first letter stands for the direction where the load is applied and the second letter for the direction of lateral deformation. Determining the Poisson's ratio for wood is difficult and literature values for timber are very scarce. Especially the ratios $\nu_{RL}$ and $\nu_{TL}$ are very small and therefore difficult to measure. For determining the Poisson's ratios of wood, no standards are available. The tests described in this research were performed on the basis of the ASTM International Standard (ASTM International 2004).

The Poisson's ratio is related to the MOE by the following equation

$$\frac{\nu_{LR}}{E_L} = \frac{\nu_{RL}}{E_R}, \qquad \frac{\nu_{LT}}{E_L} = \frac{\nu_{TL}}{E_T}, \qquad \frac{\nu_{RT}}{E_R} = \frac{\nu_{TR}}{E_T} \tag{2-5}$$

where $\nu$ is the Poisson's ratio, $E$ is the MOE and the subscripts $L$, $R$ and $T$ stand for the longitudinal, radial and tangential orthotropic wood directions.

**Modulus of Rigidity**

The modulus of rigidity (G), also called shear modulus, is defined as the ratio of shear stress to shear strain. The three MOR's of wood are denoted by $G_{LR}$, $G_{LT}$ and $G_{RT}$. The MOR in comparison to the MOE of some commonly used timber species for utility poles are given in Table 2-4 (Bolza & Kloot 1963).

Table 2-4: Compilation of moduli of rigidity values *G* of common wood species used for utility poles in NSW

| ***Species*** | ***MOE at 12% MC*** *[N/mm²]* | ***G at 12% MC*** *[N/mm²]* | ***Ratio G/MOE*** |
|---|---|---|---|
| Blackbutt *(Eucalyptus pilularis)* | 19,000 | 1,151 | 0.061 |
| Box, grey *(Eucalyptus microcarpa)* | 20,000 | 1,462 | 0.073 |
| Gum, grey *(Eucalyptus punctata)* | 18,000 | - | - |
| Gum, spotted *(Eucalyptus maculata)* | 23,000 | 1,282 | 0.056 |
| Ironbark, grey *(Eucalyptus paniculata)* | 24,000 | 1,338 | 0.056 |
| Tallowwood *(Eucalyptus microcorys)* | 18,000 | 1,179 | 0.066 |

The ratios G/MOE presented by Green et al. (2010) of a big range of species typically lie between 0.04 and 0.14.

### 2.3.2 Strength Properties

The strength properties of wood, also called mechanical properties, include various common and less common properties. Here, only the common properties such as the MOR, the compressive strength (CS) and the tensile strength (TS), which were also examined in the laboratory tests during this project, are described. In total there are more than ten different strength properties.

#### 2.3.2.1 Modulus of Rupture

The MOR, also known as flexural strength or bending strength, is the ability of a material to resist deformation in bending, mostly applied in a three or four point bending test. The MOR is the stress experienced at failure. Values determined with bending tests always include a shear component. The standards DIN 52186 Deutsche Norm (1978), ASTM D143-09 ASTM International (2009) and ASNZ 4063.1 Australian/New Zealand Standard (2010) describe the standard test for determining the MOR.

#### 2.3.2.2 Compression Strength

The compression strength, also called maximum crushing strength, is the maximum value of a uniaxial compressive stress when the material fails. The compression test for timber in longitudinal direction is described in the DIN 52185 Standard (Deutsche Norm 1976) and the ASTM D143-09 Standard (ASTM International 2009). For testing perpendicular to the grain, DIN 52192 (Deutsche Norm 1979) and ASTM D143-09 (ASTM International 2009) apply.

#### 2.3.2.3 Tensile Strength

The tensile strength is the opposite of the compression strength but its values can vary significantly. It is the maximum stress that a material can withstand when a stretching force is applied before failure. The tensile strength parallel to the grain is described in DIN 52188 (Deutsche Norm 1979) and ASTM D143-09 (ASTM International 2009) and perpendicular to the grain in ASTM D143-09 (ASTM International 2009).

## 2.4 Non-Destructive Testing

### 2.4.1 Background

Non-destructive testing (NDT) methods, also referred to as non-destructive evaluation (NDE) methods, have long been used on timber to assess structures without causing additional damage, and involve a wide group of analysis techniques. The earliest non-destructive evaluation of wood is visual inspection which has mainly been used for the selection of timber for construction purposes. Even nowadays this method is still widely used for grading wood product such as lumber, piles and poles. In the early 20th century, scientific non-destructive methods became available with the development of the theory of elasticity and more advanced measuring equipment to determine the wood properties. Hearmon (1948); Kollmann & Krech (1960) were the first researchers in Europe who conducted research on the determination of the MOE based on dynamic methods. Hearmon (1965) was the first to promote techniques using ultrasonic waves for the elastic characterization of wood. Beside visual inspection and acoustic methods, optical methods based on image processing or laser and methods which use x-rays are available. Non-destructive methods can be distinguished into non-destructive and semi-destructive methods. None of them damage a structure strongly but semi-destructive methods mostly require drilling or punching a hole to obtain information about the inside condition of a beam, pile or pole. During the last 20 years of the 20th century, researchers have developed different methods for the non-destructive evaluation of wood. Ross & Pellerin (1994); Ross (1991), started organizing symposia on NDT which stimulated the research in this area. Bucur (2006) published a comprehensive book (first published in 1995) about the acoustic properties of wood.

In this research, NDT techniques based on stress waves were performed and the literature review therefore focuses on those types of methods.

#### 2.4.1.1 Stress Waves

NDT methods using stress waves have long been used on wood members. Sound waves can be divided into sonic and ultrasonic waves. Stress waves are defined as the acoustic hearing range of humans which is usually between 16 Hz and 20,000 Hz. Ultrasound is above 20,000 Hz and outside of the threshold of human hearing. Due to the high attenuation in wood, the ultrasound frequencies typically used on wood are in the low range

between 20,000 Hz and 500,000 Hz.

When stress waves are introduced to a wood member, either by a mechanical impact or through an ultrasound transmitter, three different wave types are being triggered. They are bending waves, also called S-waves or shear waves (illustrated in Figure 2-9), longitudinal waves, also called P-waves or compression waves (also shown in Figure 2-9), and surface waves, also called Raleigh waves.

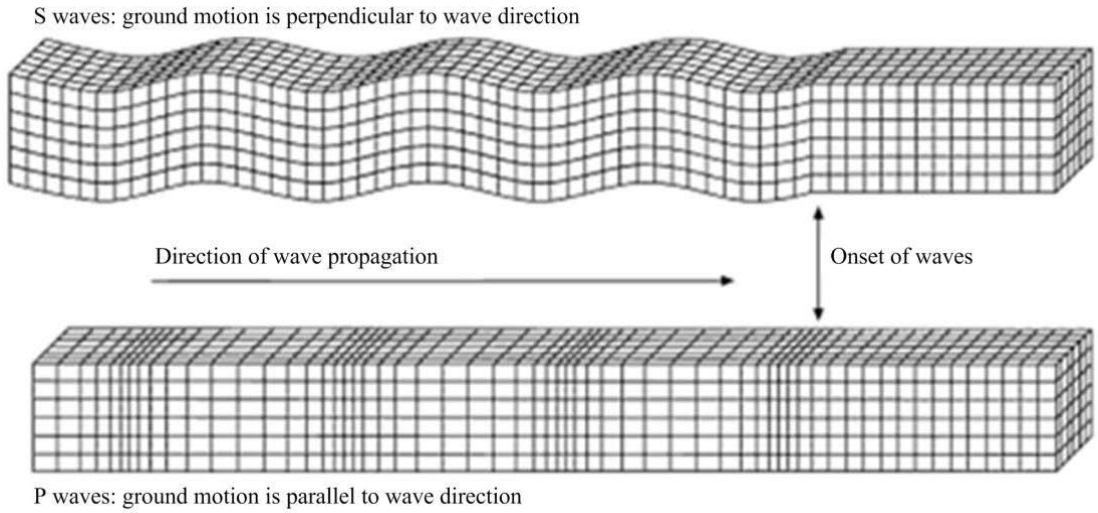


Figure 2-9: Illustration of bending and longitudinal waves Stein (2003)

While the surface waves, as the name indicates, propagate on the surface, the P-waves and S-waves are body waves which propagate within a media. As indicated in Figure 2-9, the particle motion in longitudinal waves is parallel to the direction of propagation, for shear waves it is perpendicular to the direction of propagation.

Stress waves travel through wood with different velocities depending on the direction of grain. The wave velocity in longitudinal direction is the highest and depends on the wood species, quality, density and moisture content of the specimen. The speed of sound across the grain is about one fifth to one third of the longitudinal wave velocity (Green et al. 2010). A compilation of wave velocities in longitudinal, radial and tangential direction for three wood species, measured by Burmester (1965), is shown in Table 2-5.

Table 2-5: Compilation of speed of sound *V* values for three wood species Burmester (1965)

| ***Species*** | ***V longitudinal [m/s]*** | ***V radial [m/s]*** | ***V tangential [m/s]*** |
|---|---|---|---|
| Pine *(Pinus sylvestris)* | 5,380 | 1,898 | 1,630 |
| Beech *(Fagus sylvatica)* | 4,929 | 1,996 | 1,455 |
| Spruce *(Picea abies)* | 4,780 | 1,681 | 1,283 |

The wavelength is inversely proportional to the frequency and is related to the frequency and velocity by the following equation

$$\lambda = \frac{V}{f} \tag{2-6}$$

where $\lambda$ is the wavelength, $V$ the velocity of the wave and $f$ the frequency. The propagation velocity of a stress wave can be determined using the following equation when the transmission time and the distance between two sensors are known

$$V = \frac{L}{T} \tag{2-7}$$

where $V$ is the velocity, $L$ is the distance between two sensor location points and $T$ is the time taken to travel the distance.

In order to be able to detect an anomaly in timber, the wavelength needs to be smaller than the defect. Assuming a wave velocity of 1800 m/s in radial direction and a frequency of 20,000 Hz, the resulting wavelength is 75 mm (according to Equation (2-6) and can therefore only detect damage which is larger than 75 mm. The ability to detect small-size damage and the extent of attenuation need to be traded off against each other depending on the application.

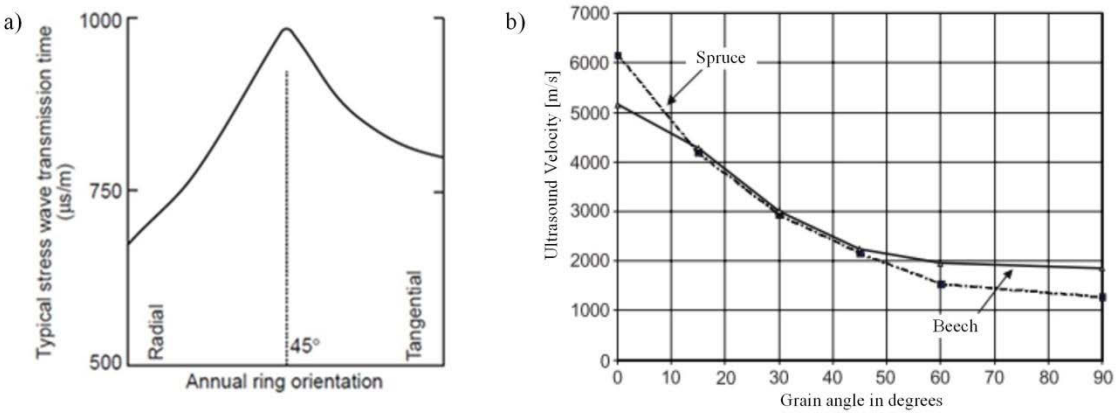


Figure 2-10: Stress wave transmission time perpendicular to the grain compared to annual ring orientation. a) Experimental results by Ross et al. (1999), b) experimental results by Niemz et al. (1999)

The influence of the annual growth rings orientation on the transmission time of stress waves in timber has been studied by Kabir (2001); Niemz et al. (1999) and Ross et al. (1999). As shown in Figure 2-10 (a) by Ross et al. (1999), the transmission time in radial direction is the shortest, as expected, but does not gradually increase towards the tangential direction. The highest transmission times are present at an annual ring orientation of 45 degrees according to Ross et al. (1999). Kabir (2001) and Niemz et al. (1999), on the other hand found that the velocity consistently decreases from the radial to the tangential direction as shown in Figure 2-10 (b).

#### 2.4.1.2 Wave Propagation

Wave propagation in wood is a complex dynamic process which depends on the wood properties, the orientation and microstructure of the wood fibres, and perhaps more importantly, on the geometric form of the material (X. Wang et al. 2007). Mattheck & Bethge (1993) investigated the speed of sound in different healthy tree species with a commercially available stress wave timing unit and discovered that the wave velocity varies between tree species but also within the same species.

When sound travels through wood it is mainly affected by the MOE and the density but also the Poisson's ratio has a minor influence. When V is known, the MOE can then be determined using the following wave equation

$$MOE_d = V^2 \cdot \rho \cdot \left[\frac{(1+\nu)(1-2\nu)}{(1-\nu)}\right] \quad (2\text{-}8)$$

where $MOE_d$ is the dynamic modulus of elasticity in longitudinal, radial or tangential direction, respectively, $V$ the wave velocity in the corresponding direction, $\rho$ the density of the material and $\nu$ the Poisson's ratio. Since wood is neither homogeneous nor isotropic, the usefulness of one dimensional wave theory may be put into question. However, several researchers have shown that one-dimensional wave theory is adequate for describing the wave behaviour in wood. Bertholf (1965) for example showed the dependency of the wave propagation velocity and the MOE of clear wood specimen. Usually, the simplified equation, neglecting the influence of the Poisson's ratio, is used for the dynamic MOE calculations, according to Equation (2-9).

$$MOE_d = V^2 \cdot \rho \quad (2\text{-}9)$$

Several researchers have found that the one-dimensional wave theory is appropriate to describe the wave behaviour in timber Bucur & Feeney (1992).

Figure 2-11 displays the displacement fields of wave propagation, obtained using finite element analysis, in isotropic and orthotropic materials by Tallavo et al. (2012). For the isotropic case, the researchers used a ratio of 1 for the modulus of elasticity ($MOE_R/MOE_T$) and for the orthotropic case 1.36. In the isotropic mode, the wave front has a circular shape while the orthotropic model shows a triangular shape. This behaviour is in agreement with literature from Payton (2003); Schubert et al. (2005).

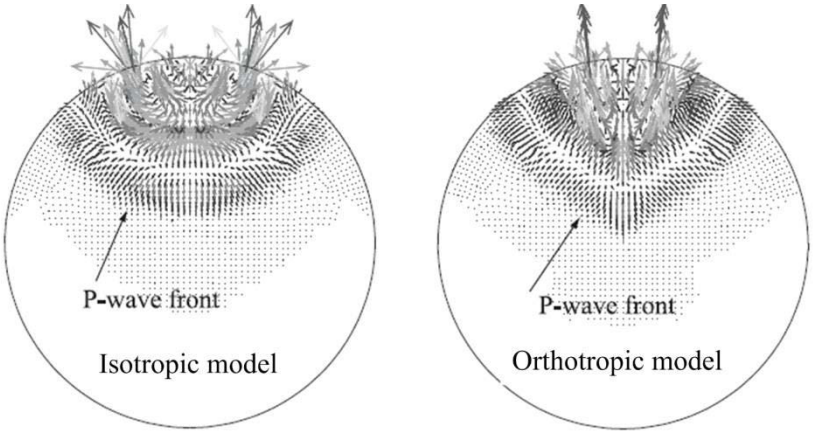


Figure 2-11: Comparison between displacement fields of wave propagation in isotropic and orthotropic media Tallavo et al. (2012)

The wave propagates faster in radial direction than in tangential direction and therefore creates the distinct pointy wave front in the orthotropic case.

#### 2.4.1.3 Factors influencing the Wave Velocity

Various wood properties as well as environmental factors have an influence on the velocity with which the wave propagates through wood as mentioned in the previous section. Following the most important factors influencing the wave velocity are presented and discussed.

**Moisture Content**

The wood moisture content is the more important of the two environmental influences beside the temperature and various researchers have examined its influence on the wave velocity. A dramatic decrease of the wave velocity in wood with increasing moisture content up to the fibre saturation point was reported by Sakai et al. (1990). The researchers also found the decrease to be linear which was confirmed by Keunecke et al. (2006). Bucur (2006) also states that the sound velocity is directly related to the presence of bound water. The influence of moisture was also investigated in this work for the two tested Eucalyptus species. The results are presented in chapter 5.4.4.

**Temperature**

The influence of the second environmental factor, the temperature, is less distinct. A linear reduction of the ultrasound velocity with increasing temperature was discovered by Sandoz (1993) on Spruce and Fir samples. This behaviour was observed below and above the fibre saturation point as well as for temperatures of below 0 degrees Celsius.

The effect decreases with a lower moisture content. Ross et al. (2000) also conducted research on the influence of the temperature on the ultrasound velocity which confirmed the same findings.

**Density**

Investigations on the influence of the density on the wave velocity resulted in different conclusions by different researchers. An decreasing wave velocity with increasing density was first reported by Bucur & Chivers (1991). Ilic (2003) and Mishiro (1996)a both reported that the wood density does not have an influence on the wave velocity at all. Carrasco & Junior (2003) stated that for a constant moisture content along the specimen, an increasing density results a higher wave propagation velocity in all of the three orthotropic directions of wood. Finally it was found by Baar et al. (2011) that a higher density positively influences the wave velocity, but that the effect is usually supressed by other factors such as the stiffness, the micro and macro structure and the chemical composition of the wood. Mishiro (1996)a who examined the ultrasonic velocity in 12 hardwoods and 7 softwoods concluded that the velocity in longitudinal direction is independent of the density in the whole but that the specimens could be classified into three groups. In the first group ultrasonic velocities increased with higher density, in the second it was independent of density, and in the third, it decreased with higher densities. He also concluded that the wave velocity in longitudinal direction is independent of the one in tangential direction and divided the specimens in two groups again. In one group, the ultrasound velocity in longitudinal direction increased with the velocity in tangential direction while in the other group the velocities in both anatomical directions decreased.

**Macroscopic and microscopic structure**

On a macroscopic scale, the influence of the width of the annual growth rings on the stress wave velocity were investigated by Bucur (2006) for spruce and maple. The waves propagated faster through specimens with smaller annual growth rings for both wood species. On a microscopic scale it is the length of the anatomical elements, namely the fibres in hardwood and the tracheids in softwood which have an influence on the wave velocity. Fibres are usually shorter compared to tracheids with average lengths of 1 – 1.5 mm while tracheids are in average around 3 mm long (these numbers have to be understood as very rough estimates over all species and can vary largely between but

also within species). Longer elements generally support faster wave propagation in longitudinal wood direction. Reaction wood as well as wood defects also have an influence on the wave velocity which has to be considered if they lay in the path of the measurement.

**Microfibril Angle**

Furthermore, it is the microfibril angle (MFA) of the thickest cell wall layer two, which has a proven influence on the MOE as reported by Bergander & Salmen (2000) and the strength and stiffness as shown by Cave & Walker (1994). Studies on the stress wave velocity with changing microfibril angle have not been conducted as yet. Donaldson (2008) provided a comprehensive literature review on studies about the MFA which mainly confirm the correlation of the MFA with the MOE in longitudinal direction and the stiffness.

**Extractives**

Grabner et al. (2005) found that an increasing content of wood extractives go hand in hand with improved mechanical properties. Information about the influence of the amount of extractives on the wave velocity has not been reported in literature.

**Slope of grain**

The slope of grain or grain angle does have a heavy influence on the wave velocity. Niemz et al. (1999) found that a displacement of only 10 degrees results in a 20% decrease of the stress wave velocity. Similar tests were also conducted by Armstrong (1991) on several soft and hardwoods and similar results were reported.

**Age**

Finally, also the age of a tree influences how fast an stress wave propagates. Farrell et al. (2008) reported that the velocity is slower in younger trees and increases in more mature trees.

Considering all these factors it becomes apparent how many different wood characteristics and environmental factors can influence the velocity of stress waves. Having as much information about the tested tree species as possible is crucial for a meaningful interpretation of the time of flight.

#### 2.4.1.4 Wave Theory

Waves may propagate in two different ways, as infinite waves in infinite media where they propagate freely in media without boundaries, or as guided waves in finite media with boundaries. The boundaries impose stress and/or strain constraints. This causes the wave to reflect and often yield a change of wave type and the direction of the wave. Therefore guided waves are present in any elastic and inelastic material (H. Wang 2004) and they follow the theory of elasticity when propagating in elastic media (Graff 1975). In a finite media, all guided waves are dispersive and the velocity is a function of the frequency and the geometric and boundary conditions. For utility poles, the guided wave case has to be considered since a pole is of finite dimensions and therefore has boundaries which interfere with the waves travelling in the pole.

The ultrasound input used for the tests in this thesis had a centre frequency of 24 kHz which means that other frequencies were also excited. This results in a wave package when the wave is propagating through the pole, and therefore the group velocity of the wave has to be considered instead of the phase velocity.

Also, when waves travel through a body, different wave modes occur. With higher frequencies more modes appear as shown in Figure 2-12. Since the maximum group velocity is the same for all modes, the frequency used for TOF measurements is not important for the wave velocity. The data used for plotting the graph in Figure 2-12 was created with the software Disperse, using material properties obtained from experimental material testing and considering timber as transversely isotropic material. The validity of considering timber as transversally isotropic material is presented in Subhani et al. (2013) where the transversally isotropic dispersion curves show a good correlation with the orthotropic material model.

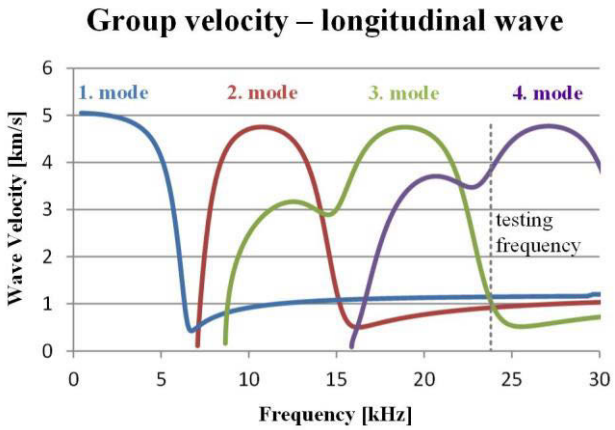


Figure 2-12: Group velocity of the P-wave of Spotted Gum (data created with Disperse software)

As mentioned above, the centre frequency used for testing was 24 kHz which lies between the 3rd and 4th mode according to Figure 2-12 and would result in a velocity smaller than the maximum velocity. However, this is only the centre frequency and other nearby frequencies are also excited which travel with the maximum group velocity, and hence, the TOF measurements will capture the fastest wave velocity.

## 2.4.2 Current Practice

### 2.4.2.1 Pole Testing

The current pole testing procedure executed in NSW by Ausgrid's pole inspectors involves the following steps:

1. visual inspection
2. sounding
3. drilling

The first step in the assessment process, the visual assessment of the pole, includes checking the pole for any visible defects, such as visible rot, fungi or insect attack. As the second step, the inspector uses the sounding technique, which involves hitting the pole with a blunt hammer between ground line and the maximum height the inspector can reach. The sound of the hits indicates the integrity of the pole, where a higher pitch sound infers that the poles inside is solid and therefore in good condition and lower frequency indicates voids or rot in the pole. It is obvious that this technique requires a lot of experience of the assessor in order to interpret the sound correctly and therefore leaves room for the eventuality of human error. The last stage of the assessment is to

examine the pole's underground condition with the sounding and drilling method. Since this is the most vulnerable area of the pole due to changing moisture content conditions and the occurrence of the highest stresses at ground level, the sounding technique on its own is not sufficient to obtain an accurate prediction of the integrity of the pole's underground section. Since this is also the area where most poles break in case of failure, special attention is required to this part of the pole. For the drilling assessment, to access the pole underground, the inspector is forced to dig the pole free to a depth of about 40 cm as shown in Figure 2-13 a.

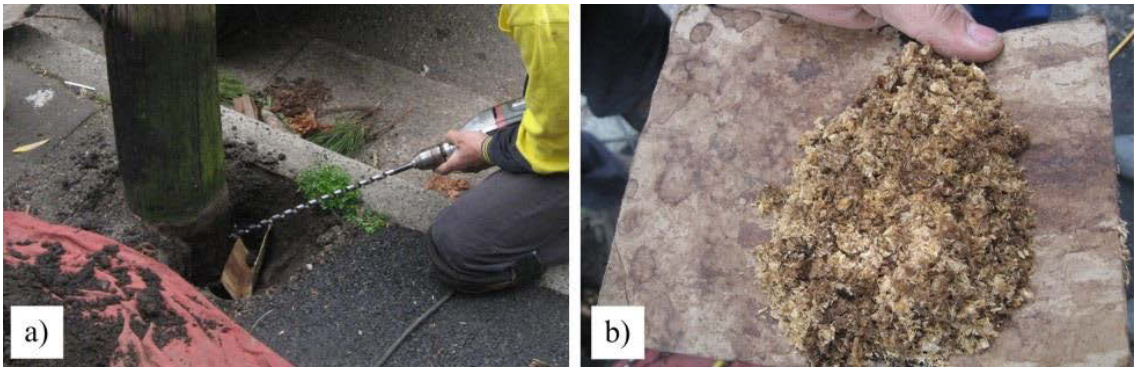


Figure 2-13: (a) Drilling method to assess underground pole condition (b) sawdust from decayed part from inside the pole

Holes at a 90 degree angle to each other are drilled through the full pole cross section and the occurring sawdust is collected and examined as shown in Figure 2-13 b. Wet sawdust indicates the presence of decay or rot inside the pole. In addition to the wet sawdust, the pole inspector can usually also feel a reduction in the resistance while drilling. This is a quite common event as long as the remaining wall thickness of sound wood in this area is enough. The pole inspector therefore notes the hole diameter and the remaining wall thickness and fills the drilling holes with wood preservatives and closes them with a plastic cap. While it is these holes that additionally weaken the pole in this critical area, Ausgrid states that this method has currently proved to deliver the most reliable results to assess the remaining strength of a pole.

#### 2.4.2.2 Time of Flight Method

The TOF is the time it takes for a stress wave to travel a distance through a medium. Measuring the TOF is one of the simplest and most common techniques for detecting interior decay and voids of wood, or determining its material properties. In the TOF method, the measured wave velocities of a wood specimen are compared to average ve-

locity values determined from sound samples of the same wood species. If the measured velocities are slower than the average velocity, this indicates mechanical or physical changes in the timber since the wave doesn't travel as quickly through damaged or decayed wood as is does through dense, solid material. If there are voids and cracks present, the wave might travel a longer distance around the damaged area as shown in Figure 2-14 which again results in a longer travel time and therefore indicates damage in the wood. The measurements can be carried out in longitudinal, radial and tangential directions but vary with grain direction.

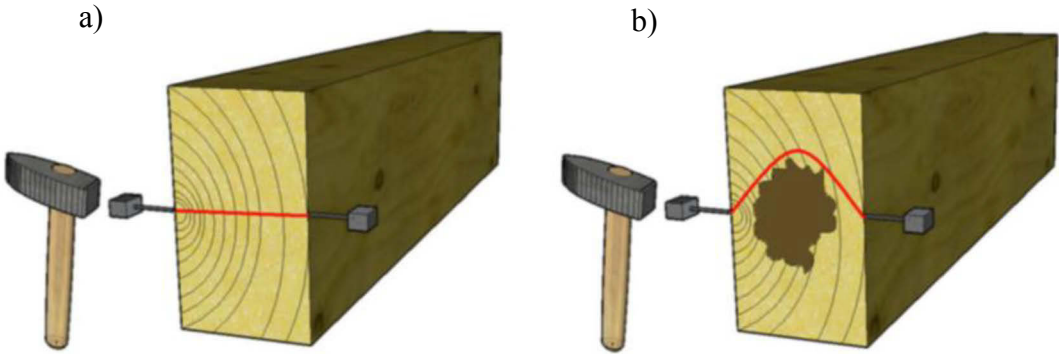


Figure 2-14: Wave path perpendicular to the grain in a) healthy and b) decayed wood member (Dackermann et al. 2013)

Furthermore, since wood is an inhomogeneous, naturally grown material, the propagation of stress waves also depends on factors such as knots, the orientation of growth rings and the moisture content. Sandoz (1989) has shown that TOF measurements of ultrasonic waves can be used for the mechanical characterization of wooded beams and increase the accuracy compared to visual grading.

Stress wave techniques with wood subjected to different levels of biodegradation have been researched by Pellerin et al. (1985) who showed that stress waves could be used to monitor the degradation of small, clear wood specimens exposed to brown-rot fungi. A strong relationship between stress wave speed and the compressive strength of exposed timber was shown. Pellerin & Ross (2002) successfully used a stress wave method for decay detection on a variety of wood structures.

#### 2.4.2.3 Acoustic Tomography

As for X-ray tomography, acoustic tomography refers to cross sectional imaging of an object from data collected by illuminating a wood member. Images can be reconstructed from a variety of characteristic parameters of a sonic or ultrasonic wave such as the

TOF, amplitude, frequency spectra of the waveform or the phase. In the presented work acoustic tomography based on the TOF method or stress wave transmission time is used. Acoustic tomography is capable of creating a two or three dimensional image of the inside of a tree, a timber beam or a wooden pole, to name a few examples. The impact can be introduced manually with a hammer or an ultrasonic impulse. A network of sensors, located around the testing specimen in one layer, captures the arriving waves. Figure 2-15 a shows a six sensor setup which was used to create a two dimensional tomographic image of a tree by Divós & Szalai (2002). In Figure 2-15 b, the picture of a three dimensional tomographic image is displayed as it was generated by Martinis et al. (2004) of the internal structure of a beech tree with a decayed area in the centre.

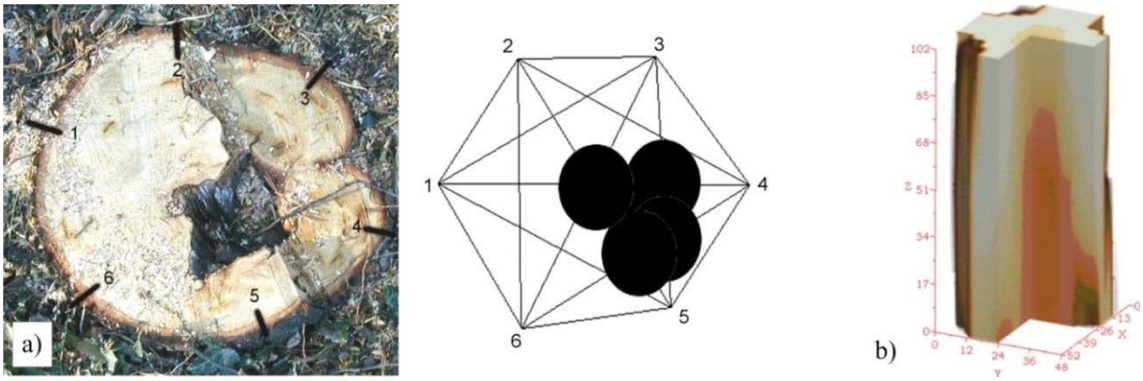


Figure 2-15: (a) Two dimensional image Divós & Szalai (2002) and (b) three dimensional image of the internal structure of a tree (Martinis et al. 2004)

Longitudinal waves are most often used for ultrasonic imaging, however shear waves and surface waves can be used as well. Bucur (2005) has shown that ultrasonic measurements can be used to create accurate three dimensional images of trees, poles or piles.

## 2.5 Conclusions

Wood is a highly complex orthotropic and heterogeneous material, whose properties vary with changing moisture content and temperature. When wood is exposed to the weather it becomes more vulnerable to fungi and insect attack which can cause damage such as rot, decay and voids which add even more variability and uncertainties to the material.

NDT methods based on sonic and ultrasonic waves are widely used in the timber industry to determine wood characteristics and detect internal damage. A lot of research has been done on several NDT techniques that employ stress wave propagation. However, due to the natural variability, the anisotropy and the inhomogeneity of the material, it is difficult to distinguish between the natural structure of wood and its failures.

# 3 RESEARCH METHODOLOGY

## 3.1 Chapter Overview

This chapter gives an overview of the methodology applied to the overall project and the research performed in this thesis. The proposed approach utilises and integrates three experimental methods, namely static material characterization, non-destructive dynamic material characterization using an ultrasonic stress-wave-based approach and damage detection and identification of in-service structures. The detailed methodology on the testing setup and the specimen prepation are given in each individual chapter.

## 3.2 Project Framework

### 3.2.1 Project Organization

The final and overall project goal was to determine the remaining strength of timber utility poles in service with a non-destructive testing method based on stress waves. The research project was conducted in collaboration with Ausgrid, an energy supplier and responsible company for the maintenance of the power grid in large parts of NSW, as industrial partner. In order to achieve the set goal, a group of four research students (three PhD and one Master student), supervised by a postdoctoral research fellow and an Associate Professor, with the assistance of various academic and staff members, was put together. The research focuses of the students were divided into the following four areas of expertise:

- Analytical stress wave propagation analysis and wavelet analysis
- Finite element analysis and model updating
- Sensor network, signal processing and experimental analysis
- Experimental investigations and material characterization

This thesis presents the research performed in the field of experimental investigation and material characterization. Figure 3-1 shows a simplified overview of the whole project and displays how the different fields of research were linked up and how each area contributed to the main goal of developing reliable and accurate non-destructive pole assessment technique.

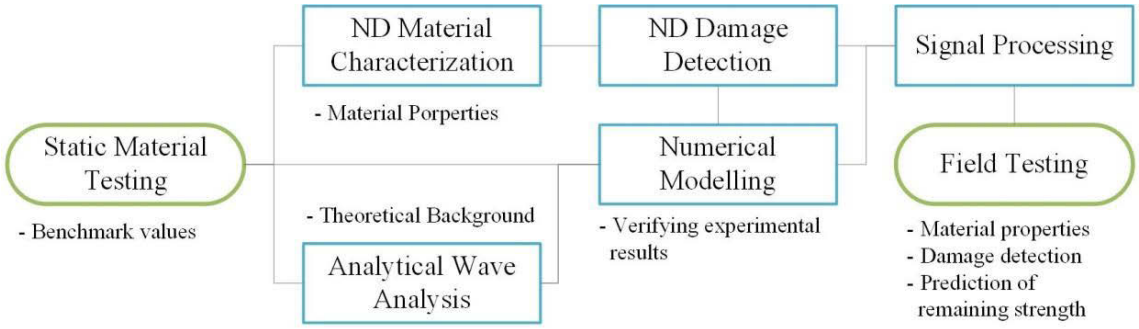


Figure 3-1: Project overview, displaying how the four main research tasks were linked up

It is obvious that the determination of the static material properties was vital in the beginning of the project since all fields of research directly depended on them, except the sensor networking and signal processing. After the determination of the benchmark material properties, the project went along with intensive exchange of information and numerical, analytical and experimental testing data.

### 3.2.2 Research Goals

The following research goals were set in the field of the experimental investigations and material characterization in order to achieve the project's main aim of determining the remaining strength of timber utility poles:

1) Determining benchmark material properties for Spotted Gum and Tallowwood with static material tests
2) Performing non-destructive material tests based on TOF method and calibrating the results with the static results in order to be able to determine the material

properties of timber poles in-situ

3) Performing non-destructive material tests based on the TOF method with the aim to find and locate internal damage in timber poles
4) Using the experimental data to calibrate numerical models to enable the simulation of more damage cases numerically and gathering more data

Following, the four main aims are explained in greater detail and the contexts of the fields of work are defined:

**1) Static Material Tests**

The static material tests presented in this thesis were carried out to supply accurate material values of two eucalyptus species, Spotted Gum *(Eucalyptus maculata)* and Tallowwood *(Eucalyptus microcorys)*, which were investigated in this research and are frequently used for utility poles in New South Wales, Australia.

The tests were necessary since only very limited literature values are available for the two mentioned species and also because of the variations within timber species. Hence, exact material properties of the investigated species in the laboratory were needed. The MOE in all three orthotropic directions and the six Poisson's ratios were statically determined.

The timber properties were needed for the generation of numerical models and for analytical analysis of the wave behaviour and propagation in the timber poles. The statically determined material properties furthermore served as benchmark values for calibrating the non-destructive, ultrasonic testing methods.

In the course of testing, not only the elastic material properties were determined but also the strength properties, namely the MOR in all three orthotropic directions, the tensile strength in longitudinal direction and the compression strength in all three directions.

**2) Ultrasonic Material Tests**

For being able to characterize poles in the field, a test method should be non-destructive and applicable in-situ. The ultrasonic test method based on the TOF fulfils both requirements. However, material properties determined by non-destructive means do not have the same accuracy as statically determined values. For this reason, the gathered values needed to be calibrated using the static material values. Using longitudinal and

shear waves, the MOE's and the shear moduli can be determined.

Environmental factors such as the humidity and the slope of grain play a vital role in the acoustic material characterization and were also investigated within the framework of these tests.

**3) Damage Detection**

Detecting damage in a timber pole from transversal wave measurements by means of acoustic tomography can be a powerful tool technique to detect and locate internal damage that can't be visually be seen.

Research in this field has previously been conducted by various researchers, however most tests have been conducted with very high ultrasonic frequencies which are suitable for laboratory tests on small clear specimens but are unsuitable for field tests due to the high attenuation of wood. For this reason, in this research, all laboratory testing was performed using the same equipment as for in-situ testing with low ultrasonic frequency excitations.

**4) Numerical Modelling**

The numerical modelling was performed on the basis of the experimental results. The models were calibrated to match the experimental behaviour as exactly as possible. Accurate numerical models are capable of simulating experimental cases and of providing additional data on different damage types with less effort and cost compared to experimental testing.

### 3.2.3 Innovations and Merits

The focus of the presented research was to compare the different testing methods. The aim was not to test as many poles as possible, which had been done previously in other projects in order to gather information about the variation of the material properties within a species. The focus was on the method itself which requires material of consistent properties to exclude additional uncertainties as introduced with varying material characteristics. This approach allowed the comparison of the static and ultrasonic method and made it possible to calibrate the ultrasonic method.

For this reason, only one 12 m pole of Spotted Gum and one of Tallowwood was used

for the testing. Each pole was cut into two 5 m segments (to be tested in full scale statically and with ultrasound) and one 2 m segment (used to cut small clear specimens for small scale static and ultrasonic material tests).

Due to the fact that the same material was tested in full scale and on small clear specimens with two different testing methods, conclusions could be drawn about the influence of knots and cracks between full scale and small clear specimen tests as well as the outcomes of the different testing methods.

Another important feature was that the same acoustic testing equipment was used for the laboratory tests as would be used for the field tests. The ultrasonic testing equipment was purchased to meet all needs to allow for the testing of the full scale poles in the field. This required low ultrasonic frequencies due to attenuation and high impulse strength to allow for the wave to travel down an embedded pole, reflect back at the bottom and return with still enough wave energy to be captured by the sensors. The laboratory tests were then designed to work with this equipment. Only by using the same equipment and testing frequencies for laboratory and field tests, the knowledge acquired through the laboratory tests can be directly transferred to the field without uncertainties.

### 3.2.4 Challenges

For several tests performed for this research, no standards are available for wood. In addition, for the material values found in literature, the performed testing methodology is often missing. For the static tests, no standards were available for the 4-point bending tests in radial and tangential direction and the Poisson's ratio tests. For the ultrasonic TOF tests, no standards for wood are available at all. Where possible, similar testing methods, or standards that were available for the testing of other materials were chosen.

The lack of standards or testing guidelines does not only make testing more difficult but also makes the comparison to the results from literature afflicted with uncertainties.

## 3.3 Overview of Tests

The static material tests were carried out according to the standards (where available) to

determine the elastic material properties of the two Eucalyptus species, Spotted Gum and Tallowwood. As mentioned above, one utility pole of each species was available for the tests. These new undamaged poles were used to determine the MOE in longitudinal direction from full scale bending testing as well as to cut small clear specimens and determine the MOE in all three directions (longitudinal, radial and tangential) and all six Poisson's ratios. For the small clear specimens, the MOEs were determined with bending, tensile and compression tests.

Non-destructive material tests based on the ultrasonic TOF method were also carried out on the full scale pole specimens and the small clear specimens. From these tests, the dynamic MOE in longitudinal and transversal direction was determined from the full scale specimen, and from the small clear specimens, the dynamic MOE in longitudinal, radial and tangential direction and the shear modulus G in all three orthotropic planes. Furthermore, the influence of the moisture content and the grain angle was investigated and is presented under the heading *'Environmental Testing Considerations'*. Table 3-1 gives an overview of the tests performed in the presented research. The table lists the purpose of the tests, the testing method, the specimens used, the material values determined and the influencing factors.

Table 3-1: Overview of executed static and ultrasonic tests

| | Static Material Characterization | Ultrasonic Material Characterization | Non-destructive Damage Detection |
|---|---|---|---|
| **Test Details** | • Laboratory<br>• Destructive<br>• Standards available<br>• Reference values | • Laboratory<br>• Non-destructive<br>• No standards | • In-situ<br>• Non-destructive<br>• No standards |
| **Test Method** | • Universal testing machines | • Ultrasonic wave transmission time ('TOF' measurements) | • Ultrasonic wave transmission time ('TOF' measurements) |
| **Specimens** | • Full scale<br>• Small clear | • Full scale<br>• Small clear | • Full scale<br>• Small clear |
| **Outcome** | • Modulus of elasticity (long, rad, tang)<br>• Poisson's ratios | • Moduli of elasticity (long, rad, tang)<br>• Shear modulus (LR, LT, RT)<br>• Poisson's ratios | • Modulus of elasticity (long, trans)<br>• Shear modulus (long, trans)<br>• Damage detection |
| **Research Tasks** | • Environmental influence | • Influence of cross section size<br>• Influence of grain angle<br>• Environmental influence | • Influence of damage (voids, cracks, rot)<br>• Environmental influence |

In a third set of tests, also based on the TOF method, different damage types were tested. Full scale pole specimens which contained cracks and knots were tested in longitudinal direction and transversal direction. For the measurements in transversal direction, artificial damage was introduced which was increased in size. The small clear specimens were tested with different artificial damage sizes in longitudinal and transversal direction as they can occur in the field in in-service timber poles. And rot-type damage was simulated with wet sawdust.

## 3.4 Conclusions

Comprehensive tests were carried out on two eucalyptus species commonly used for utility poles in NSW. Various static and ultrasonic testing methods were used to determine the elastic material properties. The non-destructive material characterization tests depended on benchmark values obtained from the static tests, while the damage detection tests depended on both previous testing results as references. All ultrasonic tests were carried out with the same measurement equipment in order to allow for comparison between the laboratory test results and the results from field testing.

Comprehensive testing data was collected for the two investigated species that were previously unavailable in the literature. The findings contribute to the overall aim of this research project which is the non-destructive determination of the remaining strength of timber utility poles in-service.

# 4 STATIC MATERIAL TESTS

## 4.1 Chapter Overview

This chapter presents the results obtained from the static material tests. These tests were performed to determine the elastic material properties such as the MOEs and the Poisson's ratios of the investigated eucalyptus species Spotted Gum and Tallowwood. The mechanical properties such as the modulus of rupture, the tensile and the compression strength were also measured and are presented and discussed in this chapter. The test setups of each of the performed tests (4-point bending, tensile, compression and Poisson's ratio) are described in detail. The main reason for these tests was to get accurate values for the elastic material properties which could be used for numerical and analytical studies and would serve as benchmark values for the dynamic acoustic material tests later on.

## 4.2 Introduction

In Australia, timber utility poles represent a significant part of the country's infrastructure for power distribution and communication networks. For many of the utilized timber species, however, the less common timber properties such as the $MOE_R$, $MOE_T$ and the Poisson's ratios are very rare in literature or altogether unknown. Since, when timber is used for construction purposes, mainly the MOE in longitudinal direction is of

interest due to the superior characteristics of wood parallel to the grain.

Stress wave methods can offer simple and cost-effective tools for identifying the in-service condition as well as the embedment length of timber poles. In order to investigate and understand the wave propagation in timber poles, numerical modelling is an essential tool. To be able to develop accurate models, correct values on various orthotropic material properties need to be available. Most values in literature commonly describe the MOE derived from bending tests (MOEB), which can deviate from MOE values derived from tension or compression tests. Schneider et al. (1990) investigated the variations between MOE's derived from bending, tension and compression test on sugar maple at 12% moisture content. The researchers found that the determined values ranged from 15.1 GPa for the MOE in compression (MOEC) up to 16.5 GPa for the MOE in tension (MOET). Wangaard (1950) compared the MOE's derived from bending and compression tests of several wood species and found that the values computed from compression tests were slightly higher than the ones derived from bending tests.

Numerical models require the full set of orthotropic material properties of timber in order to accurately simulate the real structure. This research investigates the influence of using different testing methods for the determination of the MOE, the MOR and the CS in longitudinal, radial and tangential direction as well as the tensile strength (TS) in longitudinal direction. The material properties were determined from small clear specimens as well as full scale pole sections by conducting 4-point bending, compression and tension tests. The testing results were compared against each other as well as literature values. The tested full scale pole sections, which were from the same tree trunk as the small clear specimen, were only tested in 4-point bending tests to determine the overall MOE of the whole pole and to obtain comparative values.

## 4.3 Material Testing Methodology

### 4.3.1 Testing Specimens

As mentioned above, two new undamaged utility poles, made from Spotted Gum and Tallowwood, were each cut into two 5 m pieces and one 2 m piece. The four 5 m pieces

were tested in their entirety for *MOE* determination in bending and the two 2 m pieces, which had a diameter of about 30 cm, were used to produce small clear testing samples. All specimens produced were clear, straight grained and did not contain any visible defects such as knots or splits (Figure 4-1). The elastic and mechanical properties of heart and sapwood are similar for most tree species but can show differences as Niklas (1997) demonstrated on a Black Locust tree. Hence, these tests, only the heartwood was used for manufacturing the samples. Because the raw material supply was limited, only seven test specimen and not ten, as recommended in DIN 52180 Deutsche Norm (1977), were manufactured and tested. However, because this research investigates the properties of only one tree trunk, the expected deviations were not as big as they would have been between different trees.

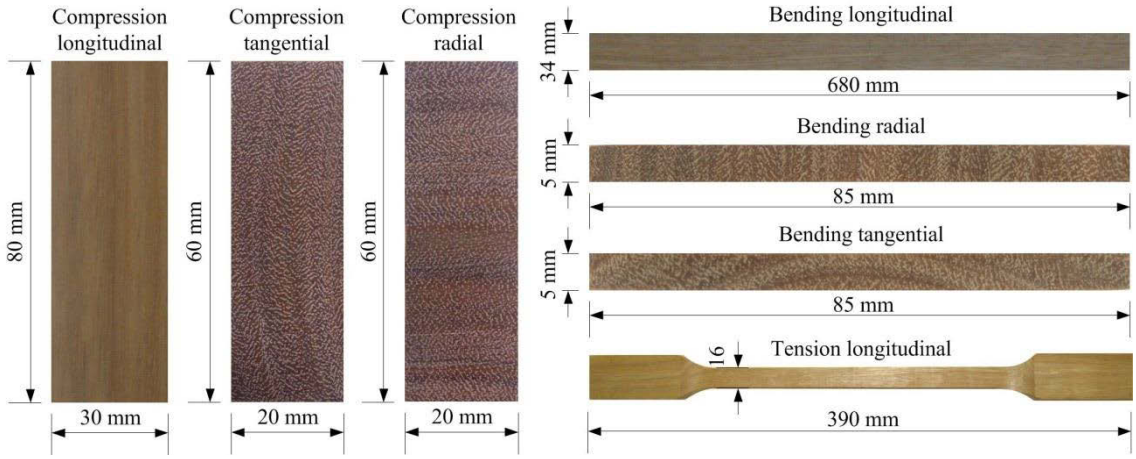


Figure 4-1: Small clear specimens used for material testing

The bending specimens in longitudinal direction were manufactured with a rectangular cross section of 34×34 mm, which allowed for bending tests in both directions and therefore delivering more results to determine the MOE since the raw material supply was limited. Since for the bending specimen in radial and tangential directions no standards are available, the specimens were cut with the same length to thickness ratio as the longitudinal specimen but wider to make them stronger. The maximum length of the specimen that could be cut from the trunk was 85 mm which allowed for a testing span of 75 mm with a resulting thickness of 5 mm according to DIN 52186 (Deutsche Norm 1978).

For the tension test, the specimens had to have a predetermined breaking point, which was achieved with so called ‘dog bone’ shaped specimen. Both, the DIN 52188 and ASTM D143-09 standard require this shape, however with small differences in shape

and dimensions. The manufactured specimens had a cross section of 16×16 mm in the tested area, giving a cross sectional area of 256 $mm^2$ opposed to 120 $mm^2$ (DIN) and 46 $mm^2$ (ASTM). This was done to allow for as many annual growth rings to be tested as possible because plantation eucalyptus is fast growing and has therefore wide annual growth rings. The German standard recommends testing an area of at least five annual growth rings to obtain meaningful results.

The specimens used for the longitudinal compression tests had a cross section of 30×30 mm and a length of 80 mm while the radial and tangential specimens were only 20×20 mm in cross section and 60 mm long. The larger cross section of the longitudinal specimen again allowed for testing of a larger area. These measurements were chosen according to the DIN standards 52185 and 52192 (Deutsche Norm 1976; Deutsche Norm 1979)a since it was the only standard which dealt with both instances.

Prior to testing all specimens were conditioned in a kiln to a wood moisture content of about 12% according to the ASNZ 1080.1 Standard (Australian/New Zealand Standard 1997). The wood density was also determined after testing according to ASNZ 1080.3 Standard (Australian/New Zealand Standard 2000)b.

### 4.3.2 Testing Machines

All tests were carried in the Materials Testing Laboratoryout at the Faculty of Engineering and Information Technology (FEIT) of the University of Technology, Sydney (UTS) in a controlled climate of 20° Celsius and 60% humidity resulting in an equilibrium wood moisture content of approximately 12%. For all tests, a 50 kN Shimadzu AG-X (ISO 7500-1, Class 1 rated machine) and a 500 kN Shimadzu REH-50 machine were used. The bigger machine (Shimadzu REH-50) was only used where the maximum range of the smaller Shimadzu AG-X was exceeded since the smaller machine was programmable and accurate to ±0.5% of the displayed force, while the 500 kN machine was manually controlled and less accurate.

### 4.3.3 4-Point Bending Tests

The 4-point bending tests were carried out to determine the MOE in bending and to obtain the MOR where the tests were destructive. The full 5 m pole sections were tested in order to obtain the MOE of the whole pole as a comparison value to the small clear

specimens. The MOE values of the full poles were expected to be significantly lower than of small clear specimen values due to the cracks, knots and higher moisture content inside the pole.

The four 5 m full scale poles were non-destructively tested in a 4-point bending test to a load of about 20% of their maximum strength (Figure 4-2 a). To stop the round poles from rotating during the tests, custom built supports were used at the loading points and as seats under the pole which were also filled with packers to stabilize the pole (Figure 4-2 b). Each pole section was loaded three times and the mid deflection and the deflection under the loading points were captured by three linear variable differential transformers (LVDT).


Figure 4-2: (a) 4-point bending test setup with (b) custom built pole supports (dimensions in mm)

The small-size longitudinal bending specimens were cut to a square cross section of 34×34 mm to be able to test them in both directions, as mentioned above. The first direction of bending was only loaded to about 20% of the maximum load (within the elastic range) to determine the MOE. Thereafter the specimens were turned by 90° and loaded until failure to also determine the MOR. A picture of the test setup is shown in Figure 4-3 a.

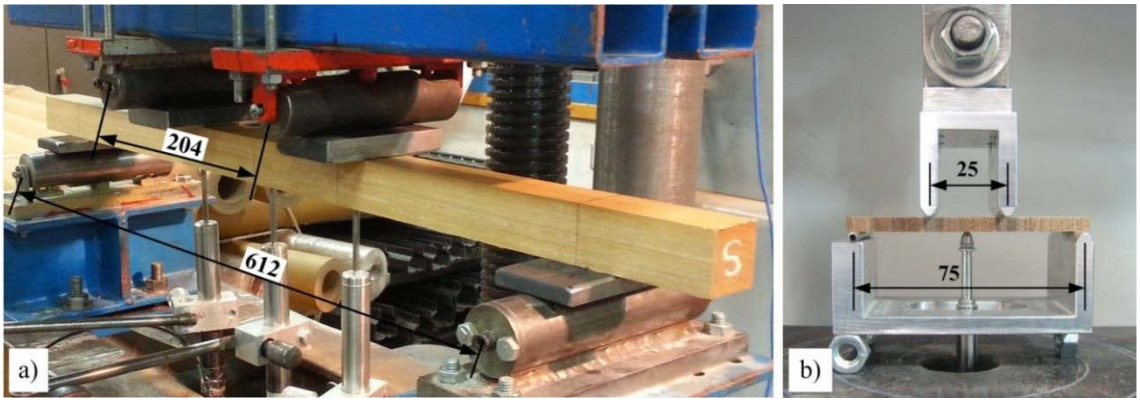


Figure 4-3: (a) 4-point bending test setup in longitudinal direction and (b) 4-point bending test setup in radial and tangential direction with custom built testing jig (dimensions in mm)

The deflection was measured with three LVDT's which were placed below the loading points, as well as in the middle of the specimen. For the calculation of the apparent MOE, however, only the middle LVDT was needed. The crosshead movement was captured by a further LVDT and the applied load by a 500 kN load cell. The testing machine was manually operated and the load was time controlled. The specimens were loaded three times in the first direction to a deflection of 4 mm and then turned by 90° and loaded twice to 4mm deflection before they were finally loaded until failure. The duration until failure was approximately 5 minutes.

The small-size bending specimens for the radial and tangential tests required a specially manufactured testing rig due to their small dimensions (Figure 4-3 b). The test setup however, was exactly the same as for the longitudinal tests with the only difference that due to space limitations only the middle LVDT could be placed to measure the deflection.

### 4.3.4 Tension Tests

From the small-size tension tests, the MOE in longitudinal direction from tension and the maximum tensile strength were determined. The specimens were cut in a 'dog bone shape' to create a predetermined breaking point. The jaws which clamp the specimen during the test exert a considerable force on the specimen and the thicker ends make sure that the specimen does not break due to shear force near the jaws.

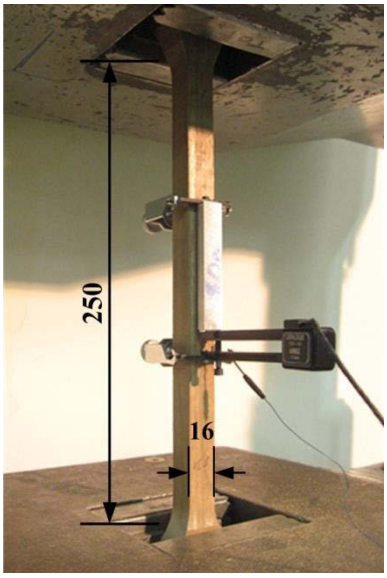


Figure 4-4: Tension test setup with 80 mm extensometer (dimensions in mm)

Figure 4-4 shows the test setup with an extensometer used to measure the elongation of the specimen over a length of 80 mm while the testing machine recorded the crosshead movement and the applied tensile force. Before the specimen failed, the extensometer was removed to prevent damage. The tension specimens were only loaded once to avoid losing the jaws grips of the specimens. The testing time until failure was between three and seven minutes because some specimen showed an extended elongation behaviour before they failed.

### 4.3.5 Compression Tests

The compression tests in longitudinal direction were performed to determine the MOE in longitudinal, radial and tangential direction as well as the crushing strength. It was setup according to the DIN 52185 standard and the alternation of length was measured with an extensometer as shown in Figure 4-5 a. A spherical seat with springs to minimize slack was used for a perfect transmission of the compression force to the specimen.

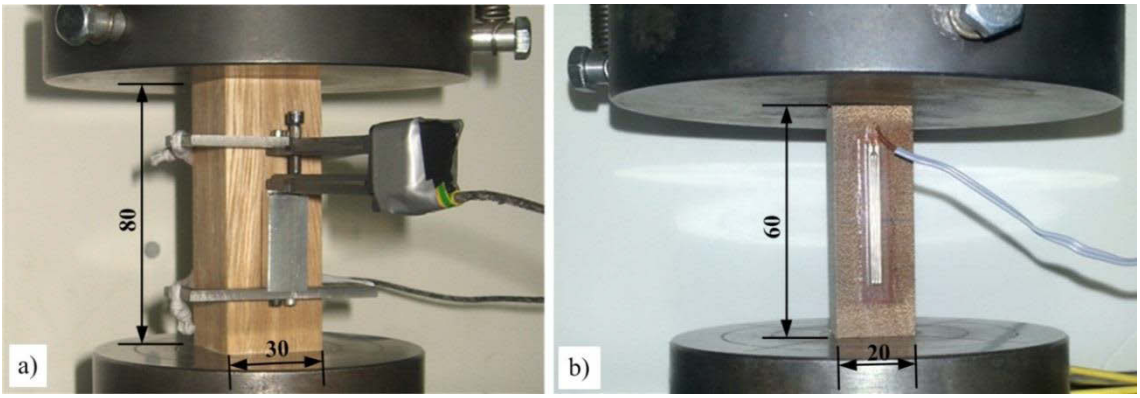


Figure 4-5:(a) Test setup of a compression parallel to grain tests equipped with a 40 mm extensometer and (b) compression perpendicular to grain test setup equipped with a 30 mm strain gauge

For the compression tests in radial and tangential direction only the German standard provided a test setup which was basically the same as for a compression test in longitudinal direction as displayed in Figure 4-5 b. The only difference was the size of the specimens which is limited in radial and tangential direction. In the longitudinal tests, the compression strain was measured with a 40 mm extensometer, while the strain of the radial and tangential specimens was measured with a 30 mm strain gauge. In both tests, the specimens were loaded within the elastic range for three times before they were tested until failure. The last loading cycle until failure took approximately three minutes.

### 4.3.6 Poisson's Ratio Test

When an object is stretched it contracts in the perpendicular direction to the applied load. The Poisson's ratio is the ratio of transverse to axial strain. Literature values for timber are very scarce. However, for numerical modelling, the project depends on accurate values for the corresponding species.

The tests are challenging and extensive because timber as an orthotropic material has six Poisson's ratios and due to a limitation in specimen size in radial and tangential direction the preparation of specimens is a complex task. Only in longitudinal direction the specimen can be cut long enough to allow for grips for the testing machine and the distribution of the strain. In radial and tangential direction, additional grips needed to be glued to the specimen as displayed in Figure 4-6. The strain in horizontal and vertical direction as well as 45 degrees was measured with 30mm strain gauge rosettes which allowed calculation of the Poisson's ratios. An extensometer was used to verify the

strain gauge readings in vertical direction.

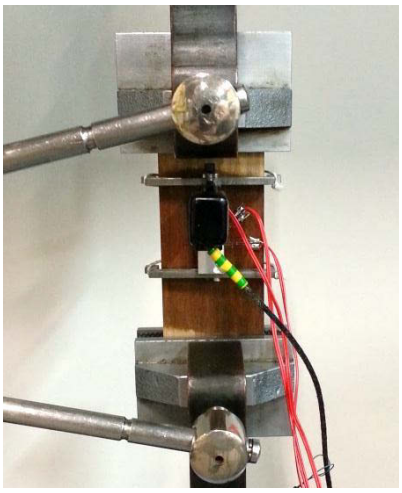

Figure 4-6: Test setup for the Poisson's ratio measurements

Two of the ratios *($\nu_{RL}$, $\nu_{TL}$)* are about an order of magnitude smaller than the others and therefore very hard to measure. This is also due to the fact that timber has a low tensile strength in radial and tangential direction compared to longitudinal. External signal amplifiers had to be used to increase the accuracy of the measured strains.

Note: In the naming of the Poisson's ratios, the first letter stands for the direction where the load is applied and the second letter for the direction of lateral deformation.

## 4.4 Results and Discussion

### 4.4.1 Modulus of Elasticity

The tests on the four 5 m long full scale pole sections produced an $MOE_L$ of 18,322 N/mm$^2$ for Spotted Gum and 14,986 N/mm$^2$ for Tallowwood. These values are approximately 30% lower than the results of the small clear specimen tests. This can be explained with mainly the cracks and knots that exist in the full scale pole sections and the higher moisture content inside of the poles which were stored in an outside location before they were delivered to the laboratory and tested about three months later. The moisture gradient was approximately 40%, ranging from 12% on the outside to about 50% in the centre of the poles.

The MOE in bending for the full scale poles were calculated using Equation (4-1) for round cross sections and the $MOE_{L,R,T}$ in bending were calculated using Equation (4-2) for rectangular cross sections, both provided in DIN 52186

$$E = \frac{2 \cdot l^3 - 3 \cdot l \cdot l'^2 + l'^3}{3 \cdot \pi \cdot d^4} \cdot \frac{\Delta F}{\Delta f} \quad (4\text{-}1) \qquad E = \frac{2(2 \cdot l^3 - 3 \cdot l \cdot l'^2 + l'^3}{8 \cdot b \cdot h} \cdot \frac{\Delta F}{\Delta f} \quad (4\text{-}2)$$

where $l$ is the span between the supports, $l'$ is the distance between the loading points, $d$ the diameter of the pole (only Equation 4-1), $b$ and $h$ the width and the thickness of the specimen (only Equation 4-2) and $\Delta F/\Delta f$ is the linear elastic slope of the load-displacement graph.

The $MOE_{L,(R,T)}$ in compression were calculated with the following equation provided in DIN 52192 which was also be applied to calculate the MOE in tension

$$E = \frac{l_0}{a \cdot b} \cdot \frac{\Delta F}{\Delta f} \quad (4\text{-}3)$$

where $l_0$ is the original length of the measured distance, $a$ and $b$ the cross section and $\Delta F/\Delta f$ is the linear elastic slope of the load-displacement graph.

Table 4-1 and Table 4-2 present a summary of all determined MOE values for both tested wood species. The values derived from the three different test methods correspond quite well to each other with the exception of the $MOE_L$ of Spotted Gum in tension which is about 10% lower than the values determined from the corresponding bending and compression testing methods. For the tension testing of Spotted Gum, all specimens failed at the predetermined breaking point but only one of the seven tested samples reached an $MOE_L$ of 28.128 N/mm$^2$, a similar value as the ones derived from bending and compression testing. The averaged MOE values of both species show the typical ratio $MOE_R/MOE_L$ of roughly 0.1 and $MOE_T/MOE_L$ of 0.05.

Table 4-1: Comparison of Spotted Gum MOE values in longitudinal, radial and tangential direction

| **Spotted Gum** (values in N/mm²) | | | | | |
|---|---|---|---|---|---|
| | ***Bending*** | ***Compression*** | ***Tension*** | ***Average*** | ***Literature Bending*** |
| $MOE_L$ | 26,512 | 27,462 | 24,467 | 26,147 | 23,000 |
| $MOE_R$ | 2,207 | 2,602 | - | 2,405 | - |
| $MOE_T$ | 1,457 | 1,540 | - | 1,499 | - |

Table 4-2: Comparison of Tallowwood MOE values in longitudinal, radial and tangential direction

| **Tallowwood** (values in N/mm²) | | | | | |
|---|---|---|---|---|---|
| | ***Bending*** | ***Compression*** | ***Tension*** | ***Average*** | ***Literature Bending*** |
| $MOE_L$ | 20,720 | 21,548 | 20,983 | 21,078 | 18,000 |
| $MOE_R$ | 2,227 | 2,372 | - | 2,300 | - |
| $MOE_T$ | 1,317 | 1,535 | - | 1,426 | - |

A comparison with literature values is only possible for the MOE in longitudinal direction where average values of 23,000 N/mm² for Spotted Gum and 18,000 N/mm² for Tallowwood in dry conditions (12% MC) are stated in Bootle (2005). However, it is not specified which test methods were applied, but since bending is the most common testing method it must be assumed that it concerns those values. For both tested timbers, the values are roughly 10% higher than the average literature value, which lies well within the variations of wood. In comparison with other species usually used for utility poles in New South Wales, such as Grey Ironbark (24,000 N/mm²), Blackbutt (19,000 N/mm²) or Grey Gum (18,000 N/mm²), the two tested species are representable regarding the MOE.

As stated earlier, the longitudinal 4-point bending specimens had a rectangular cross section and were tested twice, for 0 and 90 degrees. The resulting values showed no significant differences for the MOE which concludes that the angle of the annual growth rings in respect to the applied load does not have an influence on the MOE.

For each test, seven specimens were tested, with the exception of the bending tests in radial and tangential direction where twelve specimens were manufactured and tested. Especially for the tangential bending test as many specimens as possible needed to be tested. This is due to the small dimensions, where only one to two annual growth rings could be tested and the DIN standards recommend testing at least five annual growth rings to obtain reliable results. Since both species, Spotted Gum and Tallowwood, have

very small variations between early and latewood, it was not important which side of the specimen was exposed to tension and which to compression forces. This assumption was verified by testing the same specimen from both sides within the elastic range and comparing the MOE values which did not reveal significant difference. The standard deviation was with 8% about twice as high as the one derived from the same tests with the radial specimens. The standard deviation of all tests was in a range between 3% and 9% with the only exception being the $MOE_C$ in longitudinal direction with a standard deviation of 15%. Some conspicuously high as well as low values were obtained for no obvious reasons and were disregarded in the analysis.

### 4.4.2 Poisson's Ratio

The Poisson's ratios determined from the static tests for Spotted Gum and Tallowwood are presented in Table 4-3. As a basis for comparison, the averaged, minimum and maximum Poisson's ratio values of 11 hardwood species as presented in (U.S.) Forest Products Laboratory (2010) are listed in Table 4-5.

Table 4-3: Summary of the Poisson's ratio values of Spotted Gum and Tallowwood

| **Poisson's Ratios** | | | | | | |
|---|---|---|---|---|---|---|
| | $\nu_{LR}$ | $\nu_{LT}$ | $\nu_{RT}$ | $\nu_{TR}$ | $\nu_{RL}$ | $\nu_{TL}$ |
| **Spotted Gum** $\bar{x}$ | 0.49 | 0.55 | 0.66 | 0.48 | 0.045 | 0.047 |
| (n = 3), COV [%] | 31.5 | 22.4 | 4.2 | 3.6 | 21.6 | 29.1 |
| **Tallowwood** $\bar{x}$ | 0.46 | 0.83 | 0.69 | 0.43 | 0.043 | 0.050 |
| (n = 3), COV [%] | 31.3 | 7.0 | 2.0 | 3.9 | 23.5 | 13.7 |

The Poisson's ratios of both species are very similar with the exception of $\nu_{LT}$ where the value for Tallowwood is 50% higher than the value for Spotted Gum. The coefficients of variation of the test results of both species are rather high with exception of the RT and TR plane of both woods and the LT plane of Tallowwood. The results of the tested samples were repeatable and the high COVs are therefore not a product of random factors. The gluing of the grips also does not seem to be the source of the variation since the specimens that were produced in one piece (LR, LT) also yielded high COV values. For the two smallest Poisson's ratios $\nu_{RL}$ and $\nu_{TL}$, the higher COV may be explained by the significantly smaller ratios (around one order of magnitude smaller). Therefore, they are more difficult to measure which has also been reported in literature. Often these

values are being calculated using the relationship as given in Equation (2-5). This relationship, however, has never been proven to be significant for wood. In literature, COV values for statically determined Poisson's ratios can only scarcely be found. The only reported values found were provided by Niemz & Ozyhar (2011) who tested European beech. The COV values reported by the researchers were in the same range as the ones yielded from the testing of the Spotted Gum and Tallowwood specimens and ranged between 4% and 67%. The COV values were also lower for tests in the RT and TR planes and highest in the LR plane. It is difficult to tell where the high COV values result from and why they show such big differences in the different planes.

Green et al. (2010) states that experimentally determined Poisson's ratio values do not always closely meet the relationship given in Equation (2-5). The MOE/ν as calculated from the experimental testing are given in Table 4-4.

Table 4-4: Relations of the MOE's and Poisson's ratios

| **Relations MOE/ν** | | | |
|---|---|---|---|
| | $\nu_{LR}/E_L = \nu_{RL}/E_R$ | $\nu_{LT}/E_L = \nu_{TL}/E_T$ | $N_{RT}/E_R = \nu_{TR}/E_T$ |
| Spotted Gum | 1.22 | 0.67 | 0.85 |
| Tallowwood | 1.16 | 1.11 | 1.00 |

Overall, the relations were more closely met for Tallowwood than Spotted Gum. The ratios range between 0.67 and 1.22 for the two tested species. The data from Green et al. (2010) was analysed for 10 hardwood species with the calculated ratios ranging from 0.5 and 1.7 as presented in Equation (2-5). Spotted Gum and Tallowwood therefore lie within the range of the compared data.

#### 4.4.2.1 Comparison

In comparison to the Poisson's ratio values of the 11 hardwood species as presented in Table 4-5, the tested values of Spotted Gum and Tallowwood are mostly close to or above the maximum values.

Table 4-5: Average, minimum and maximum Poisson's ratio values of 11 hardwood species from (U.S.) Forest Products Laboratory (2010)

| **Average Poisson's ratio values of 11 hardwoods** | | | | | | |
|---|---|---|---|---|---|---|
| | $\nu_{LR}$ | $\nu_{LT}$ | $\nu_{RT}$ | $\nu_{TR}$ | $\nu_{RL}$ | $\nu_{TL}$ |
| Averages $\bar{x}$ | 0.38 | 0.49 | 0.67 | 0.33 | 0.056 | 0.036 |
| Minimum | 0.30 | 0.40 | 0.56 | 0.26 | 0.033 | 0.023 |
| Maximum | 0.50 | 0.64 | 0.77 | 0.43 | 0.086 | 0.051 |
| Spotted Gum | 0.49 | 0.55 | 0.66 | 0.48 | 0.045 | 0.047 |
| Tallowwood | 0.46 | 0.83 | 0.69 | 0.43 | 0.043 | 0.050 |

The compilation of the 11 hardwoods consists of White Ash, Yellow Birch, Black Cherry, African and Honduras Mahogany, Sugar and Red Maple, Red and White Oak, Sweet Gum and Black Walnut. Of these species, the Poisson's ratio values of Black Walnut match best with the ones of Spotted Gum and Tallowwood - and not the only Eucalyptus species in the list, Sweet Gum whose values are significantly lower. The most obvious trend that can be observed from the average values is that the $\nu_{RT}$ values are the highest, followed by $\nu_{LT}$, $\nu_{LR}$, $\nu_{TR}$, $\nu_{RL}$ and$\nu$ $\nu_{TL}$. The largest differences are between $\nu_{LT}$ and $\nu_{RT}$ with the $\nu_{RT}$ values being 37% higher, while $\nu_{LT}$ is 29% higher than LR and LR 15% higher than $\nu_{TR}$. $\nu_{RL}$ and $\nu_{TL}$ are approximately one order of magnitude smaller with $\nu_{RL}$ being 56% higher than $\nu_{TL}$. 9 of the 11 hardwood species in the compilation follow exactly this order.

The Poisson's ratios of Spotted Gum also follow this trend with only the two smallest ratios $\nu_{RL}$ and $\nu_{TL}$ having almost the same values with 0.045 and 0.047. For Tallowwood, however, it is the $\nu_{LT}$ ratio which is bigger than the $\nu_{RT}$ ratio while the $\nu_{RL}$ and $\nu_{TL}$ ratios are very similar again with values of 0.043 and 0.050 as it is the case for Spotted Gum. Overall, the ratios of the two tested woods are very similar with exception of $\nu_{LT}$ where the value of Tallowwood is 0.83 compared to 0.55 for Spotted Gum which is 51% higher. The $\nu_{LT}$ Poisson's ratio of Tallowwood is also higher than all the $\nu_{LT}$ ratios of the 11 hardwoods, where African mahogany has the highest value with 0.64. Bucur (2006) mentions various researchers who found Poisson's ratios of >1 for composite materials, cellular materials and wood-based composite. The determined value for Tallowwood may therefore be within the realms of possibility.

### 4.4.3 Mechanical Properties

The mechanical properties obtained from the tests comprise the MOR in longitudinal, radial and tangential direction, the Compression Strength (CS) in all three directions and the Tensile Strength (TS) in longitudinal direction for Spotted Gum and Tallowwood as presented in Table 4-6. Literature values for these properties are very scarce and could only be found for the MOR and the compression strength in longitudinal direction from Bolza & Kloot (1963).

Table 4-6: Compilation of the obtained strength properties in comparison to the available literature values from the Commonwealth Scientific Organization, Australia Bolza & Kloot (1963)

| **Test** | **Spotted Gum** (values in N/mm²) | | **Tallowwood** (values in N/mm²) | |
|---|---|---|---|---|
| | ***Tested*** | ***Literature*** | ***Tested*** | ***Literature*** |
| $MOR_L$ | 141.4 | 142.0 | 121.8 | 134.0 |
| $MOR_R$ | 19.5 | | 19.2 | |
| $MOR_T$ | 14.9 | | 13.2 | |
| $MOR_L$ | 78.2 | 75.8 | 68.4 | 76.5 |
| $CS_R$ | 23.5 | | 19.5 | |
| $CS_T$ | 21.0 | | 24.0 | |
| $TS_L$ | 159.0 | | 107.3 | |

As it can be seen from the table, the values determined from the static testing correspond well with the literature values, especially for Spotted Gum. The tested properties of Tallowwood were usually lower than the ones derived from Spotted Gum, whereas in the literature the values of both species are very similar.

Figure 4-7 displays a comparison of two typical loading curves of the 4-point bending tests. Spotted Gum usually started to splitter on the tension side and also showed compression marks on the top side which resulted in a slow failure and a long creeping phase. Tallowwood, on the other hand, failed suddenly due to simple tension failure and showed no signs of compression failure. This can be explained with the TS and CS strength values in Table 4-6 where the ratio of TS/CS of Spotted Gum is 2 compared to a value of 1.57 for Tallowwood. For safety reasons in constructions, the slower failure mode is desirable.

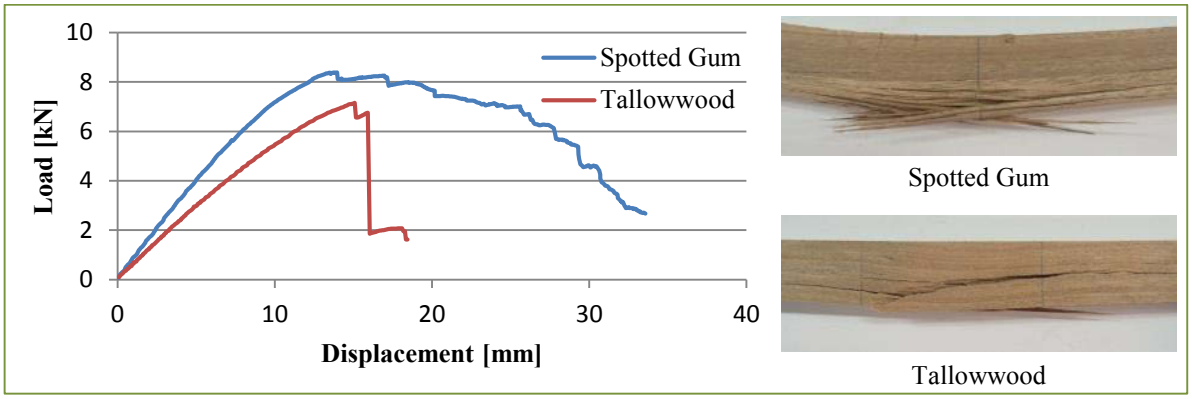


Figure 4-7: Comparison of the typical failure behaviour (curves) and failure mode (pictures) of Spotted Gum and Tallowwood for the 4-point bending tests

The results of the compression tests in radial and tangential direction of Spotted Gum and Tallowwood showed a long period of linear behaviour after the linear-elastic range and before failure as shown in Figure 4-8. This phenomenon has not been documented in literature as yet. A similar phenomenon was observed with tension tests in longitudinal direction.

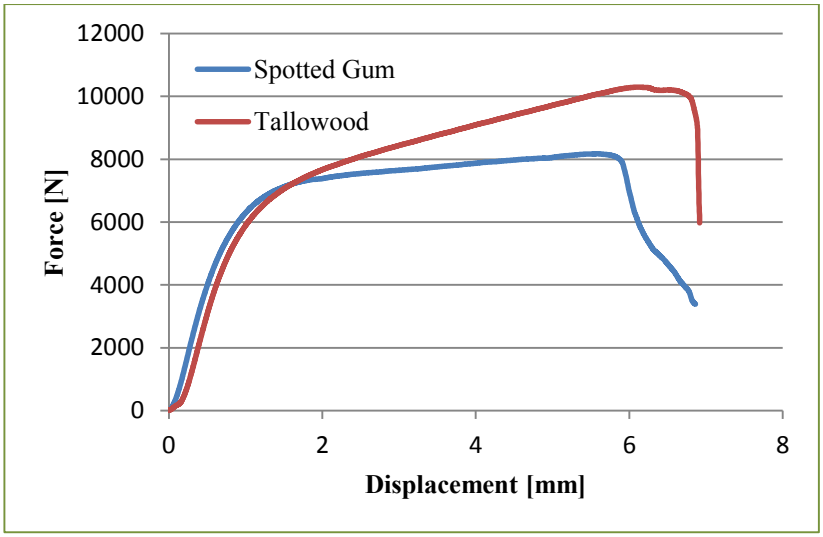


Figure 4-8: Behaviour of Spotted Gum and Tallowwood at compression in radial and tangential direction

The average density of all the tested specimens was 1.06 g/cm$^3$ for Spotted Gum and 1.09 g/cm$^3$ for Tallowwood at 12% moisture content. The density and moisture content were determined according to the ASNZ 1080.3 Standard (Australian/New Zealand Standard 2000)b. The moisture content of all specimens was determined after testing and ranged always around 12% ±1% complying with ASNZ 1080.1 Standard (Australian/New Zealand Standard 1997).

## 4.5 Conclusions

The fact that material tests on timber always include uncertainties due to the inhomogeneous and anisotropic characteristics and the lack of standards for certain tests make it a challenging task compared to steel or concrete testing. Missing data for the radial and tangential direction makes tests indispensable.

The comparison of the different MOE tests showed that all three methods produce similar results. Especially the bending and compression values matched very well for both species. Since the results matched that well and the compression test requires smaller specimens and is easier to carry out, it could be considered as standard test for the determination of MOE values.

The tension tests in radial and tangential direction were not conducted within the framework of these tests but would complete the comparison of all MOE values. To complete the investigation on all elastic properties, the Poisson's ratio and the shear modulus could be investigated.

### 4.5.1 Comparison of Standards

For wood testing, the 4-point bending test in longitudinal direction, the compression test in longitudinal direction and tensile tests in longitudinal direction are standardized in all three considered standards (ASTM International (2009); Australian/New Zealand Standard (2010); Deutsche Norm (1978)). The testing methods and the specimen shapes and proportions do not vary considerably between the standards. When it comes to testing in transversal direction to the grain in either bending tension or compression, less testing recommendations are available. The DIN standard deals with compression tests in radial and tangential direction while the ASTM standard describes the testing setup and specimen preparation for the tensile test across the grain. For bending in the two secondary directions of wood, no standards are available. References to the comparability of the results obtained from the three different testing methods for the MOE were only found in Schneider et al. (1990) and Wangaard (1950) for tests in longitudinal direction. For measuring the Poisson's ratio of wood no standards are available at all and for the values that can be found in literature, information on the testing methodology is largely missing.

### 4.5.2 Testing Recommendations

Testing recommendations are given for the two tests where no standards were available, the bending tests in radial and tangential direction and the Poisson's ratio tests. The testing rig that was built for the 4-point bending tests in radial and tangential direction allowed for convenient and reproducible testing and yielded good testing results. Special attention had to be paid to the preparation of the specimens which is more challenging due to the fact that they are quite small and fragile because they have to be cut in the wood's secondary direction.

The Poisson's ratio test was designed according to the ASTM E132-4 Standard (ASTM International 2004) standard. Due to the size limitations of the wooden specimens, the testing method had to be adapted to be applicable to the wood samples. Again, special attention had to be paid to the accurate preparation of the specimens. Testing was only possible with the testing machine that allowed controlling loads with an accuracy of 0.1 N since very small loads were needed especially in the RT, TR, RL and TL directions.

# 5 ULTRASONIC MATERIAL TESTS

## 5.1 Chapter Overview

In this chapter, the results obtained from the ultrasonic material tests are presented. These tests are non-destructive which means that this testing methodology does not cause damage to the tested specimen nor does it permanently alter the specimen that is tested. The results obtained from the ultrasonic material tests are compared against the benchmark values determined from the static material tests as presented in chapter 4.

## 5.2 Introduction

Stress wave methods are simple and cost-effective tools for identifying the in-service condition of timber poles. Such acoustic methods are capable of characterizing a wood member non-destructively as well as detecting internal damage such as voids caused by termites or rot. With stress-wave-based testing, the material properties of timber poles such as the MOE can be determined from the direct relationship between the longitudinal wave velocity and the MOE according to the following equation

$$E = {V_P}^2 \cdot \rho \qquad (5\text{-}1)$$

$$G = {V_S}^2 \cdot \rho \qquad (5\text{-}2)$$

where $V_P$ is the longitudinal wave velocity, $V_S$ is the shear wave velocity and $\rho$ is the density of the tested material. The information about wood characteristics is essential in order to be able to predict the remaining strength of a pole. Since wood is neither homogeneous nor isotropic, the usefulness of one dimensional wave theory may be put into question. However, several researchers have shown that one-dimensional wave theory is adequate for describing the wave behaviour in wood. As such, Bertholf (1965), Kollmann & Krech (1960) showed in their research the dependency of the wave propagation velocity and the MOE of clear wood specimen.

The 'time of flight' (TOF) method is based on the wave transmission time (WTT) and describes the time an acoustic wave takes to travel a distance through a medium. Sonic and ultrasonic waves in the lower frequency range of up to 50 kHz are usually used for field testing because of the high attenuation of acoustic waves in wood. In the laboratory, frequencies of up to 10 MHz are applied on small clear specimens in experimental studies. The wave velocities in longitudinal direction are the highest and range from 3050 – 6100 m/s as reported by Gerhards (1982), who determined the values on small clear timber specimens with a moisture content of 9 to 15%. The velocities in radial and tangential direction are usually around a third of the longitudinal wave velocity, with the radial direction featuring slightly higher velocities than the tangential direction. This is due to the fact that the anatomical elements, such as fibres and tracheid, are aligned in longitudinal direction and the wood rays in radial direction, while in tangential direction, along the annual growth rings, no structural elements exist.

Different wave velocities have been determined for a large variety of wood species, predominantly in longitudinal direction, but only a few studies have performed static and dynamic testing to characterize the material properties of the same tree. Further, no research has been undertaken that compares different static testing methods with dynamic results of the same tree. Smulski (1991) reported on dynamically determined MOE values for four hardwood species (maple, birch, ash and oak), which were between 22 and 32% higher than statically obtained MOE values from bending tests. Similar values were also presented by Burmester (1965), with dynamic MOE values being 19 to 34% higher than the static MOE values derived from bending tests on beech and two tropical hardwood species.

Several factors influence the wave velocity in wood. The most important may be the microscopic and macroscopic structure of wood where the microfibril angle and the length of the anatomical elements (fibres and tracheids) play a vital role. Bergander & Salmen Bergander & Salmen (2000) showed that a small cell wall layer results in a high longitudinal MOE and therefore higher acoustic wave velocities. The influence of the density on the TOF was subject to several studies, with different researchers deriving at different conclusions. Bucur & Chivers (1991) found that an increasing density leads to slower wave propagation velocities, while de Oliveira & Sales (2006) observed the opposite behaviour. Other researchers stated that the density doesn't have any influence on the wave velocity Ilic (2003); Mishiro (1996)a or that it has a positive effect but is suppressed by other factors such as the micro and macro structure of the material Baar et al. (2011).

As with all wood properties, also the wave velocity is influenced by the wood moisture content. A linear behaviour of the wave velocity as a function of the moisture content below the fibre saturation point (FSP) was correspondingly reported by Bucur (2006), Keunecke et al. (2006), Sakai et al. (1990). When measuring the TOF in longitudinal direction, the grain angle is further an important influencing factor, since wave velocities decrease with increasing grain angle. Niemz et al. (1999) reported that a displacement of only 10 degrees results in a reduction of the wave velocity of 20%. Similar findings were also presented by Armstrong (1991). Furthermore, temperature has an influence on the TOF, which is of special importance when measurements are carried out in the field Sandoz (1993).

## 5.3 Ultrasonic Testing Methodology

For TOF measurements of wood there are no standards defined. However, the ASTM standard provides a 'Standard Test Method for the Laboratory Determination of Pulse Velocities and Ultrasonic Elastic Constants of Rock' in ASTM International (2008). Where applicable this standard was applied.

### 5.3.1 Testing Specimens

As for the static material tests, the specimens used for the ultrasonic material tests were also cut from the same two Spotted Gum and Tallowwood poles. A number of small clear specimens were cut from the heartwood and were free of any visible wood defects such as knots or cracks, i.e. assembled block specimens for L, R and T wave measurements, disc specimens for grain angle investigations and solid block specimens for moisture studies. To measure the TOF in transversal direction, cross-sectional specimen still containing the natural wood defects were also cut from the poles. Furthermore, the four full scale 5 m pole sections, which were non-destructively tested in bending, were also used for the ultrasonic material characterization. Figure 5-1 shows a compilation of the small clear, the cross-sectional and the full pole specimens that were used for the ultrasonic material characterization.

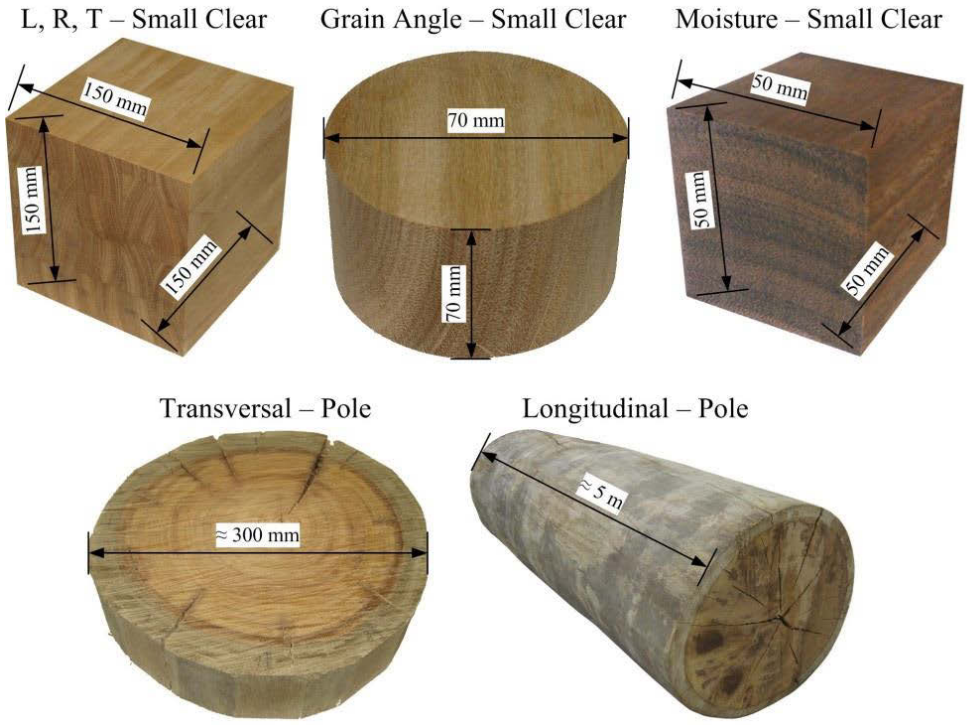


Figure 5-1:Small clear and full-scale pole specimens used for the ultrasonic material characterization tests

All tested small size specimens had dimensions that could be cut from the stem in one piece except for the cubic small clear specimen that was used to measure the TOF in longitudinal, radial and tangential direction. This specimen had a size of 150/150/150 mm and therefore had to be glued together from several small pieces to create a specimen with the annual growth rings aligned strictly radial and tangential.

This size was chosen for two reasons; firstly the TOF measurements are more accurate the longer the wave transmission time is and secondly, the ratio of the frequency, and therefore the wavelength, to the specimen size does have an influence on the wave propagation. Bucur (2006) mentions a minimum diameter of the specimen of two times the wave length in order to reduce the influence of the boundaries and to allow for the wave to propagate as free waves.

### 5.3.2 Testing Instrumentation

For the ultrasonic material testing, ultrasonic stress waves were generated, recorded and analysed using the testing system illustrated in Figure 5-2. In the testing, an ultrasonic impulse was created using a commercial flaw detector. The generated wave was captured with a piezoelectric transducer of the same device (receiving transducer) and the wave form was recorded with an acquisition system from National Instruments with a sampling rate of 1 million samples per second. The TOF was calculated using the software Matlab. Since no standard exists for the ultrasonic testing of wood, the tests were carried out according to common practices mentioned in the literature and used in the industry.

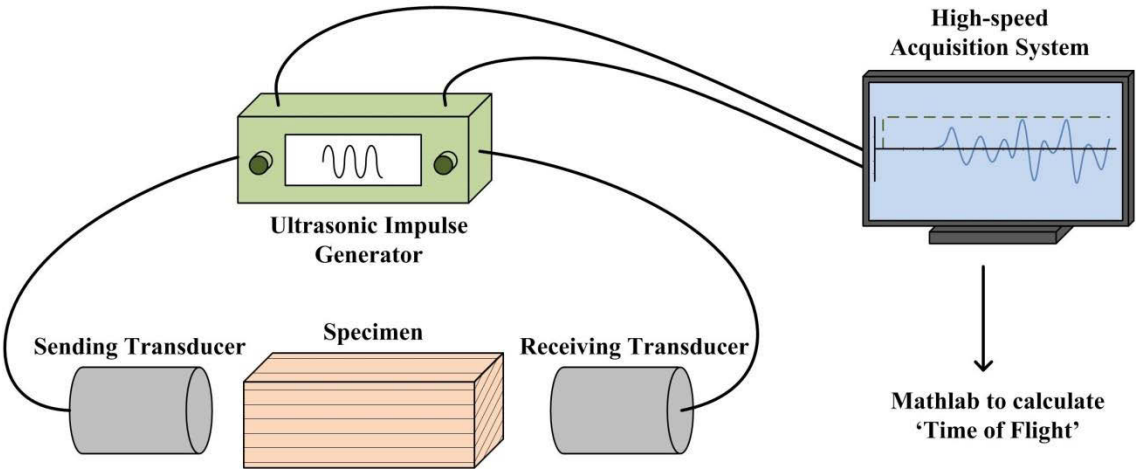


Figure 5-2: Diagram of the non-destructive testing setup.

The commercially available testing unit from Proceq Switzerland named Pundit Lab was used for the wave generation and capturing as displayed in Figure 5-3. The entire unit consisted of a display unit which was connected to a sending and receiving transducer via two BNC cables. For the testing, two types of transducers were used, i.e. one pair to excite longitudinal waves with a frequency of 24 kHz and one pair of shear wave transducers with a frequency of 250 kHz. The frequency of 24 kHz of the P-wave trans-

ducers was chosen due to the high attenuation of wood - the unit had to be capable of sending wave pulses through timber poles with travel distances of up to 6 m. For the shear wave transducers, only the 250 kHz model was available that was perfectly capable of sending shear waves through the small clear specimens.

Figure 5-3: Ultrasound testing unit 'Pundit Lab' (Proceq 2011)

The Pundit lab testing device has a measurement resolution of 0.1 µs and different gain settings of 1x, 10x and 100x. The energizing pulse voltage can be adjusted in steps of 125 V, 250 V, 350 V and 500 V as well as the ultrasonic pulse length from 1 µs to 100 µs.

#### 5.3.2.1 Transducers

Both pairs of transducers used, the P-wave as well as the S-wave transducers, were based on the piezoelectric effect, which is the linear electromagnetic interaction between the mechanical and the electrical state in crystalline material with no inversion symmetry Gautschi (2002). The inverse piezoelectric effect is used to produce ultrasonic waves as describe by Krautkrämer & Krautkrämer (1983).

Piezoelectric transducers are rugged, hermetically sealed units that use this effect and can measure the short duration when dynamic tensile and compression stresses occur. In order to transfer the ultrasonic signal from the sending transducer to the specimen and again from the specimen to the receiving transducer without losing much energy, a coupling medium is necessary which doesn't allow for air to be trapped between the transducers and the specimen. In this research, the couplant used for the P-wave transducers was a water based gel that was easy to wash off from the specimen. For the S-wave transducers, a specially designed high-viscosity couplant, similar to honey, was used

since low viscosity gels are not suitable for transferring the shear wave to the specimen.

### 5.3.3 Time of Flight Measurements

A series of pre-testing was run to find appropriate settings for the different testing applications. It was concluded that for the small clear specimens the lowest gain setting of 1x was sufficient due to the short measurement distance and the lower attenuation since the samples were damage free. The changing voltage settings seemed to have only a minor influence on the transmitted wave energy while a longer transmitting pulse duration clearly increased the strength of the signal.

Accurate TOF measurements depend on a clear wave signal of the first arriving wave. To automatically measure the TOF, a triggering level of the arriving wave energy needed to be set up. A high level of noise or very low arriving wave energy may trigger the measurement too early or miss an arriving wave at all. In Figure 5-4, the arriving wave signal of a small clear and a damaged specimen (as used in the tests in Chapter *6 Damage Detection*) using different levels of gain are displayed. The variable factor in these tests was only the gain level, since it was previously observed that the gain has the largest influence on the wave energy. The voltage was set to the highest setting of 500 V and the impulse length was chosen to be 20 µs, so the impulse length would be shorter than the TOF.

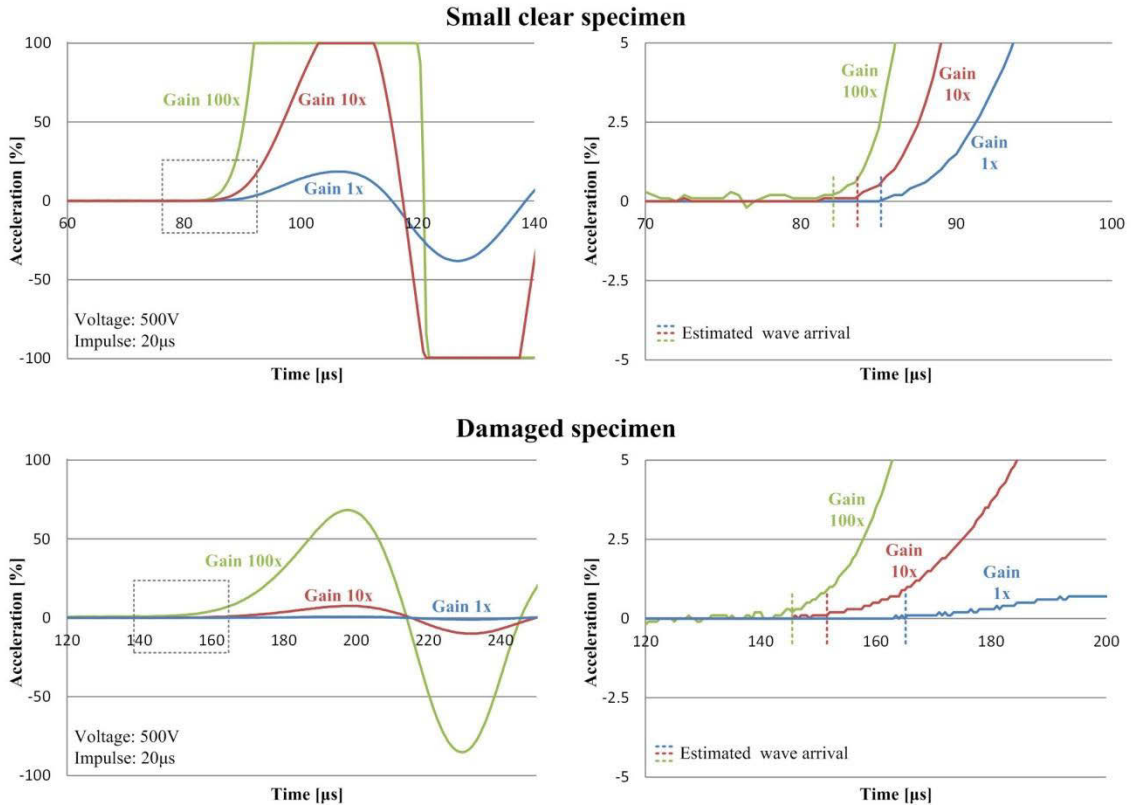


Figure 5-4: Arriving wave signals from various gain levels, tested on a small clear and damaged specimen

From these tests, it can be seen that the gain level significantly influences the TOF measurements. Higher wave energy reaches the trigger level of the device earlier than a wave with lower energy. Also manually estimated wave arrivals clearly show different arrival times. For the case of the small clear specimen, the TOF decreased by about 1.5 µs when the gain setting was increased by one order of magnitude. The lower the gain setting the lower is the noise which is very desirable in order to accurately read the wave arrival. With a larger distance between sender and receiver or with increasing damage, the attenuation increases and results in less wave energy arriving at the receiving transducers. This phenomenon occurs to the point where the readings become very inaccurate and difficult to interpret or the wave energy becomes too small for a reading due to a too small signal to noise ratio.

For the damaged case, the arriving wave with a gain setting of 1x has a very small slope which makes it impossible to determine when the wave arrived. Noise, however, also leaves some uncertainty about the exact wave arrival time with higher gain settings but the uncertainty is of a smaller range. The readings of the damaged case show results which vary from around 146 µs for the highest gain setting to 151 µs for the medium

setting and approximately 166 µs for the lowest gain setting.

The trigger level of the wave arrival time was adjusted manually for all experiments and the point of the wave arrival time was determined from the point where the wave energy only kept increasing on a level higher than the average noise. For heavily damaged specimens, however, the wave arrival point was very difficult to identify as shown in the 'Damaged specimen' plots of Figure 5-4 with the 1x gain setting. A small amount of wave energy is clearly arriving but the curve shows decreases in wave energy. In such cases, the beginning of the arriving wave had to be estimated.

Based on these observations, the testing settings for this research were chosen to be the maximum voltage of 500 V, the maximum gain level of 100x and a pulse length of 20 µs for all tests. The higher wave energy and therefore more accurate readings on damaged specimens and the ability of the wave to travel further had to be traded off against a higher noise level and the cut off wave peaks which made it impossible to determine the wave attenuation.

### 5.3.4 Time of Flight Calculations

For the Pundit Lab testing device, a product specific software named Pundit Link was available that allowed to control the device from a computer and was capable of displaying and analysing the captured data as shown in Figure 5-5.

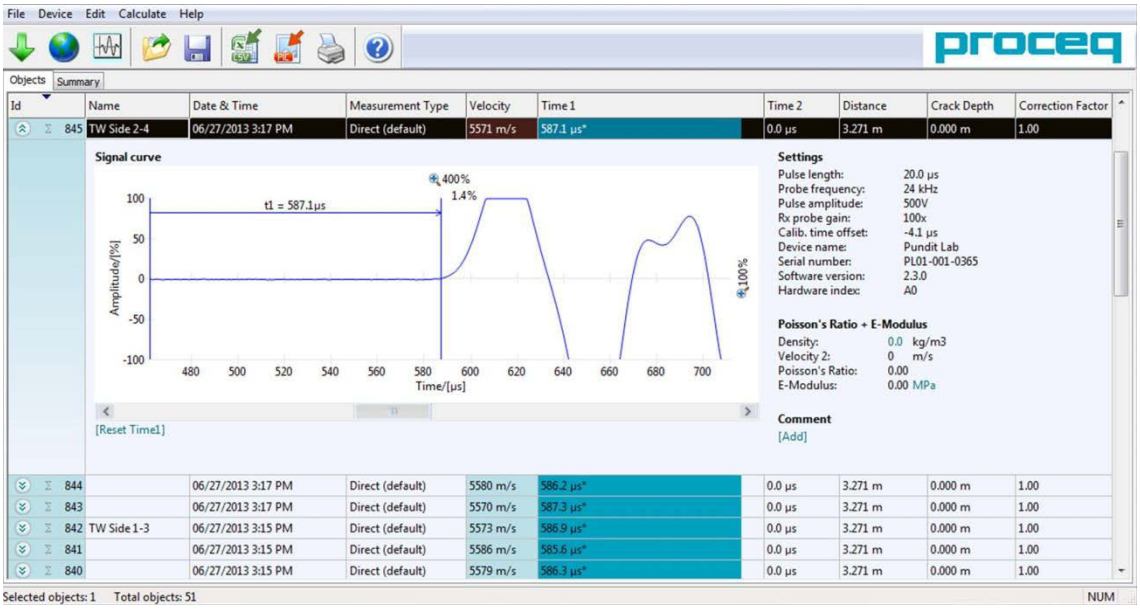


Figure 5-5: Pundit Link software used for the TOF measurements (Proceq 2011)

Using this software was the most efficient way of analysing the large amount of date which was collected during the tests. However, first, a pre-testing series was executed where the wave signals were also captured using a National Instruments high-speed acquisition system and the TOF measurements were calculated using Matlab. Since both TOF calculations yielded exactly the same results, the testing data was thereafter only analysed using the Pundit Link software.

### 5.3.5 Ultrasonic Material Characterization

#### 5.3.5.1 Small Clear Specimens

For the ultrasonic material testing based on TOF measurements, for each wood species, a timber block of 150×150×150 mm was glued together from smaller pieces as shown in Figure 5-6 a. The larger size of the specimen (compared to the small clear specimen of the static testing) was chosen because the length of the small clear specimen would have been smaller than the wave length. This criteria is necessary for waves with plane wave characteristics in an infinite medium, was stated in Bucur (2006). Furthermore, a longer propagation time of the ultrasound signal allows for more accurate TOF measurements. Due to the larger size of the specimens, they had to be glued together from smaller pieces to minimize the influence of the curvature in tangential direction and to have the annual growth rings as perfectly aligned in the orthotropic directions as possible.

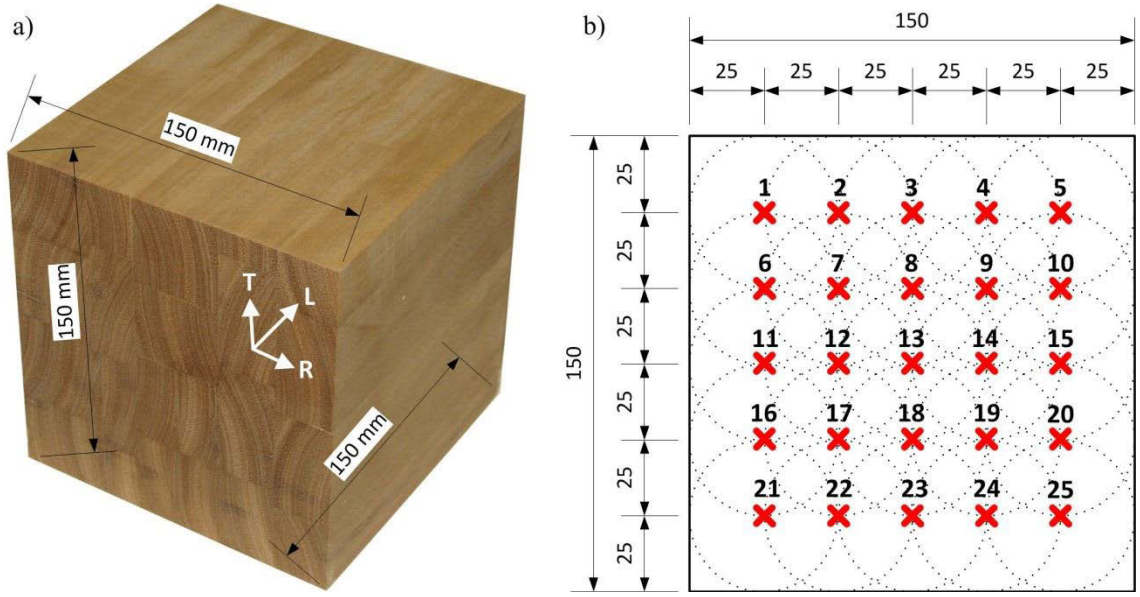


Figure 5-6:a) Timber block used for ultrasonic material characterization, and b) indication of the 25 measurement locations used in each plane.

The ultrasonic material properties of wood and adhesive are similar according to Sanabria et al. (2010) who performed ultrasonic tests on glued laminated timber. Hence, it is assumed that the glue line causes a reflection of the wave but does not affect the TOF. For the manufactured test specimen PVA glue that produces very thin glue lines was used. Dill-Langer et al. (2006) showed that only an open glue line affects the TOF due to a change of impedance. To verify this behaviour, tests on an intact specimen in tangential direction were carried out, which was, after measuring the TOF, cut in into 4 pieces and glued back together. It was found that the standard deviation of the measured TOF was in the same range for the measurements on the intact specimen as well as on the one with three glue lines.

For the TOF measurements of the timber block, recordings were not only taken in the middle but also in a 25 mm raster over the entire surface, which resulted in 25 measurement points for the longitudinal, radial and tangential directions (see Figure 5-6 (b)). For the measurements of the longitudinal wave, flat transducers with a diameter of 50 mm were used.

On the same specimens with the same raster, shear wave measurements were also taken in all three orthotropic directions. The shear wave transducers which excited ultrasound pulses with a frequency of 250 kHz also excited a longitudinal wave and not only a shear wave. When analysing the results this has to be taken into account in order to cor-

rectly interpret the curves. Figure 5-7 shows the measurement curves in the LT and TL directions.

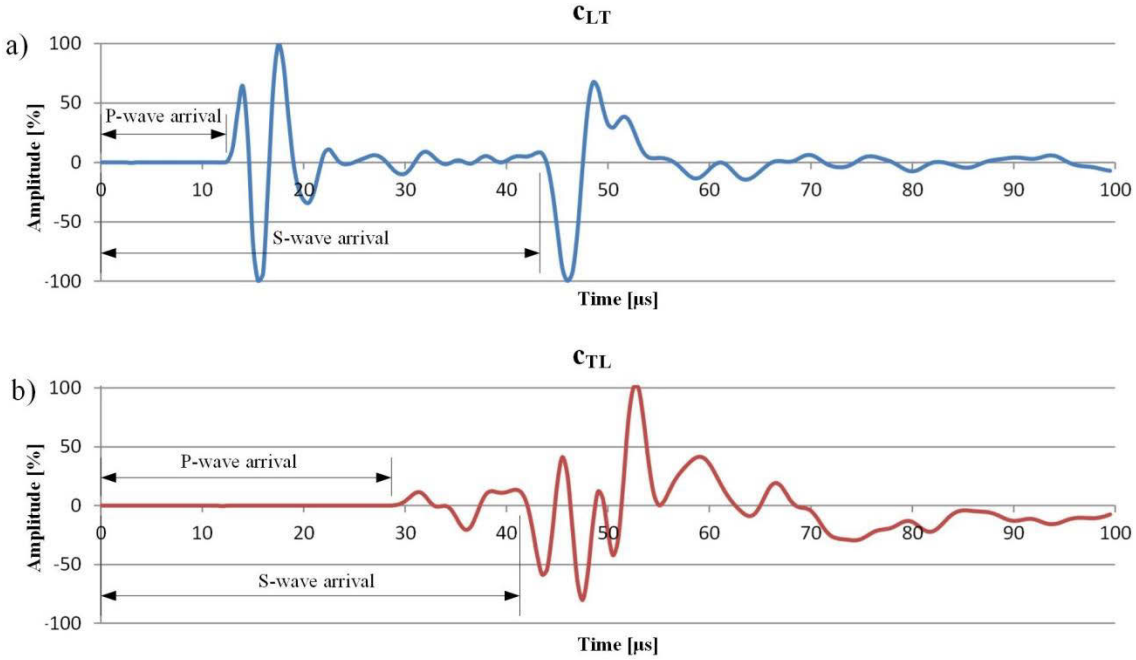


Figure 5-7: a) Arrivals of P-wave and S-wave with a large timely distance resulting in clear peaks and b) arrivals of P-wave and S-wave with a small time distanc,e resulting in interference of the two waves

The measurement in the LT direction (a) shows two clear peaks. The first peak indicates the arriving P-wave and the second peak the arrival of the S-wave. Due to the fact that the longitudinal wave travels much faster along the grain than the shear wave in LT direction, it arrives much earlier and the two peaks can be clearly distinguished. In the second case (b), the longitudinal wave travels slower and the arrivals of P-wave and S-wave lie much closer together. This makes distinguishing between the two waves and determining the exact moment of arrival more challenging.

#### 5.3.5.2 Pole Specimens

The ultrasonic measurements on the entire poles in longitudinal direction were carried out on the same four 5 m pole sections that had been tested statically. For the measurements in transversal direction, 150 mm thick cross-sectional specimens were cut from the poles (see Figure 5-8) and transversal measurements were performed in four directions, every 45°, to measure the TOF across the grain. It is obvious that on a round pole section, only radial measurements can be taken when measuring from one side of the pole to the other.

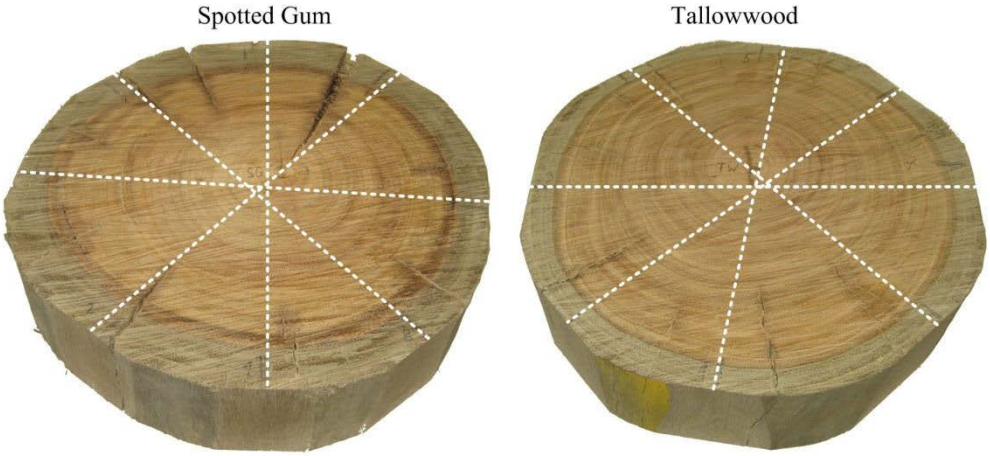


Figure 5-8: Cross-sectional pole sections transversal TOF measurements

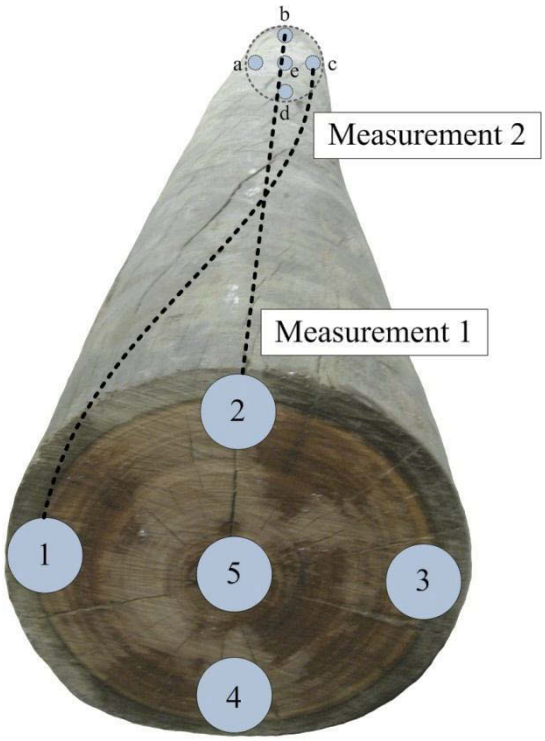


Figure 5-9: TOF measurement setup in longitudinal direction of the full poles

The TOF of the full scale 5 m poles in longitudinal direction was measured at four locations on both ends on the outside of the pole as well as in the centre according to Figure 5-9 (locations 1-5 and a-e). Since the Tallowwood poles showed spiral growth of almost exactly 180° over the 5m length of the pole, the measurements were also taken with a 180° rotation to measure along the grain (i.e. 1-c, 2-d, 3-a, 4-b) instead of measuring along the axis. The results of the different measurement locations are presented in chapter 5.4.1.2.

The 24 kHz transducers were used for measuring the TOF and the cross-sectional pole specimens had to be levelled at the points of measurement, as displayed in Figure 5-8, to allow for perfect coupling. The cross-sectional pole specimens had a diameter of roughly 300 mm. Since a naturally grown tree stem is not perfectly round and the pith is not located perfectly in the centre, the measurement axis did not run exactly through the pith in all measured directions. However, when working on full poles, this cannot be avoided either. Nonetheless, the measurements were predominantly in radial direction. Both pole sections also showed cracks which resulted from the dry laboratory climate. The moisture content on the outside of the poles to a depth of approximately 20 mm was about 12%, while in the centre of the pole, the moisture content was around 22% for both species. The cross-sectional pole specimens were cut from the centre of the pole and tested immediately after they had been cut and therefore represented the same moisture conditions as the whole poles.

The measurements along as well as across the grain of the full poles were only possible with the P-wave transducers of 24 kHz. The attenuation and scattering of the 250 kHz shear wave transducers were too big to capture reliable results.

### 5.3.6 Moisture Content Tests

The moisture content of wood has an influence on the stress wave velocity as it has been shown by various researchers for a wide variety of wood species. For the two used eucalyptus species, however, no data could be found in literature. Since utility poles are exposed to weathering, they undergo a constant change of the wood moisture content. This change mostly occurs within the outermost layer of the pole, depending on the duration of a continuing similar ambient humidity.

According to Gerhards (1982), the wave velocity decreases by 1% with every 1% increase in moisture content. This is valid for cases below the fibre saturation point (FSP), whereas for cases above the FSP, the same effect can be monitored, however, less distinctive.

The transportation of moisture in wood is different in all three orthotropic directions. It is fastest in the longitudinal direction, which is the main direction of moisture transport in wood, followed by the radial and tangential directions. Franke et al. (2012) conducted

long-term measurements of approximately 2 years on a glue laminated timber block which was first exposed to a laboratory environment of 90% humidity and temperatures of 15-30°C for 250 days before it was moved outside where, for the remaining time, it was exposed to changing temperatures and moisture contents in a covered location. The results confirmed the assumption that the moisture content change on the inside of a timber beam is slower compared to the outside. Similar research was conducted by Gamper et al. (2012) who monitored timber beams of structures exposed to extreme climate changes such as indoor swimming pools and ice arenas and who concluded the same findings.

Since in-situ timber utility poles are also exposed to a changing ambient climate, the situation is similar, with the difference that the poles are not covered but exposed to outdoor weathering. Furthermore, they are embedded in soil which also heavily influences the moisture content of the embedded part. These circumstances together with the effect of the different speeds of acclimatization on the outside and inside of a timber member are responsible for a changing moisture gradient in the pole.

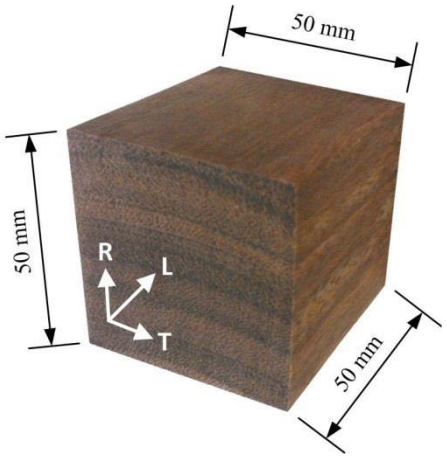


Figure 5-10: Specimens used for TOF measurements at different wood moisture contents

20 specimens (10 Spotted Gum, 10 Tallowwood) were conditioned in 5 different climates, which were 90%/30°C, 60%/20°C, 50%/10°C, 60%/105°C and fully water soaked. The resulting wood moisture contents are presented in chapter 5.4.4. The test specimens as shown in Figure 5-10 had a size of 50/50/50 mm and were cut along the orthotropic planes so that the TOF could be measured in pure longitudinal, radial and tangential direction. The size was chosen according to the size of the P-wave transducer's diameter. While a larger size would have increased the measurement accuracy, the

curvature in tangential direction as well as the longer condition time made the cutting of larger specimens unsuitable. The fastest wave transmission times in longitudinal direction were around 9 µs which, with a measurement accuracy of 0.1 µs, resulted in a measurement accuracy of 1.1%. The P-wave velocities as well as the S-wave velocities were measured resulting in 9 TOF measurements per specimen. In total, including both wave TOF measurements on both tested species with 5 different moisture contents, 90 TOF measurements were taken.

### 5.3.7 Grain Angle Tests

To determine the influence of the slope of grain on the wave propagation velocity, three disk specimens, one for each orthotropic plane, were cut as displayed in Figure 5-11. The disks had a diameter of 70 mm and were 40 mm thick.

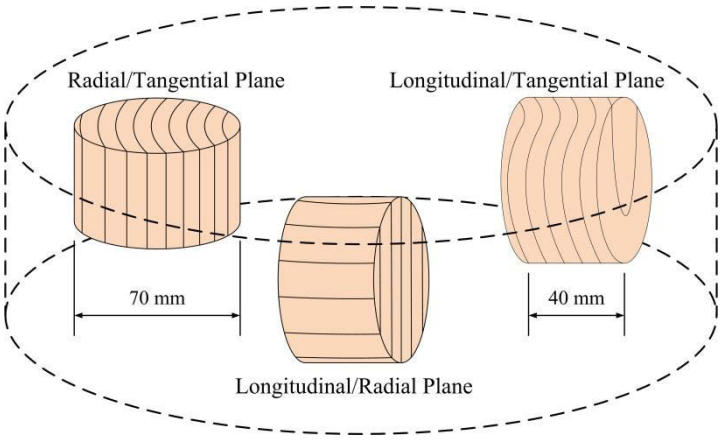


Figure 5-11: LR, LT and RT disc specimens, as cut for grain angle tests

The TOF was measured in 11.25 degree increments, which equalled to 16 measurements around the disk (see Figure 5-12). Since the transmission time was measured in both directions of the disk, wave velocity measurements in 32 directions were taken (Figure 5-12 (b)). To determine averaged time recordings, three measurements in each direction were taken. Since proper coupling of the flat transducers with the round specimen surface was not possible, tapered transducer caps with a tip diameter of only 5 mm were manufactured. Before using the transducers with the caps for TOF measurements, they were calibrated according to the TOF measurements captured without the additional caps. For both tests, a water based gel was used as coupling media between the transducers and the specimens.

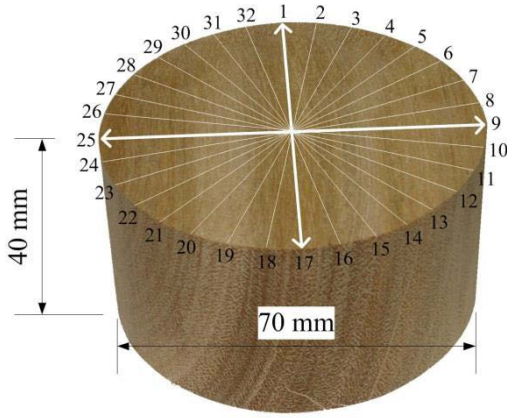


Figure 5-12: Disk specimen used for the grain angle tests with indication of the 32 measurement points

Prior to testing all, specimens were conditioned in a controlled environment of 20°C and 60% humidity, to a wood moisture content (MC) of about 12%, which was measured in the kiln after the tests according to ASNZ standards. The wood density was also determined after testing according to ASNZ standards.

### 5.3.8 Calculation of the Elastic Constants

Several standard references deal with the theory of wave propagation in orthotropic media Hearmon (1961); Royer & Dieulesaint (2000); Wasley (1973). The determination of the MOE and the shear modulus are quite straight forward thanks to the direct relationship with the P-wave and the S-wave velocities. For an isotropic material, the Poisson's ratio can also be determined easily by applying the following equation

$$\nu = \frac{V_P^2 - 2V_S^2}{2(V_P^2 - V_S^2)} \tag{5-3}$$

where $V_P$ is the longitudinal wave velocity and $V_S$ is the shear wave velocity. Calculating the Poisson's ratio for an orthotropic material, however, is more complicated since velocity measurements are required not only along the principal axes but also at an angle to the main orthotropic directions

As described in chapter 2.3.1 on page 17, an orthotropic material with its 12 elastic constants (nine are independent) can be described with the compliance matrix. The inverse of the compliance matrix [$S_{ij}$] is the stiffness matrix [$C_{ij}$].

$$[C] = \begin{bmatrix} C_{11} & C_{12} & C_{13} & 0 & 0 & 0 \\ C_{21} & C_{22} & C_{23} & 0 & 0 & 0 \\ C_{31} & C_{32} & C_{33} & 0 & 0 & 0 \\ 0 & 0 & 0 & C_{44} & 0 & 0 \\ 0 & 0 & 0 & 0 & C_{55} & 0 \\ 0 & 0 & 0 & 0 & 0 & C_{66} \end{bmatrix} \quad (5\text{-}4)$$

An orthotropic material can be characterized by measuring as many velocities as there are unknown orthotropic constants (i.e. nine), six along the principal orthotropic axes, yielding the diagonal terms ($C_{11}$, $C_{22}$, $C_{33}$, $C_{44}$, $C_{55}$, $C_{66}$) and three at an angle to the principal axes, to determine the off-diagonal terms ($C_{12}$, $C_{13}$, $C_{23}$) of the stiffness matrix. The six diagonal stiffness terms have the general form

$$C_{ii} = v^2{}_{ii} \cdot \rho \quad (5\text{-}5)$$

and the three off-diagonal stiffness components have the form

$$C_{ij} = \frac{\Gamma_{ij}}{n_k \cdot n_j} - C_{ii} \quad (5\text{-}6)$$

where $\Gamma$ is the Christoffel tensor and $n_{j,k}$ are the propagation vectors.

For the determination of the off-diagonal terms of the stiffness matrix with wave velocities measured at 45° angle to the principal axes (i.e. in LR plane $n = \left\{\frac{1}{\sqrt{2}}, \frac{1}{\sqrt{2}}, 0\right\}^T$, in the LT plane $n = \left\{\frac{1}{\sqrt{2}}, 0, \frac{1}{\sqrt{2}}\right\}^T$ and in the RT plane $n = \left\{0, \frac{1}{\sqrt{2}}, \frac{1}{\sqrt{2}}\right\}^T$) the specialized equations based on Equation (5-6) are

$$C_{12} = \sqrt{(C_{11} + C_{66} - 2\rho \cdot (v_{12})^2) \cdot (C_{66} - C_{22} - 2\rho \cdot (v_{12})^2)} - C_{66} \quad (5\text{-}7)$$

$$C_{13} = \sqrt{(C_{11} + C_{55} - 2\rho \cdot (v_{13})^2) \cdot (C_{55} - C_{33} - 2\rho \cdot (v_{13})^2)} - C_{55} \quad (5\text{-}8)$$

$$C_{23} = \sqrt{(C_{22} + C_{44} - 2\rho \cdot (v_{23})^2) \cdot (C_{44} - C_{33} - 2\rho \cdot (v_{23})^2)} - C_{44} \quad (5\text{-}9)$$

where $v_{ij}$ are the S-wave velocities at a 45° angle. Theoretically, instead of using the S-wave velocity, also the P-wave velocity can be used, however one calculation always results in imaginary values which always were the P-waves in our case. The same observations were made by Bucur & Archer (1984) where the calculations using the P-wave resulted in imaginary values and were therefore without any practical use for structural considerations.

The elastic compliances are related to the stiffness terms and the elastic constants (E, G and ν) by the following equations, which, once the stiffness terms are calculated, makes determining the elastic constants easy

$$S_{11} = \frac{C_{22} \cdot C_{33} - (C_{23})^2}{\Delta C} = \frac{1}{E_{11}}$$

$$S_{22} = \frac{C_{33} \cdot C_{11} - (C_{13})^2}{\Delta C} = \frac{1}{E_{22}}$$

$$S_{33} = \frac{C_{11} \cdot C_{22} - (C_{12})^2}{\Delta C} = \frac{1}{E_{33}}$$

$$S_{12} = \frac{C_{23} \cdot C_{31} - C_{33} \cdot C_{21}}{\Delta C}$$

$$S_{13} = \frac{C_{21} \cdot C_{32} - C_{11} \cdot C_{31}}{\Delta C} \qquad (5\text{-}10)$$

$$S_{23} = \frac{C_{13} \cdot C_{21} - C_{11} \cdot C_{23}}{\Delta C}$$

$$S_{44} = \frac{1}{C_{44}} = \frac{1}{G_{44}}\ ; \qquad S_{55} = \frac{1}{C_{55}} = \frac{1}{G_{55}}\ ; \qquad S_{66} = \frac{1}{C_{66}} = \frac{1}{G_{66}}$$

where

$$\Delta C = C_{11}\, C_{22}\, C_{33} + 2\, C_{12}\, C_{23}\, C_{31} - (C_{12})^2\, C_{11} - (C_{13})^2\, C_{22}$$

And the six Poisson's ratios are:

$$\nu_{21} = -\frac{S_{21}}{S_{22}}; \qquad \nu_{31} = -\frac{S_{31}}{S_{33}}; \qquad \nu_{32} = -\frac{S_{32}}{S_{33}}$$
$$\nu_{12} = -\frac{S_{12}}{S_{11}}; \qquad \nu_{13} = -\frac{S_{13}}{S_{11}}; \qquad \nu_{23} = -\frac{S_{23}}{S_{22}} \tag{5-11}$$

Since ultrasonic Poisson's ratio measurements often comprise significant measurements errors, Kohlhauser & Hellmich (2012) presented an approach, using combined ultrasonic and mechanical tests according to Equations (5-12) – (5-20).

$$\nu_{21} = \frac{1}{2\sqrt{2}E_2E_3}\sqrt{\frac{n_{21}}{C_{11}C_{22}}} \tag{5-12}$$

$$\nu_{31} = \frac{1}{2\sqrt{2}E_2E_3}\sqrt{\frac{n_{31}}{C_{11}C_{33}}} \tag{5-13}$$

$$\nu_{32} = \frac{n_{32}}{f g_{12} g_{32}}\sqrt{n_{21}n_{32}\frac{C_{22}}{C_{33}}} \tag{5-14}$$

where

$$n_{21} = n_{12} - h$$

$$n_{31} = {c_3}^2 - 2E_3c_3d_{31} + E_3^2e_{31} - h \tag{5-15}$$

$$n_{32} = {c_3}^2 - 2E_3c_3d_{32} + E_3^2e_{32} - h$$

and

$$f = -16c_1c_2E_3^2$$

$$\tag{5-16}$$

$$g_{12} = c_3 - E_3d_{12}$$

$$g_{32} = c_3 - E_3 d_{32}$$

$$n_{12} = c_3^2 - 2E_3 c_3 d_{21} + E_3^2 e_{21}$$

$$h = \sqrt{f g_{12}^2 + n_{12}^2}$$

with

$$e_{21} = c_2^2 - 2E_2 c_2 b_2 + E_2^2 a_2^2$$

$$e_{31} = c_2^2 - 2E_2 c_2 a_1 + E_2^2 a_2^2 \qquad (5\text{-}17)$$

$$e_{32} = c_2^2 - 2E_2 c_2 b a_2 + E_2^2 a_2 b_1$$

$$d_{12} = c_2 - E_2 a_2, \quad d_{21} = c_2 + E_2 a_1, \quad d_{31} = c_2 + E_1 E_2 - 3c_1 \qquad (5\text{-}18)$$

$$d_{32} = c_2 + E_1 E_2 - c_1$$

$$c_1 = C_{11} E_2, \quad c_2 = C_{22} E_1, \quad c_3 = C_{33} E_1 E_2 \qquad (5\text{-}19)$$

$$a_1 = E_1 + C_{11}, \quad a_2 = E_1 - C_{11}, \quad b_1 = E_1 + 3C_{11}, \quad b_2 = E_1 - 3C_{11} \qquad (5\text{-}20)$$

This approach was applied using the ultrasonic and mechanical testing results of this research and the results of both approaches are presented in the following results chapter. Kohlhauser & Hellmich (2012) obtained more accurate Poisson's ratios for different materials applying this approach. Among the tested materials was also Spruce to represent the orthotropic case.

## 5.4 Results and Discussion

### 5.4.1 Moduli of Elasticity

Following, the results of the MOE determined from the testing of the assembled block specimens and the full pole specimens are presented. The dynamic MOEs were calculated using Equation (5-1).

The wave velocities measured on the assembled block specimens were intended to serve as benchmark measurements due to the larger size of the specimens and therefore the higher possible measurement accuracy. Furthermore, the specimens were free of any visible damage and conditioned to a moisture content of 12%. The corresponding measured density values were 1.06 g/cm$^3$ for Spotted Gum and 1.09 g/cm$^3$ for Tallowwood.

#### 5.4.1.1 Small Clear Specimens

The derived wave velocities in all three orthotropic directions together with the coefficients of variation (COV) and MOE values are listed in Table 5-1.

Table 5-1: Summary of wave velocities with COV and MOE values in longitudinal, radial and tangential direction of Spotted Gum

| **Spotted Gum** | | | |
|---|---|---|---|
| | ***Longitudinal*** | ***Radial*** | ***Tangential*** |
| Wave velocity [m/s] | 5,521 | 1,982 | 1,760 |
| COV [%] | 0.9 | 0.9 | 0.9 |
| MOE [N/mm$^2$] | 32,313 | 4,165 | 3,282 |

Table 5-2: Summary of wave velocities with COV and MOE values in longitudinal, radial and tangential direction of Tallowwood

| **Tallowwood** | | | |
|---|---|---|---|
| | ***Longitudinal*** | ***Radial*** | ***Tangential*** |
| Wave velocity [m/s] | 5,137 | 2,095 | 1,820 |
| COV [%] | 0.8 | 1.0 | 1.2 |
| MOE [N/mm$^2$] | 28,764 | 4,783 | 3,610 |

The listed wave velocities are the averages of the 25 measurement locations as illustrated in Figure 5-6 b. The measurements were very consistent across the entire cross-section with resulting COVs of approximately 1% for the measurements in all three di-

rections. The slightly higher values for the measurements in radial and tangential direction of Tallowwood are most likely due to the curvature and the imperfect alignment of the growth rings, which are inherent features of the investigated testing specimen and cannot be avoided. The wave velocities measured in longitudinal direction are 5,521 m/s for Spotted Gum and 5,137 m/s for Tallowwood, resulting in MOE values of 32,313 N/mm$^2$ and 28,764 N/mm$^2$, respectively, by applying Equation (5-1).

Table 5-3 and Table 5-4 show a comparison of the static and dynamic MOE values for all three directions. The 23% and 36% higher dynamic MOE values in longitudinal direction correspond well with values reported by Burmester (1965) and Smulski (1991). For the values in radial direction, the difference was about three times bigger than the values obtained in longitudinal direction. The largest difference between the static and dynamic values was found in the tangential direction for both species, with values of approximately 2.2 times higher for Spotted Gum and 2.5 times higher for Tallowwood. Overall, the relationship was more closely met for Spotted Gum than for Tallowwood but for both species the correlations are very weak, especially in radial and tangential direction.

Table 5-3: Comparison of static and dynamic MOE values (in N/mm$^2$) in longitudinal, radial and tangential direction of Spotted Gum small clear and full pole specimens

| **Spotted Gum** (values in N/mm$^2$) | | | | |
|---|---|---|---|---|
| | ***Static*** | ***Dynamic*** | ***Difference S/D*** | ***Factor D/S*** |
| $MOE_L$ (Small Clear) | 26,174 | 32,313 | 23% | 0.81 |
| $MOE_R$ (Small Clear) | 2,405 | 4,165 | 73% | 0.58 |
| $MOE_T$ (Small Clear) | 1,499 | 3,282 | 119% | 0.46 |
| $MOE_L$ (Pole) | 18,322 | 33,328 | 82% | 0.55 |
| $MOE_R$ (Pole) | - | 3,494 | - | - |

Table 5-4: Comparison of static and dynamic MOE values (in N/mm2) in longitudinal, radial and tangential direction of Tallowwood small clear and full pole specimens

| **Tallowwood** (values in N/mm²) | | | | |
|---|---|---|---|---|
| | ***Static*** | ***Dynamic*** | ***Difference S/D*** | ***Factor D/S*** |
| $MOE_L$ (Small Clear) | 21,078 | 28,764 | 36% | 0,73 |
| $MOE_R$ (Small Clear) | 2,300 | 4,783 | 108% | 0,48 |
| $MOE_T$ (Small Clear) | 1,426 | 3,610 | 153% | 0,40 |
| $MOE_L$ (Pole) | 14,986 | 28,755 | 92% | 0,52 |
| $MOE_R$ (Pole) | - | 4,522 | - | - |

Considering that the relationship in Equation (5-1) is only based on the wave velocity and the material density, the reasons for the deviating MOE values for these two Eucalyptuses is a result of their high densities. The wave velocities measured in longitudinal direction are on the upper limit of the typical wave velocity range of most woods, which is approximately 3050 – 6100 m/s as reported by Gerhards (1982) on small clear specimens with a moisture content of 9 to 15%. Softwoods with much lower densities of around 450 kg/m$^3$ can reach the same velocities because of their longer tracheids with lengths of approximately 3.0 mm in comparison to hardwood fibres with lengths of approximately 1.0 – 1.5 mm.

Ilic (2003) measured the dynamic MOE of 55 wood species in longitudinal direction on small wood beams, among them Spotted Gum. To determine the wave velocity, the resonance frequency method was applied. For Spotted Gum with a density of 961 kg/m$^3$, the researcher measured a velocity of 4970 m/s, which results in a $MOE_d$ of 23,800 N/mm$^2$. This again confirms, as with the static tests, that the two poles tested in this study, are of wood with above average MOE values.

#### 5.4.1.2 Pole Specimens

The measured wave velocities as measured on the full pole sections according to Figure 5-9, are presented in Table 5-5. The column *'Along grain'* thereby lists the measured wave velocities along the grain which was along the pole axis for Spotted Gum but at a 180° displacement for Tallowwood due to the twisted grain. The column *'Angle 13°'* (the angle of the spiral growth of the Tallowwood pole sections) indicates the wave velocities in the alternative direction of measurement which was along the pole axis for Tallowwood and at a 180° displacement for Spotted Gum. For the measurements on the

inside of the pole, indicated as *'Middle'* in Table 5-5, this distinction was not made and only the direction of the faster wave velocity was measured (along the grain for Spotted Gum and at an angle of 13° for Tallowwood). For the measurements through the *'Pith'* this distinction is invalid.

It is important to notice that, in contrary to the small clear specimens, the full poles had a varying moisture content which was measured to be around 22% on the inside of the pole and approximately 12% on the outside. This is the reason why the measured velocities were higher on the outside than in the middle and the pith as confirmed in chapter 5.4.4.

Table 5-5: Wave velocities measured in the pole in longitudinal direction

| **Wave velocities longitudinal** (values in m/s) | | | | |
|---|---|---|---|---|
| | | ***Along axis*** | ***Angle 13°*** | ***Difference*** |
| Spotted Gum | Outside (MC≈12%) | 5,607 | 5,238 | - 6.6% |
| | Middle (MC≈22%) | 5,343 | | |
| | Pith | 5,151 | | |
| Tallowwood | Outside (MC≈12%) | 4,838 | 5,136 | + 5.8% |
| | Middle (MC≈22%) | | 4,850 | |
| | Pith | 4,812 | | |

When comparing the measurements along the grain with the ones at an angle it is obvious that the ultrasonic wave propagates the fastest along the grain. The slowing down of the waves at a 13° angle to the grain direction was 6.6% for Spotted Gum and 5.8% for Tallowwood. These values were also compared to measurements made with varying grain angles as presented in chapter 5.4.5. It is further noted that the calculated wave velocities of the measurements on the outside of the pole specimens, where they had a moisture content of 12%, are almost the same as the ones measured on the small clear specimens (which also had a moisture content of 12%) for Tallowwood and even 1.5% faster for Spotted Gum. Despite the fact that the full pole sections didn't contain any visible knots or defects (besides fine cracks along the grain), this analogy was unexpected. The calculated $MOE_d$ values in longitudinal directions therefore are almost the same as the ones calculated from the small clear specimens.

With this test alone, two observations are made: Firstly that the grain angle has a significant influence on the wave velocity, and second, the moisture content also heavily in-

fluences the velocity of the wave propagation. Both findings are investigated in greater detail in chapter 5.4.4 and chapter 5.4.5.

The wave velocities as measured on the cross-sectional pole sections are presented in Table 5-6. Since the pole discs were cut from the poles just before they were tested, the moisture content was, as for the full poles, approximately 12% on the outside and 22% on the inside.

Table 5-6: Wave velocities measured in the cross-sectional pole sections in transversal direction

| **Wave velocities transversal** | | |
|---|---|---|
| | ***Spotted Gum*** | ***Tallowwood*** |
| Wave velocity [m/s] | 1,815 | 2,037 |
| COV [%] | 2.9 | 0.4 |
| MOE [N/mm$^2$] | 3,494 | 4,522 |

Despite the cracks, the measured velocities were very constant with coefficients of variation of only 2.9% and 0.4%, respectively. The higher COV value of Spotted Gum is due to the heavier cracking of the pole disk as can be seen in Figure 5-8. Typically, cracks form in the longitudinal direction, and the wider they are, they become deeper in radial direction. The main influence of cracks on the wave velocity is therefore on wave measurements in the tangential direction where the wave has to travel through or around cracks. This phenomenon is important for the damage detection tests presented in chapter 6 but does not much affect the radial measurements.

In comparison with the radial measurements of the assembled block specimens, the wave velocities of Spotted Gum were 8.5% lower while the ones of Tallowwood were 2.9% lower. The higher velocities of the waves measured on the Tallowwood pole disks in comparison with the assembled block specimens again are the result of less cracking. However, even the heavy cracks in the Spotted Gum disk did not influence the wave velocities much.

## 5.4.2 Shear Moduli

### 5.4.2.1 Acoustic Results

The six shear wave velocities measured for Spotted Gum and Tallowwood are presented

in Table 5-7 and Table 5-8, with $c_{LR}/c_{RL} > c_{LT}/c_{TL} > c_{RT}/c_{TR}$ for both species. The reason for the wave velocity being the fastest in the LR plane, followed by the LT and RT planes, is the orthotropic anatomy of wood as observed with the longitudinal waves. The velocities measured in the same plane yielded almost the same values in all three orthotropic planes. Furthermore, the shear wave velocities in the direction of propagation along the grain are very similar for both wood species unlike the longitudinal wave velocities where the values for Spotted Gum were about 8% higher than the ones for Tallowwood. In the wave propagation direction transversal to the grain, the values measured for Tallowwood were slightly higher than the values measured for Spotted Gum which was also the case for the longitudinal wave velocities.

Table 5-7: Summary of the shear waves measured for Spotted Gum

| **Spotted Gum** | | | | | | |
|---|---|---|---|---|---|---|
| | $c_{LR}$ | $c_{RL}$ | $c_{LT}$ | $c_{TL}$ | $c_{RT}$ | $c_{TR}$ |
| Wave velocity [m/s] | 1,267 | 1,259 | 1,178 | 1,191 | 875 | 880 |
| COV [%] | 0.9 | 0.4 | 1.2 | 1.2 | 1.4 | 0.7 |
| G [N/mm$^2$] | 1,739 | | 1,530 | | 840 | |

Table 5-8: Summary of the shear waves measured for Tallowwood

| **Tallowwood** | | | | | | |
|---|---|---|---|---|---|---|
| | $c_{LR}$ | $c_{RL}$ | $c_{LT}$ | $c_{TL}$ | $c_{RT}$ | $c_{TR}$ |
| Wave velocity [m/s] | 1,257 | 1,259 | 1,121 | 1,140 | 914 | 909 |
| COV [%] | 1.5 | 0.8 | 0.9 | 1.9 | 1.0 | 1.5 |
| G [N/mm$^2$] | 1,725 | | 1,393 | | 905 | |

The resulting shear moduli (G) were calculated with Equation (5-2) using the average of the two wave velocities measured in the same orthotropic plane. For G, no static tests were performed and no literature values are available. However, a study by Keunecke et al. (2006) revealed that, unlike the MOE values, the stress-wave-based determined G values corresponded well with the statically determined values of G. This was concluded for spruce and yew wood. In chapter 5.4.2.3 the G values of Spotted Gum and Tallowwood are compared against reference values of 10 other hardwood species.

Ratios between $G_{LR}$, $G_{LT}$ and $G_{RT}$ are given as 3.25/2.5/1 for hardwoods by Scheer (1986)a and as 10/9.4/1 by Bodig & Jayne (1982) for both soft and hardwoods. The ra-

tios for Spotted Gum are 2.1/1.8/1 and for Tallowwood 1.9/1.5/1. For the averaged G values of 10 hardwood species compiled by (U.S.) Forest Products Laboratory (2010), the ratios are 4.6/3.3/1. Both, Spotted Gum and Tallowwood therefore have a large shear modulus in the RT plane. The ratios as given by Scheer (1986)b match the testing results much better than the ones given by Bodig & Jayne (1982) which are a combination of softwoods and hardwoods.

For Spotted Gum and Tallowwood, there are no anatomical studies available. Wagenführ (2007) provides the wood characteristics for Blue Gum and lists Spotted Gum and Tallowwood as a similar species. A compilation of the available values for Spotted Gum and Tallowwood as well as a comprehensive list of values for Blue Gum is presented in Table 2-2. Therefore, the wood properties cannot be justified by their anatomical structure. It is obvious however, that both eucalypts have superior strength properties along and across the grain.

#### 5.4.2.2 Analytical Results

To provide a comparative basis for the ultrasonic results, the shear moduli were also determined analytically. The analytical relations between the MOE, the shear modulus and the Poisson's ratio for orthotropic materials were first presented by Saint-Venant (1856) and experimentally verified by Hudson (1993) for rock material. The following Equations (5-21), (5-22) and (5-23) show the analytical derivation of the three shear moduli

$$G_{LR} = \frac{E_L \cdot E_R}{E_L + E_R + 2\nu_{LR} \cdot E_R} \tag{5-21}$$

$$G_{LT} = \frac{E_L \cdot E_T}{E_L + E_T + 2\nu_{LT} \cdot E_T} \tag{5-22}$$

$$G_{RT} = \frac{E_R \cdot E_T}{E_R + E_T + 2\nu_{TR} \cdot E_R} \tag{5-23}$$

where $G$ is the shear modulus, $\nu$ is the Poisson's ratio, $E$ is the MOE and the subscripts $L$, $R$ and $T$ are the longitudinal, radial and tangential orthotropic directions of wood. For

calculating the analytical shear moduli, the statically determined benchmark material property values were used.

In Table 5-9, the calculated analytical G values are presented for Spotted Gum and Tallowwood and are compared with the values obtained from the ultrasonic tests. For four of the six shear moduli, the analytical method yielded lower G values. Only for $G_{LR}$ of Spotted Gum and Tallowwood the analytical method yielded values which are 15% and 10% higher respectively. The $G_{LT}$ values of both species are 13% lower than the ones determined from the ultrasonic method while the $G_{RT}$ values of Spotted Gum and Tallowwood are significantly lower with -31% and -36% respectively.

Table 5-9: Comparison of ultrasonic and analytical results

| **Spotted Gum and Tallowwood** (values in N/mm²) | | | |
|---|---|---|---|
| | ***Ultrasonic*** | ***Analytical*** | ***Difference D/A*** |
| Spotted Gum $G_{LR}$ | 1,739 | 2,001 | 15% |
| $G_{LT}$ | 1,530 | 1,338 | -13% |
| $G_{RT}$ | 840 | 579 | -31% |
| Tallowwood $G_{LR}$ | 1,725 | 1,902 | 10% |
| $G_{LT}$ | 1,393 | 1,209 | -13% |
| $G_{RT}$ | 905 | 575 | -36% |

The comparison of the ultrasonic with the analytical results clearly shows the same trend for both tested species overestimation of the $G_{LR}$ values and underestimation of the $G_{LT}$ and $G_{RT}$ values. The difference of the $G_{RT}$ values is thereby more than twice as high as the values for the other two shear moduli. The analytical approach using the equations derived from tests on rock can only be considered partially applicable since the equations clearly yield much better results than formulas that apply to isotropic materials but with differences of greater than 30% the deviation is still very large.

#### 5.4.2.3 Comparison

To be able to position the measured G values of Spotted Gum and Tallowwood, a compilation of G values presenting the averages, minimum and maximum shear moduli values of 10 hardwoods is shown in Table 5-10 as presented in (U.S.) Forest Products Laboratory (2010). When comparing the *G* values derived for Spotted Gum and Tallowwood with statically determined values of the 10 hardwood species, one can see that the values are very high, as with other elastic properties.

Table 5-10: Average, minimum and maximum shear moduli of 10 hardwood species from (U.S.) Forest Products Laboratory (2010)

| **Average G values of 10 hardwoods** (values in N/mm²) | | | |
|---|---|---|---|
| | $G_{LR}$ | $G_{LT}$ | $G_{RT}$ |
| Averages $\bar{x}$ | 1,193 | 862 | 260 |
| Minimum | 622 | 511 | 251 |
| Maximum | 1,666 | 1099 | 268 |
| Spotted Gum | 1,739 | 1,530 | 840 |
| Tallowwood | 1,725 | 1,393 | 905 |

The 10 hardwood species that were used for comparison are: White Ash, Basswood, Yellow Birch, Black Cherry, Eastern Cottonwood, Sugar and Red Maple, Sweet Gum, Black Walnut and Yellow Poplar. For $G_{RT}$, values of only 4 species were available. All shear moduli of the two tested species, Spotted Gum and Tallowwood, clearly lie above the average and even above the maximum values of the 10 hardwoods used for comparison. While $G_{LR}$ of Spotted Gum is 45% higher than the average and 4% than the maximum $G_{LT}$ is 77% higher than the average and 39% than the maximum and $G_{RT}$ is 322% higher than the average and 313% than the maximum. Since the shear moduli of Spotted Gum and Tallowwood are very similar the differences in comparison to the 10 hardwoods are very similar.

Both maximum values of the 10 compared species are from Black Cherry which therefore is most similar to the tested species. The only wood with shear moduli in a similar range for $G_{LR}$ and $G_{LT}$ to Spotted Gum and Tallowwood is Yew, as presented by Keunecke et al. (2006). The shear moduli are 1,740 N/mm² for $G_{LR}$, 1,650 N/mm² for $G_{LT}$ and 368 N/mm² for $G_{RT}$. The researchers state the high ray percentage (as proposed by Burgert (2000)), the thick cell wall and the microfibril angle as causes for the high shear moduli. By modelling the elastic properties of softwoods, Astley et al. (1998) showed that $G_{LR}$ and $G_{LT}$ can double or triple with increasing MFA. Considering these findings, some of the mentioned factors must also be the cause for the very high G values of Spotted Gum and Tallowwood.

### 5.4.3 Poisson's Ratios

#### 5.4.3.1 Acoustic Results

When statically determining the Poisson's ratios, all six values can be directly measured. For the ultrasonic tests, however, only three Poisson's ratios can be determined while the three remaining ones have to be calculated using the relationship

$$\frac{\nu_{ij}}{E_i} = \frac{\nu_{ji}}{E_j}, \quad i \neq j, \quad i,j = L,R,T \tag{5-24}$$

In Table 5-11, the results from the ultrasonic tests using the orthotropic and isotropic approaches are presented in comparison to the Poisson's ratios derived from the static method. For both species, the orthotropic Poisson's ratios derived from Equations (5-7) – (5-9), yielded negative values for $\nu_{RT}$ and $\nu_{TR}$. The values of $\nu_{LT}$ are 1.89 and 2.17, respectively, and therefore very high. Also, the very small ratios $\nu_{RL}$ and $\nu_{TL}$ are around three to five times higher than the static values. For the calculations, the shear wave velocity had to be used, which was not measured experimentally. Therefore, the Hankinson formula, which had proved to produce very accurate results for the prediction of velocities at various angles to the grain (see Chapter 5.4.5.1), was used to calculate the S-wave velocity at 45°. The reason for the poor agreement of static and ultrasonic orthotropic values is assumed to be due to the fact that unlike other timbers, the radial and tangential velocities are almost the same and the calculation fails at predicting accurate Poisson's ratio values under these conditions.

Table 5-11: Poisson's ratios determined from the ultrasonic measurements

| **Ultrasonic Poisson's ratios** (MC ≈12 %) | | | | | | | |
|---|---|---|---|---|---|---|---|
| ***Species*** | ***Method*** | $\nu_{LR}$ | $\nu_{LT}$ | $\nu_{RT}$ | $\nu_{TR}$ | $\nu_{RL}$ | $\nu_{TL}$ |
| Spotted Gum | static | 0.53 | 0.55 | 0.66 | 0.48 | 0.045 | 0.047 |
| | orthotropic | 1.01 | 1.89 | -0.06 | -0.05 | 0.130 | 0.192 |
| | isotropic | 0.47 | 0.48 | 0.38 | 0.30 | 0.061 | 0.048 |
| Tallowwood | static | 0.46 | 0.83 | 0.69 | 0.43 | 0.043 | 0.050 |
| | orthotropic | 0.75 | 2.17 | -1.08 | -0.82 | 0.124 | 0.273 |
| | isotropic | 0.47 | 0.48 | 0.38 | 0.29 | 0.078 | 0.060 |

Using the simpler Equation (5-3) for the isotropic case, yielded results that more closely

met the statically determined Poisson's ratios - $\nu_{LR}$ and $\nu_{TL}$ (for both species) and $\nu_{RL}$ and $\nu_{TL}$ (for Spotted Gum) are within 2% and 30% deviation of the static Poisson's ratios, while the remaining Poisson's ratios are between 42% and 81%. All these values lie within the known range of Poisson's ratios for wood. The ratios from the orthotropic approach, however, yielded negative values and values above 1 which are out of the typical range for wood. While the orthotropic calculation must be dismissed for calculating the Poisson's ratios based on ultrasonic TOF measurements, the isotropic equation yields reasonable results and can be recommended as a simple way of calculating the Poisson's ratios.

The results from the combined ultrasonic TOF measurements and the statically determined MOE values as presented by Kohlhauser & Hellmich (2012) are shown in Table 5-12 in comparison to the solely static Poisson's ratios.

Table 5-12: Poisson's ratios determined from the combined ultrasonic and static measurements

| **Acoustic/Static Poisson's ratios** (MC ≈12 %) | | | | | | | |
|---|---|---|---|---|---|---|---|
| ***Species*** | ***Method*** | $\nu_{LR}$ | $\nu_{LT}$ | $\nu_{RT}$ | $\nu_{TR}$ | $\nu_{RL}$ | $\nu_{TL}$ |
| Spotted Gum | static | 0.53 | 0.55 | 0.66 | 0.48 | 0.045 | 0.047 |
| | orthotropic | 0.88 | 2.15 | 0.87 | 0.54 | 0.130 | 0.192 |
| Tallowwood | static | 0.46 | 0.83 | 0.69 | 0.43 | 0.043 | 0.050 |
| | orthotropic | 0.82 | 1.88 | 0.89 | 0.56 | 0.089 | 0.127 |

Kohlhauser & Hellmich (2012) were able to improve the accuracy of calculating Poisson's ratios with their combined approach over the solely acoustic method. This is mostly also true for our results, however, the results still pale in comparison with the isotropic calculations. Especially for $\nu_{LT}$ the calculations yield way too high values. Also the Poisson's ratios for $\nu_{RL}$ and $\nu_{TL}$ end up being significantly higher than the static values. For the tested species this approach therefore can't be recommended.

### 5.4.4 Practical Testing Consideration: Moisture Content

For the moisture content investigation, the ultrasonic wave velocity was measured on small clear block specimens with 6 different moisture contents. It has been shown by several researchers that the stress wave velocity decreases with increasing moisture content. This trend is linear up to the fibre saturation point (FSP) as de Oliveira et al. (2005); Sakai et al. (1990) showed in their research investigations. After the FSP, the

wave velocity further decreases in a liner manner, however, the decrease is less distinctive. This was also confirmed for the species tested in this work, Spotted Gum and Tallowwood, for the longitudinal and radial direction. Figure 5-13 shows the measured P-wave and S-wave velocities for different moisture contents for both species. The velocities were measured with 5 varying moisture contents from 0% to the FSP and one fully water saturated (WS) specimen. The graphs for the remaining measured directions are displayed in Appendix B on page 153.

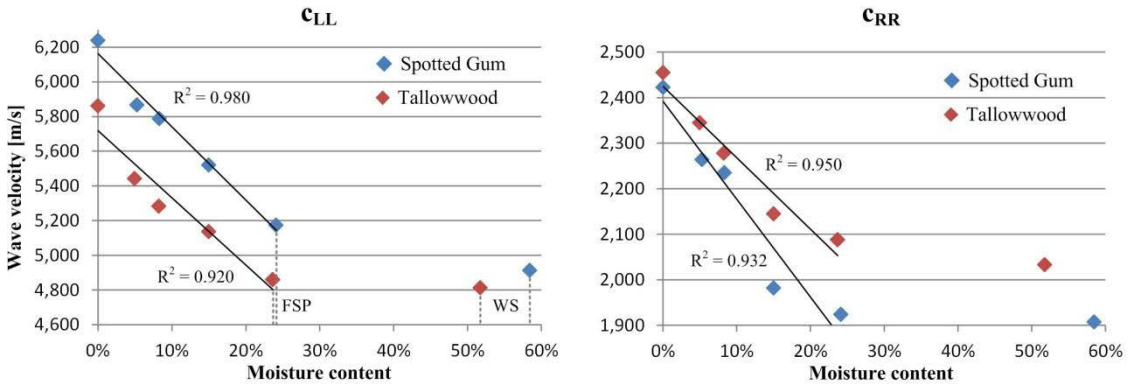


Figure 5-13: Influence of the wood moisture content on the P-wave and S-wave velocities

The Tallowwood specimens demonstrate a greater dependency of the wave velocity on changing moisture content. For all six cases, the wave velocity measured on Tallowwood showed a greater decrease. Because of a lack of information on the micro fibril angel and extractives for the examined two species, it is difficult to conclude why the wave velocities are higher or lower in the different orthotropic directions.

From the tests, the FSP as well as the wood's full water saturation (WS) point could be determined. For Spotted Gum the FSP was at 24.1% while it was at 23.7% for Tallowwood and the WS point was at 59.8% MC for Spotted Gum and at 52.9% MC for Tallowwood. Nzokou & Kamdem (2004) showed that extractives lower the equilibrium moisture content, particularly at higher relative humidity. The test results from Spotted Gum and Tallowwood confirm these findings since the fibre saturation points (FSPs) of around 24% are on the low end as shown in Figure 5-14. According to Siau (1984), the FSP corresponds to the moisture content of a wood specimen placed in a relative humidity of 98%.

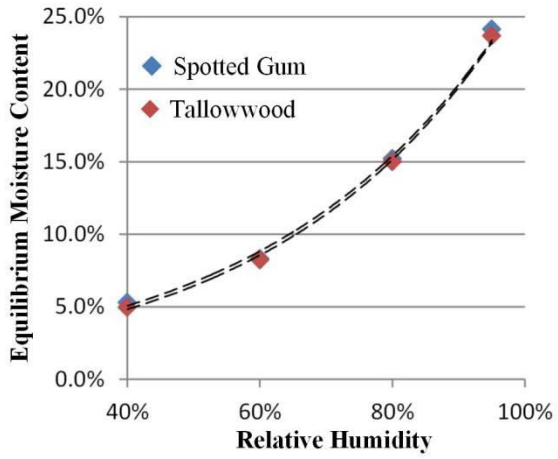


Figure 5-14: Sorption Isotherm for Spotted Gum and Tallowwood

### 5.4.5 Practical Testing Consideration: Grain Angle

The results obtained from the grain angle tests of the three disc specimens of both species are shown in Figure 5-15. The change in the TOF from radial to tangential direction occurs gradually with the fastest TOF measured in radial and the slowest measured in tangential direction. This is contrary to the observations made by Ross et al. (1999) on Douglas fir at 12% MC. Their tests clearly revealed the longest TOF at 45 degrees with a TOF of 995 µs/m in comparison to a TOF of 668 µs/m in radial direction and 800 µs/m in tangential direction. Despite the fact that the eucalyptus species used for this investigation are hardwoods with a density almost twice as high as the one of Douglas fir, which is a softwood, these different wave propagation behaviours are significant and should be subject for further studies.

a)

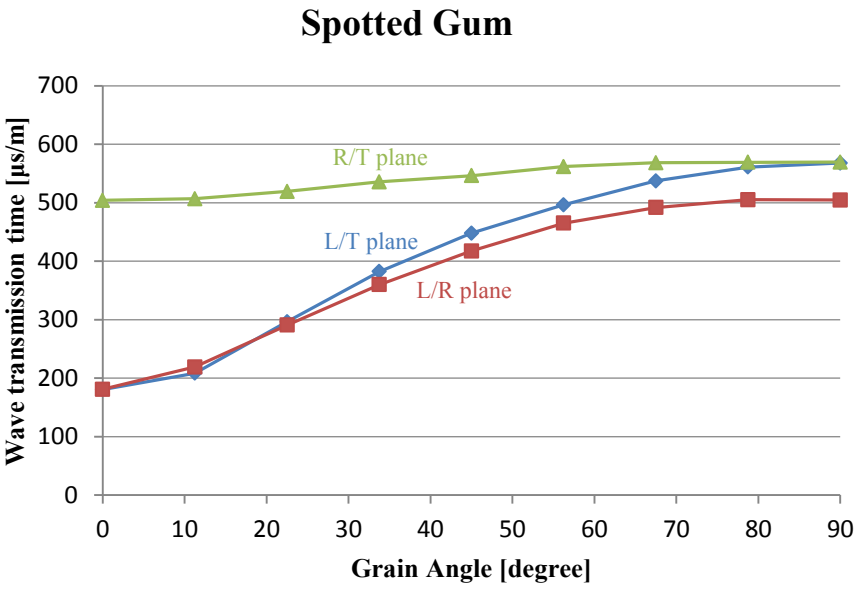

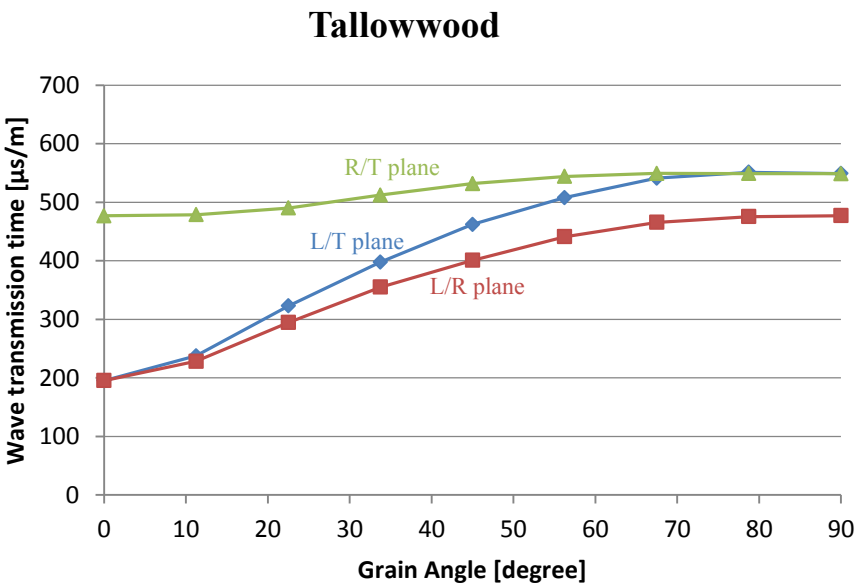


b)

Figure 5-15: Wave velocities as a function of the grain angle in all three orthotropic directions of a) Spotted Gum and b) Tallowwood.

Figure 5-16 displays changes in wave velocity in percentage as a function of the grain angle. The measured wave transmission times (WTTs) in radial and tangential direction are very similar, with the tangential direction only being 11% slower for Spotted Gum and 13% for Tallowwood. For both species, the wave velocity in radial direction is almost constant up to a grain angle of about 10%. Approaching the tangential direction, the TOF remained nearly constant from about 60 to 90 degrees. The major change of the TOF therefore occurred between 10 and 60 degrees.

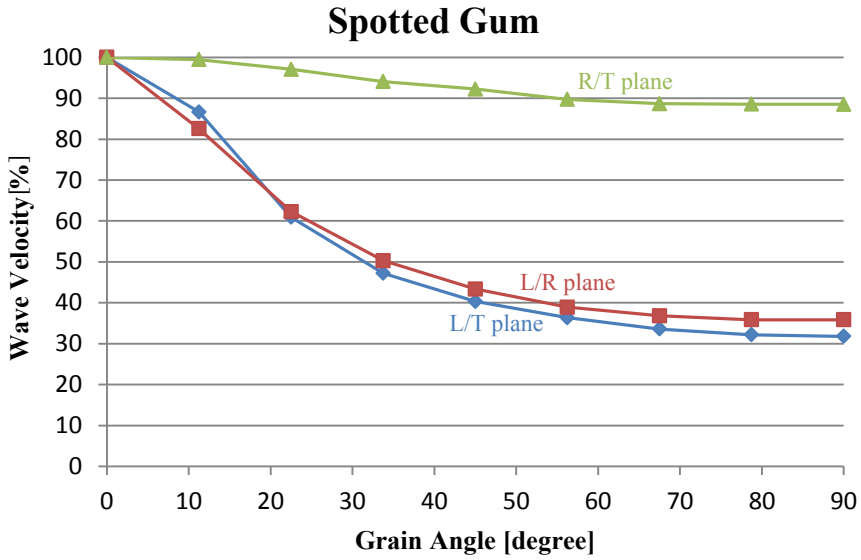


a)

b)

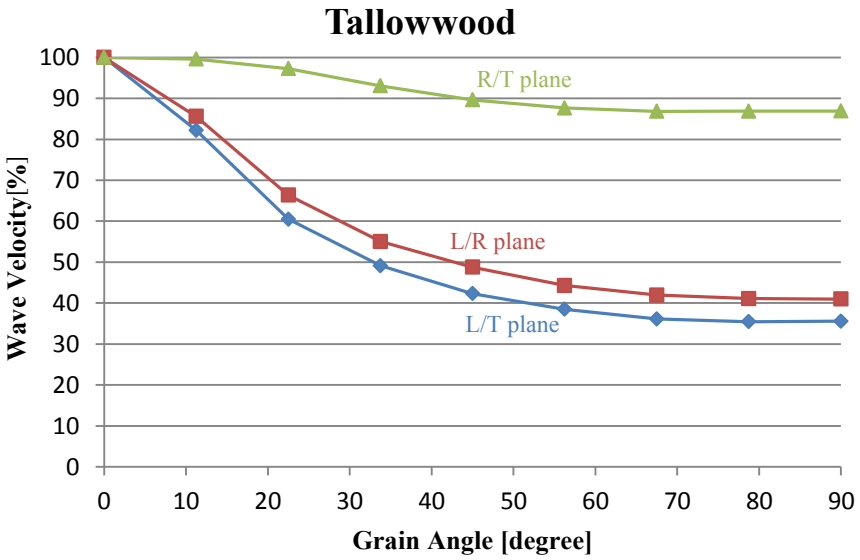


Figure 5-16: Change of wave velocity as a function of the grain angle in all three orthotropic planes (in percentage) for (a) Spotted Gum and (b) Tallowwood

In the L/R and L/T planes, the most rapid change in the wave velocity occurs between 0 and about 25 degrees. After this point, the velocity decreases more slowly until it remains almost constant from 70 to 90 degrees. This behaviour is also observed in the L/R and L/T planes of both species. Very similar observations were made by Niemz et al. (1999) on spruce and beech specimens. The researchers reported a 20% decrease in velocity for spruce and 15% for beech. The average values for both planes (L/R and L/T) for Spotted Gum and Tallowwood reveal a reduction of the wave velocity of 13% for both species. These results match very well with the ones from Niemz et al. (1999) of beech, which is also a hardwood. Hence, measurements at a 10 degree grain angle in the L/R plane of Spotted Gum, for example, would result in a MOE of 22.1 GPa instead of 32.4 GPa, which equals to an error of 32%. This indicates that the grain angle has a significant influence on measurements along the grain, where most measurements are conducted i.e. for the grading of lumber. In the secondary R/T plane, the grain angle has a smaller influence and wood could be regarded as transversally isotropic (no distinction between the velocities in radial and tangential direction) when measuring the TOF.

#### 5.4.5.1 Hankinson Formula

The Hankinson formula (5-25) is an empirical equation which was developed by Hankinson (1921) for predicting the strength properties of wood at various grain angles, and is expressed as

$$N_\theta = \frac{P \cdot Q}{P sin^2\theta + Q cos^2\theta} \tag{5-25}$$

where $N_\vartheta$ is the strength at angle $\theta$, $P$ the strength parallel to the grain, $Q$ the strength perpendicular to the grain and $\theta$ the grain angle. It was originally developed to describe the compressive strength of spruce, but Hankinson discovered that it could also be applied for other wood species. In 1939, Kollmann proposed to slightly modify the formula to make it applicable for tensile strength tests by altering the trigonometric exponent between 1.5 and 2.0 which led to reasonable strength predictions Kollmann & Cote (1968). So far, the formula has been successfully applied to predict mechanical properties such as the MOE, compressive strength and bending strength of wood with trigonometric exponents between 1.5 and 2.5. Schneckenberger (1991) conducted comprehensive research on the slope of grain on the wave velocity and showed that the equation developed by Hankinson can also be applied to wave velocity predictions at various grain angles and proposed an exponent of 1.7. For the wave velocity the equation can be written as follows

$$V_\theta = \frac{V_\parallel \cdot V_\perp}{V_\parallel sin^n\theta + V_\perp cos^n\theta} \tag{5-26}$$

where $V_\vartheta$ is the wave velocity at angle $\theta$, $V_\parallel$ the wave velocity parallel to the grain, $V_\perp$ the wave velocity perpendicular to the grain, $\theta$ the grain angle and $n$ the trigonometric exponent which was proposed to be 1.7 by Schneckenberger (1991) .

Figure 5-17 shows the measured wave velocities at grain angles from 0 to 90 degrees applied to each orthotropic plane, with the results from the Hankinson formula shown as dotted line. Trigonometric exponents of 1.4 and 1.5 for the L/R and L/T planes and of 1.9 and 2.0 for the R/T plane yielded the best results. Using these exponents, the Hankinson formula can predict the wave velocity at almost any angle very accurately. Only at a grain angle of around 10 degrees, the experimentally measured velocities are approximately 1% to 3% higher than the calculated results, which is still a very close match. The application of the Hankinson formula with the determined trigonometric exponents can therefore be highly recommended for the two tested Eucalyptus species.

a)

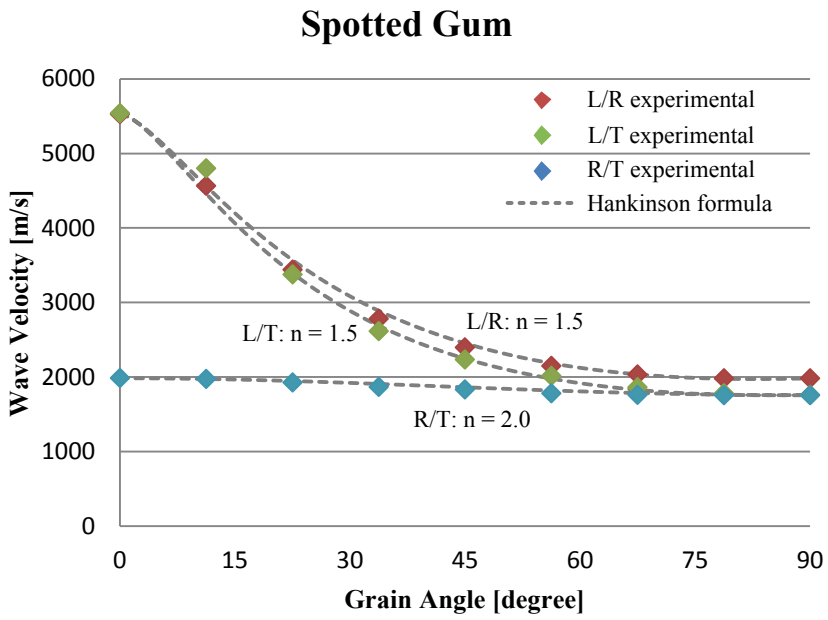


b)

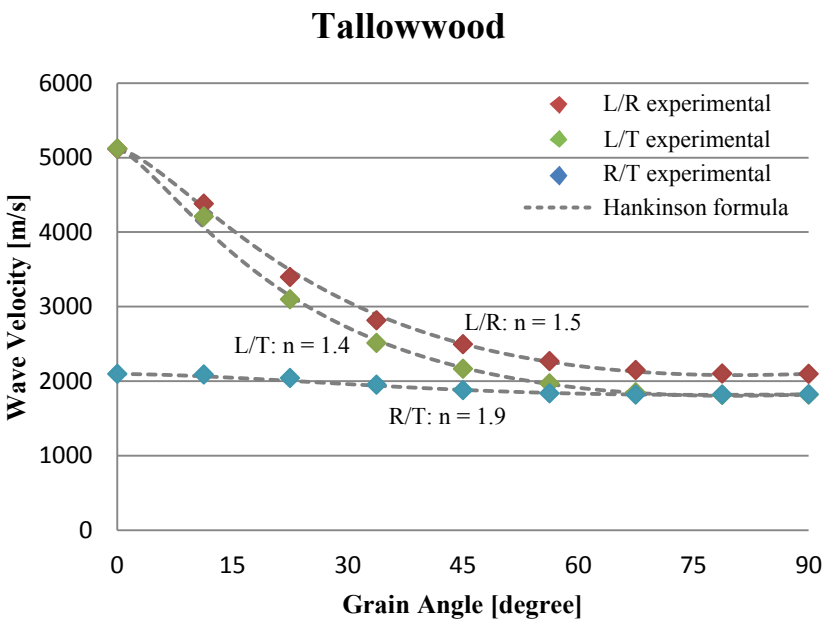


Figure 5-17: Hankinson formula in comparison to the experimental wave velocity results for a) Spotted Gum and b) Tallowwood at grain angles from 0 to 90 degrees

Besides the Hankinson formula, which is the most widely used equation, there are other formulas to calculate the influence of the grain angle. The Osgood formula is a generalization of the Hankinson formula and introduces an additional, species dependent, factor as shown in the equation below Kim (1986)

$$N_\theta = \frac{P \cdot Q}{Q + (P - Q) \cdot (P sin^2\theta + a \cdot Q cos^2\theta) \cdot sin^2\theta} \quad (5\text{-}27)$$

where $N_\vartheta$, $P$, $Q$ and $\theta$ are defined as in the Hankinson formula and $a$ is the species dependent factor which Osgood defined as 0.35 for Southern Yellow Pine. As a basis for the formula, data from compression tests was used. When $a$ is chosen as 1, the Osgood formula reduces to the Hankinson formula.

The Jacoby formula was introduced by Mishiro (1996)b to calculate the wave velocity at an angle to the grain and can be written as

$$V_\theta = V_0 \cdot cos^n\theta + V_{90} \cdot sin^n\theta \tag{5-28}$$

where $V_\vartheta$ is the wave velocity at angle $\theta$, $V_0$ the wave velocity parallel to the grain, $V_{90}$ the wave velocity perpendicular to the grain, $\theta$ the grain angle and $n$ the trigonometric exponent.

The following analytical relationship by Jones (1975), was the only analytical formula used to predict the wave velocity depending on the angle of grain. This constitutive equation was developed for anisotropic materials in general and not for wood specifically. It also requires data of the shear wave velocity and the Poisson's ratios as presented in the following equation

$$\overline{Q_\theta} = \frac{E_{LL}}{1 - \nu_{LR}\nu_{RL}} cos^4\theta + 2(\upsilon_{RL}Q_{LL} + 2G_{LR})sin^2\theta cos^2\theta + \frac{E_R}{1 - \nu_{LR}\nu_{RL}} sin^4\theta \tag{5-29}$$

where $\overline{Q_\theta}$ is the wave velocity at angle $\theta$, $E$ the MOE, $\nu$ the Poisson's ratios, $G$ the shear modulus, $Q_{LL}$ the wave velocity in longitudinal direction, and the LL, LR, RL the orthotropic directions and planes.

Table 5-13 and Table 5-14 show a summary of the mean absolute percentage error (MAPE) and the mean absolute error (MAE) for both tested species that were used to compare each formula with the experimental data and determine their usefulness. MAPE and MAE were calculated using the following equations

$$MAPE = \frac{1}{n}\sum_{i=1}^{n}\left|\frac{y_i - f_i}{y_i}\right| \tag{5-30}$$

$$MAE = \frac{1}{n}\sum_{i=1}^{n}|f_i - y_i| \tag{5-31}$$

where $f_i$ is the predicted and $y_i$ is the true value.

Table 5-13: Comparison of MAE and MAPE of all formulas for Spotte Gum

| **Spotted Gum** | | | | |
|---|---|---|---|---|
| ***Plane*** | ***Hankinson*** | ***Osgood*** | ***Jacoby*** | ***Jones*** |
| LR MAPE [%] | 1.1 | 1.4 | 9.7 | 22.6 |
| MAE [m/s] | 46 | 48 | 375 | 618 |
| LT MAPE [%] | 1.6 | 2.6 | 10.5 | 22.6 |
| MAE [m/s] | 71 | 95 | 369 | 618 |
| RT MAPE [%] | 0.7 | 0.3 | 0.5 | - |
| MAE [m/s] | 18 | 7 | 12 | - |

Table 5-14: Comparison of MAE and MAPE of all formulas for Tallowwood

| **Tallowwood** | | | | |
|---|---|---|---|---|
| ***Plane*** | ***Hankinson*** | ***Osgood*** | ***Jacoby*** | ***Jones*** |
| LR MAPE [%] | 0.8 | 1.6 | 7.8 | 21.5 |
| MAE [m/s] | 30 | 56 | 307 | 587 |
| LT MAPE [%] | 0.7 | 1.8 | 10.5 | 21.5 |
| MAE [m/s] | 28 | 60 | 365 | 587 |
| RT MAPE [%] | 0.5 | 0.9 | 2.5 | - |
| MAE [m/s] | 13 | 22 | 62 | - |

From the two tables, it can be seen that the Hankinson formula yielded the best fit with the experimental date for the LR and LT planes of both wood species with a MAPE of 0.7 – 1.6%. These results are remarkable and the application of the Hankinson formula can be strongly recommended for both tested species. In the RT plane, the Osgood as well as the Jacoby formula yielded more accurate results on a very low error level. The Osgood formula with its additional species dependent parameter did not yield results that matched the experimental data as well as the Hankinson's formula. The MAPE was between 1.4 – 1.8% for the LR and LT planes and 0.3 – 0.9% for the RT plane, which also are outstanding results, however, due to the fact that an additional parameter must be considered, it is more difficult to apply. The Jacoby formula, the simplest of the three compared empirical equations yielded more inaccurate results with MAPE between 7.8 – 10.5% in the LR and LT plane. The results for the RT planes revealed a better match with values of 0.5 – 2.5%.

The only analytical equation tested yielded the most inaccurate results with MAPE of over 20%. Due to its analytical derivation it cannot be adjusted by a trigonometric exponent. The use of the Jones equation can therefore not be recommended for the two tested timber species. Kabir (2001) did a similar comparison on the wave velocity on various grain angles, using the Hankinson, Osgood and Jacoby equations on Rubber Wood and also concluded that the Hankinson formula produced the best results

In Table 5-15 the determined trigonometric exponents which best fitted the experimental results are presented. For the Osgood formula, the species dependent variable is displayed in parenthesise.

Table 5-15: Summary of trigonometric exponents for all formulas for Spotted Gum and Tallowwood

| **Trigonometric Exponents** | | | | | | |
|---|---|---|---|---|---|---|
| | **Spotted Gum** | | | **Tallowwood** | | |
| ***Plane*** | ***Hankinson*** | ***Osgood*** | ***Jacoby*** | ***Hankinson*** | ***Osgood*** | ***Jacoby*** |
| **LR** | 1.4 | 0.9 (0.37) | 3.3 | 1.5 | 0.9 (0.36) | 3.1 |
| **LT** | 1.5 | 1.0 (0.37) | 3.4 | 1.4 | 0.9 (0.36) | 3.4 |
| **RT** | 1.9 | 1.0 (0.37) | 2.1 | 1.9 | 0.9 (0.36) | 2.2 |

For the Hankinson formula, values for $n$ of 1.5 – 2.5 are recommended. For the best fit of the experimental results, twice a value of 1.4 had to be chosen for the two tested species. The Osgood formula yielded the best results with the species dependent factor being 0.37 for Spotted Gum and 0.36 for Tallowwood, in comparison to 0.35 as recommended by Osgood for Southern Yellow Pine.

### 5.4.6 Comparison E/G Ratios

Bodig & Goodman (1973) and (U.S.) Forest Products Laboratory (2010) present the elastic parameters as factors based on the MOE in longitudinal direction. The factors determined for Spotted Gum and Tallowwood are presented in Table 5-16.

Table 5-16: Elastic parameters as factors based on the static and dynamic longitudinal MOE

| **Elastic Ratios based on $E_L$** | | | | | | |
|---|---|---|---|---|---|---|
| | $E_L$ [N/mm$^2$] | $E_R/E_L$ | $E_T/E_L$ | $G_{LR}/E_L$ | $G_{LT}/E_L$ | $G_{RT}/E_L$ |
| Spotted Gum (static) | 26,174 | 0.092 | 0.057 | 0.066 | 0.058 | 0.032 |
| (dynamic) | 32,312 | 0.074 | 0.046 | 0.054 | 0.047 | 0.026 |
| Tallowwood (static) | 21,078 | 0.109 | 0.068 | 0.082 | 0.066 | 0.043 |
| (dynamic) | 28,763 | 0.080 | 0.050 | 0.060 | 0.048 | 0.031 |

The results are presented as factors of the statically determined MOE's as well as the dynamic MOE's and represent the factors to determine the statically determined benchmark values.

## 5.5 Conclusions

In this research, the MOE of all three orthotropic directions were determined for two eucalyptus species, Spotted Gum and Tallowwood (two species commonly used for utility poles in New South Wales, Australia) using static as well as non-destructive ultrasonic material testing methods. For the static testing, bending, tensile and compression tests were conducted, while for the non-destructive testing, ultrasonic tests based on the TOF method were carried out. For the static testing, the MOE values obtained from various types of tests showed good agreement with each other, especially in the longitudinal direction. For the ultrasonic-based MOEs in longitudinal direction, the results obtained using a commonly applied equation corresponded well to literature. For ultrasonic measurements across the grain, however, calculated MOE values were up to 2.5 times higher than the values obtained from the static tests. It can therefore be concluded that due to the high densities of the investigated eucalyptus species, the commonly applied formula appears to be unsuitable. Investigations related to the grain angle confirmed results from Niemz et al. (1999), that indicated a rapidly decreasing wave velocity with increasing grain angle. This finding is of great importance for further non-destructive tests on utility poles but also for ultrasound-based timber grading. Further investigations on new full scale timber poles are planned to study the influence of cracks on the TOF and resulting MOE values. In addition, examinations on artificially damaged small clear specimens will be conducted to investigate the influence of voids inside timber poles to the TOF and MOE.

# 6 DAMAGE DETECTION

## 6.1 Chapter Overview

This chapter presents the research conducted on detecting damage in small clear specimens as well as pole sections in transversal direction. All investigated damage types represent actual cases as they most often occur in the field. The information about the damage types was obtained from the industrial partner of this research project, Ausgrid. The testing was not only conducted experimentally but also verified with a 3-dimensional, orthotropic numerical model.

## 6.2 Introduction

The damage detection principal used in this study was that stress waves take longer to travel through or around a damaged area compared to their straight propagation in a healthy specimen. The applied method based on TOF measurements uses ultrasonic waves that travel from a sending transducer to a receiving transducer. Hence, the testing methodology was largely the same as presented in chapter 5, including the testing setup and instrumentation, as well as some testing specimens.

The detection of internal decay is an important aspect to guarantee the safety of wooden utility poles. In the past, various non-destructive methods have been applied with the aim to identify internal damage in wooden poles. Acoustic tomography (AT) is one such method and uses a similar approach to X-ray assessment which is widely applied in the medical field.

Figure 6-1 shows a typical damage pattern as it frequently occurs at ground line of a timber pole. The specimens produced in the presented research are based on this type of damage. To test the effect of damage on transversal wave measurements, specimens were produced with a hole in the middle; further, to simulate the effect of a hole on longitudinal TOF measurements, specimens with a reduction in diameter were manufactured and tested.

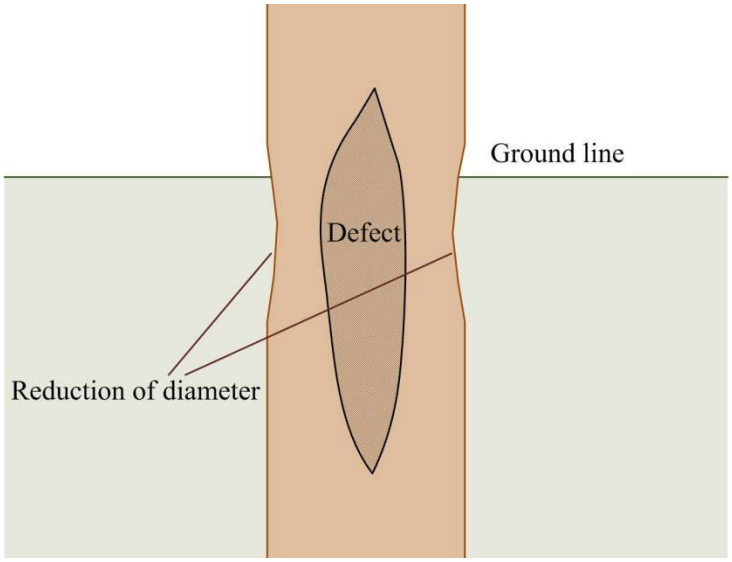


Figure 6-1: Illustration of typical damage as it occurs at ground line of timber utility poles

The influence of internal damage, such as a hole or void caused by rot or termites, and external damage, called necking which can be caused by decay or physical damage, on the strength of the pole are different.

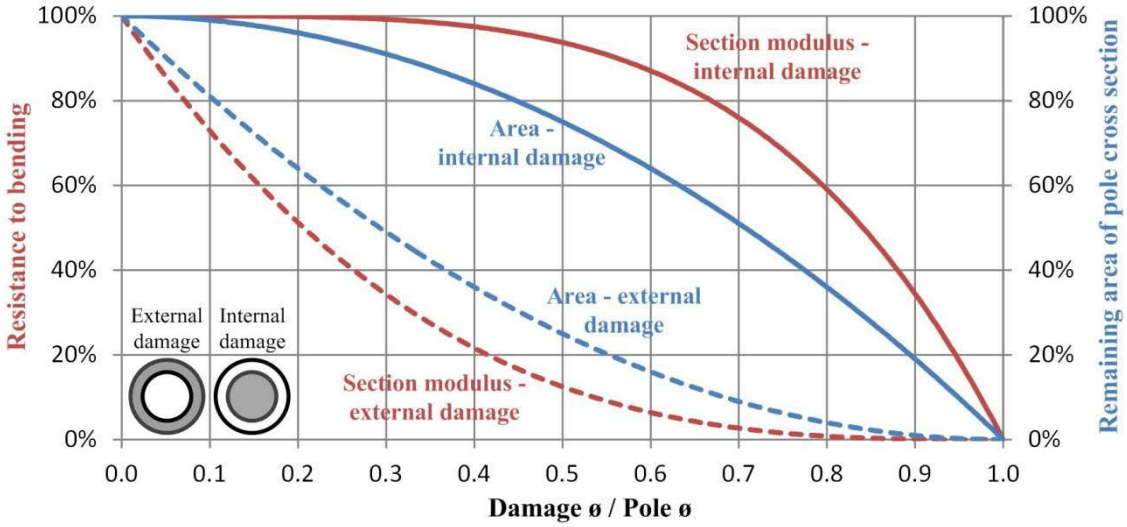


Figure 6-2: Influence of internal and external damage on the poles resistance to bending and remaining cross-section area

Figure 6-2 shows the effect of internal and external damage on its remaining resistance to bending and the remaining cross-sectional area, plotted against the damage to pole diameter ratio. While the same damage to pole diameter ratio of internal damage causes a smaller reduction of the cross-sectional area, external damage results in a bigger loss of cross-sectional area. The section modulus is a simple geometric relation which does not consider the material properties and is calculated from the size and shape of a beam. It is a measure for a member's ability to withstand a force and the resulting internal stresses. For a circular tube, as it is the case for a pole structure with internal damage, the section modulus is the quotient of the moment of inertia and the distance between the neutral axis and the outermost fibre and is calculated using the following equation

$$S = \frac{\pi(D^4 - d^4)}{32D} \tag{6-1}$$

where $S$ is the section modulus, $D$ the pole diameter and $d$ the damage diameter.

From Figure 6-2, it can be seen that external damage has a larger effect to the poles stability than internal damage. While a damage to pole diameter ratio of 80% results in an almost complete loss of strength in the case of external damage, the pole's strength still remains 60% of its original strength if the damage is internal. In reality, however, both damage types often occur simultaneously as shown in Figure 6-1.

According to X. Wang et al. (2004), the presence of decay greatly affects the wave transmission time. This effect was confirmed by Lin et al. (2008) who inflicted holes of varying sizes in wooded specimen and measured the ultrasonic TOF of the specimen with the different sized holes. The researchers found that there was generally a linear relationship between the ratio of the hole diameter to the specimen diameter and the velocity of the TOF measurements. The researchers placed eight sensors at equal circumferential distances around their specimen and measured all paths as shown in Figure 6-3.

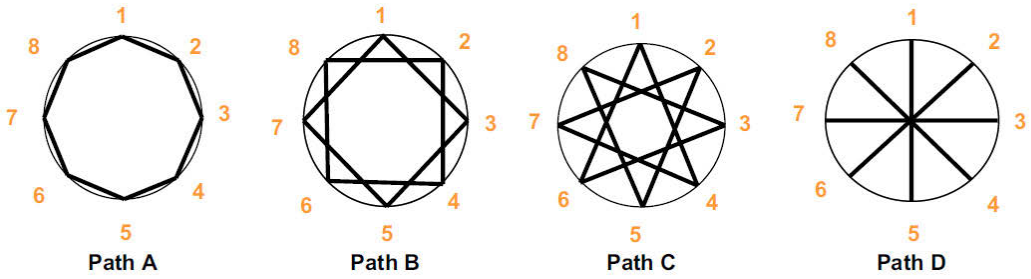


Figure 6-3: Paths for eight sensor arrangement (Lin et al. 2008)

A defect in the pole will affect these paths in different ways. In Lin et al.'s (2008) experiment, the researcher introduced a hole in the centre of the wooden specimen and incrementally increased the radius of the defect and observed the TOF differences in each path. From the results it was found that the relationship between the size of the hole and the ultrasonic wave velocity is linear as depicted in Figure 6-4.

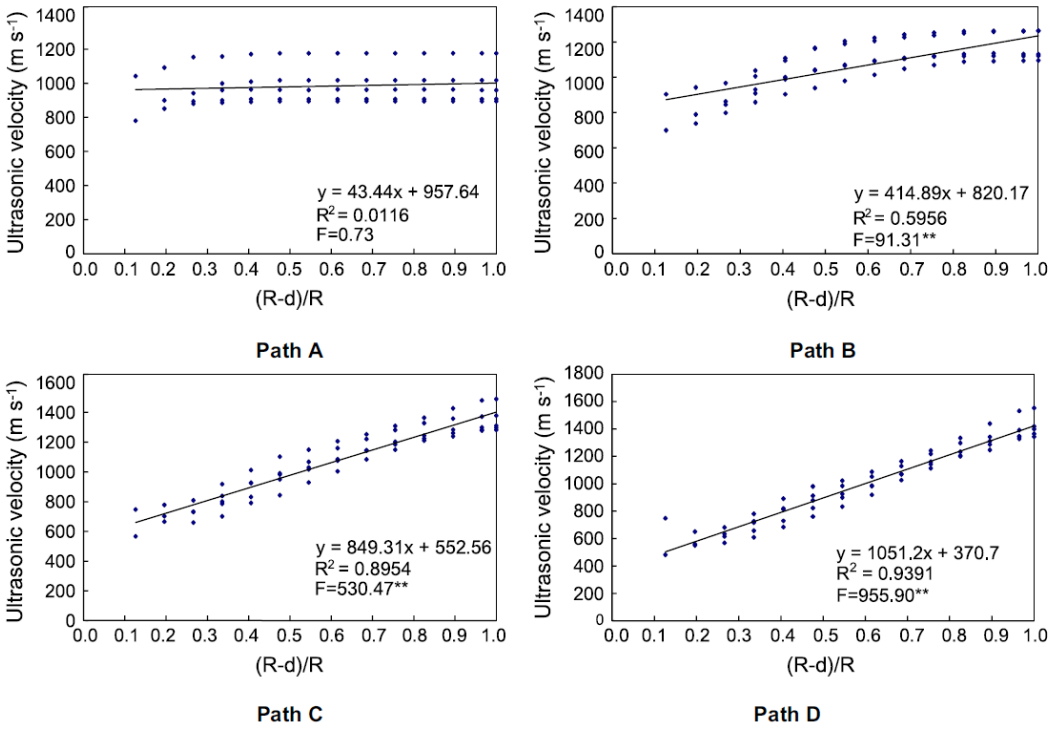


Figure 6-4: Linear relationship between hole size and velocity Lin et al. (2008)

### 6.2.1 Acoustic Tomography

The purpose of measuring the TOF on damaged specimens is to construct a tomographic image of the inside of a pole, displaying possible voids and decayed areas. In comparison to a hole or void, decay is more difficult to detect due to the similar density as the intact wood tissue. Acoustic tomography is widely used for geophysical and medical ultrasonic imaging applications. Unlike X-rays, stress waves strongly interact with the media through which they travel. When encountering a boundary caused by a material with different impedance, processes such as reflection (wave bounces back) and refraction (wave propagates through but changes direction) occur as shown in Figure 6-5.

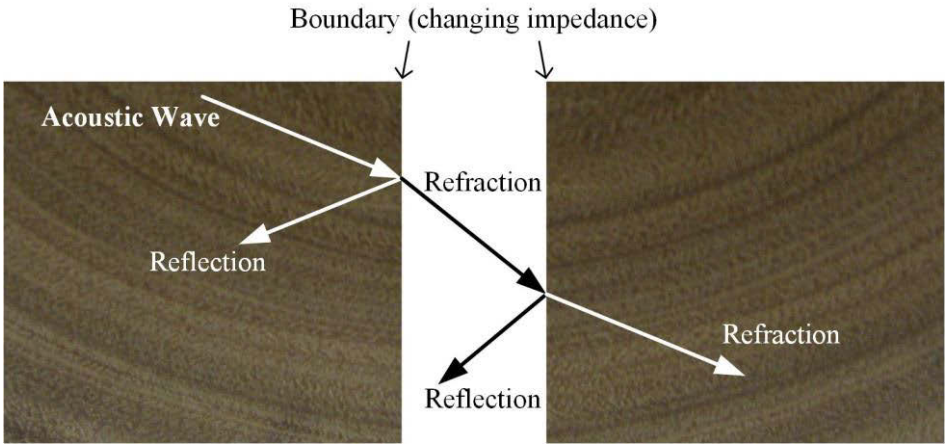


Figure 6-5: Reflection and refraction of stress waves from an impedance discontinuity

In the case of wood this can be the boundary between intact solid wood and decay or air as in a void. In homogeneous material these phenomena can be very strong which makes the reconstruction of ultrasonic images more difficult. This behaviour is also responsible for the loss of wave energy in heavily damaged or cracked wood specimens besides the normal attenuation of stress waves in wood.

Several researches have applied acoustic tomography on standing trees and wooden poles with Tomikawa et al. (1990) being one of the first to apply the technique for inspecting the internal condition of utility poles. On living trees, various researchers have applied this methodology (Comino et al. 2000; Gilbert & Smiley 2004; Lin et al. 2008; X. Wang et al. 2004). Creating an image of the cross-section of a living trees is easier since cracks are typically not present. However, due to the high moisture content, it is harder to distinguish between healthy and rotten wood. Especially early stages of rot have been reported to be difficult to identify. However, the rotten part of a tree or structure has already lost most of its structural load-bearing capacity and it is therefore of great important to be able to identify these areas. When measuring the TOF at several layers, it is possible to compute three-dimensional images as shown in chapter 2.4.2.2 with the image in Figure 2-15 b by Martinis et al. (2004).

The purpose of the presented study is to apply acoustic tomography based on ultrasonic measurements to two eucalyptus species (Spotted Gum and Tallowwood) since most research has been undertaken on European species whose properties are considerably different to the ones of eucalyptus species. In addition, the study investigates the feasibility of using TOF data (measured with the same equipment as for the ultrasonic mate-

rial testing) for the determination of the size of damage in the cross-sectional direction of eucalyptus timber poles.

## 6.3 Damage Detection Methodology

As for the ultrasonic material tests, the only standard dealing with TOF measurements for orthotropic materials is the ASTM International (2008) which, where applicable, was referred to for these tests.

### 6.3.1 Testing Specimens

For the damage detection study, the tested specimens were from the same two new utility poles, one Spotted Gum and one Tallowwood, as the ones used to produce the specimens for the static and ultrasonic material tests. All small clear specimens produced were straight grained and free of any visible defects such as knots or splits. The tested cross-sectional pole sections were cut from the middle of the poles and therefore had the same moisture gradient as the full 5 m pole sections. The small clear testing specimens were produced using only the heartwood of the poles as with the specimens for the other tests. As mentioned above, the difference of the wave propagation behaviour between heartwood and sapwood is not expected to be notable and has not been distinguished in literature. Nonetheless, only the heartwood was used for manufacturing the specimens. A compilation of the specimens used for the damage detection tests is shown in Figure 6-6.

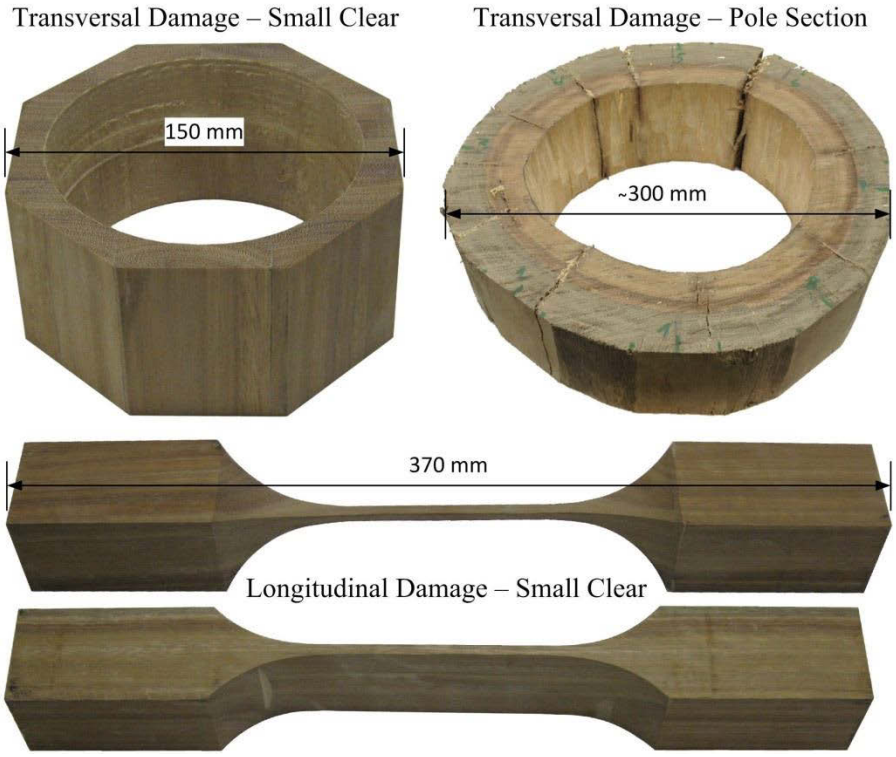


Figure 6-6: Small clear specimens and cross-sectional pole sections used for damage detection

For the ultrasonic tests with small clear specimens, one sample for each test was prepared. As shown with the ultrasonic material tests, the variation of the wave velocity between different small clear specimens was very small (COV ≈1%) and was therefore neglected for the damage detection tests. All specimens were again produced in the wood workshop of the Faculty of Engineering and Information Technology (FEIT) at the University of Technology in Sydney.

### 6.3.2 Small Clear Specimens – Longitudinal

The small clear specimens used to simulate damage in longitudinal direction had an initial size of 370/50/50 mm before their diameter was reduced in the mid-section in steps of 10 mm and finally 5 mm for the smallest dimension tested which was 5 mm as shown in Figure 6-7.

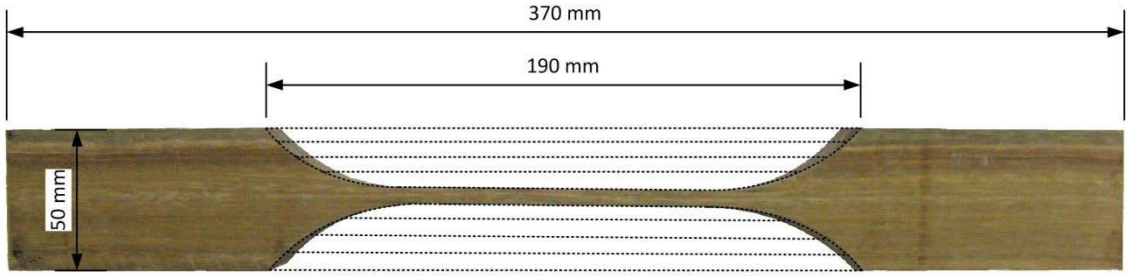


Figure 6-7: Small clear specimens used for longitudinal damage simulation

Two specimens were produced from Spotted Gum in which the diameter of one specimen was reduced in only one dimension and the diameter of the second specimen was reduced in both dimensions, resulting in a final cross section of 50/5 mm for the first case and 5/5 mm for the second case. The transducers used for all ultrasonic tests were the flat 50 mm transducers with a frequency of 24 kHz.

### 6.3.3 Small Clear Specimens – Transversal

The specimen used for the damage in transversal direction investigation is shown in Figure 6-8. The specimen was produced from the assembled block specimen initially used for the ultrasonic determination of the material properties. The specimen was cut to an octagonal shape to allow for perfect coupling with the flat 50 mm transducers. To generate damage of different sizes, damage voids were created in four steps from 41 mm to 121 mm. The different damage cases correspond to a damage area of 7% to 62% of the cross-sectional area.

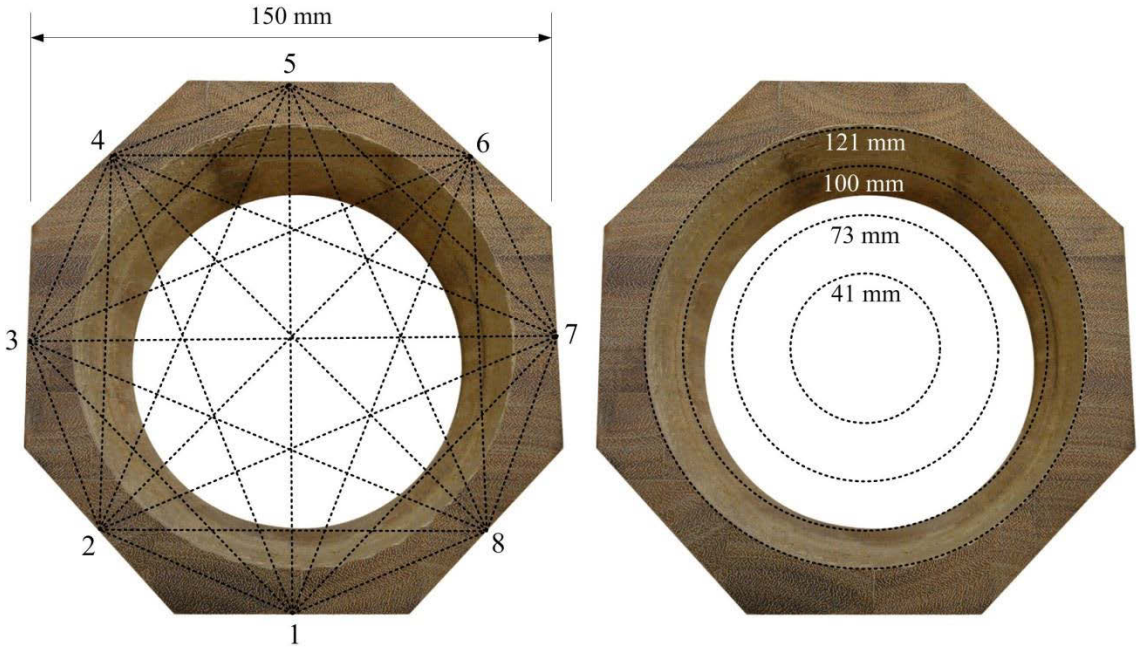


Figure 6-8: Small clear specimens used for the transversal damage simulation

Measurements were taken from each of the eight measurement points to the remaining seven receiving locations as indicated in Figure 6-8. This resulted in a total of 28 measurements per damage case. Unlike in a tree trunk, the annual growth rings were aligned strictly radially and tangentially and not circular.

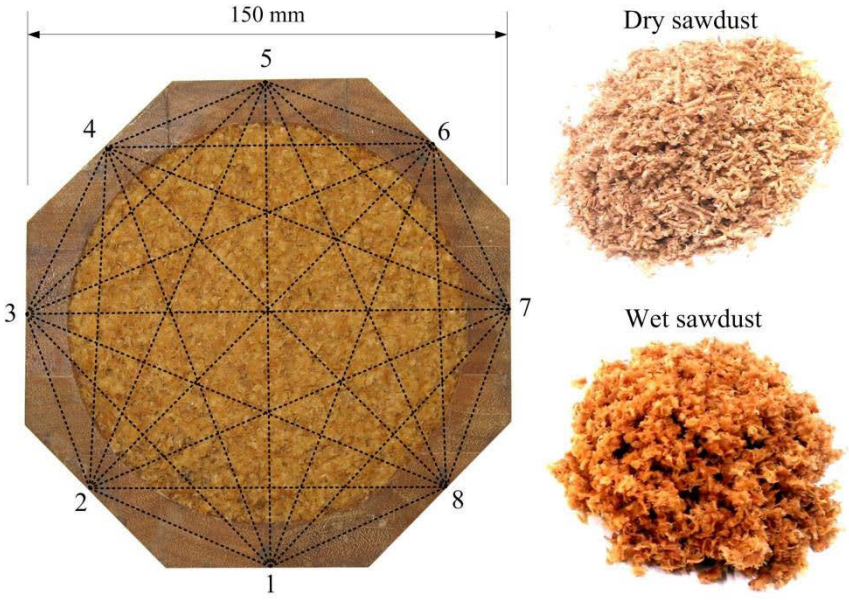


Figure 6-9: Small clear specimen filled with sawdust to simulate rot

Figure 6-9 shows the same specimen as in Figure 6-8 but filled with we sawdust. This was done to simulate rot as it may occur when a pole is attacked by fungi. Tests were conducted with the void filled with dry and wet sawdust and with different levels of

compression.

In addition to the experimental work, the damage cases were also modelled numerically to verify the results.

### 6.3.4 Pole Sections – Transversal

Ausgrid (2011) states the following in their pole inspection standard: ”Ausgrid requires that all poles have a minimum wall thickness of greater than 50 mm anywhere at or below ground line. If the minimum was thickness measurements obtained from the internal inspection are 50 mm or less, at or below ground line, the pole is classified as defective.” For this reason, the maximum damage size was chosen to leave a remaining circle of wood of minimum 50 mm.

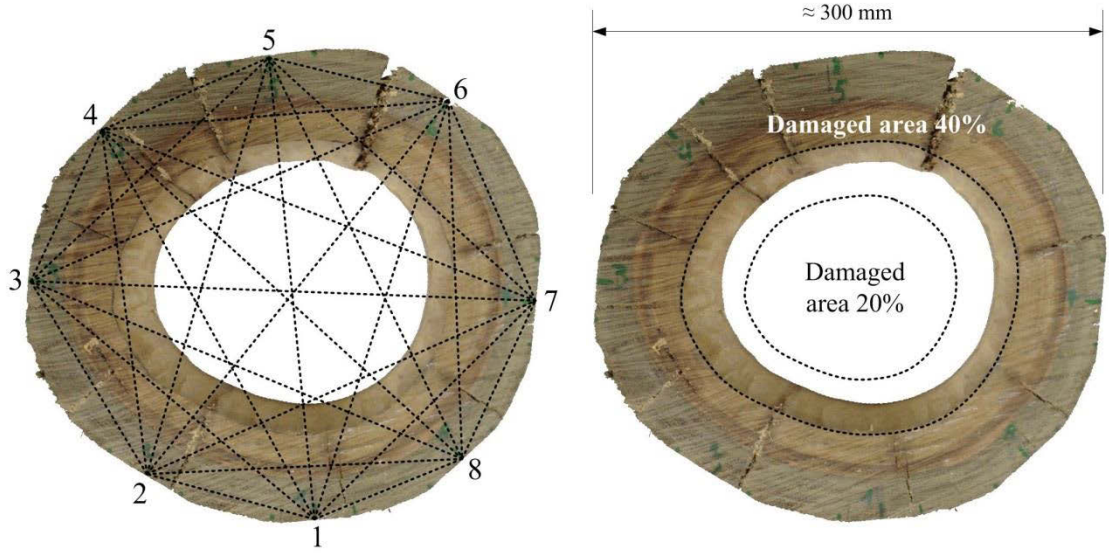


Figure 6-10: Cross-sectional pole section specimen used for transversal damage detection

Figure 6-10 shows the Spotted Gum pole section as it was used for transversal damage detection. The specimen was first tested with no damage, than with a hole which occupied an area of 20% of the whole pole cross section and finally with a damaged area of 40%. The hole was cut parallel to the outside edge and not round as with the small clear specimens. The remaining circle of wood with a 40% damage was 50 mm for the Tallowwood and 54 mm for the Spotted Gum specimen.

#### 6.3.4.1 Influence of Cracks

To better understand the influence of cracks on the TOF, a simple test with two separate specimens with an increasing gap in between the specimens was performed. The crack

size was increased from 0.5 mm to 20 mm. Measurements were taken only in transversal direction since this is the only plane where cracks occur in wood.

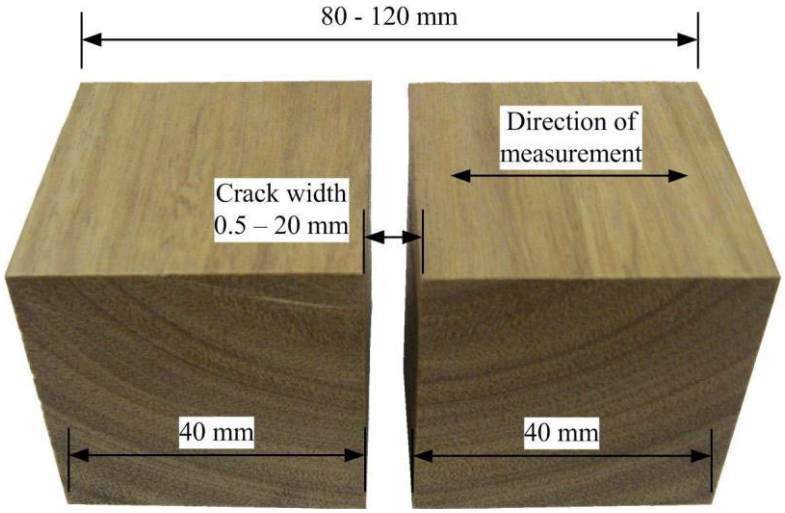


Figure 6-11: Specimens used for measuring the TOF with increasing crack size

### 6.3.5 Numerical Modelling

For the accurate numerical modelling of the experimental case, an orthotropic model was created. For the numerical model of Spotted Gum, the material properties from the static tests were used as input parameters, i.e. $\rho$ = 1060 kg/m$^3$, $E_x$ = 1,499 N/mm$^2$, $E_y$ = 2,405 N/mm$^2$, $E_z$ = 26,174 N/mm$^2$, $G_{yz}$ = 1,739 N/mm$^2$, $G_{xz}$ = 1,530 N/mm$^2$, $v_{xy}$ = 0.48, $v_{yz}$= 0.45, $v_{xz}$ = 0.047, $G_{xy}$ = 840 N/mm$^2$.

The ultrasonic pulse signal used for the numerical simulation had to reflect the ultrasonic transducer signal used in the experiment. Baskaran (2007) described the typical trigger pulse of a piezoelectric transducer with the following formula

$$F(t) = \left\{\left[1 - \cos\left(\frac{2\pi f}{3}t\right)\right]\cos(2\pi f t)\right\}, for\ 0 \le t \le \frac{3.0}{f} \ldots \quad (6\text{-}2)$$

where $f$ = frequency and $t$ = time. Substituting a frequency of 24 kHz into the equation the pulse depicted in Figure 6-12 is obtained.

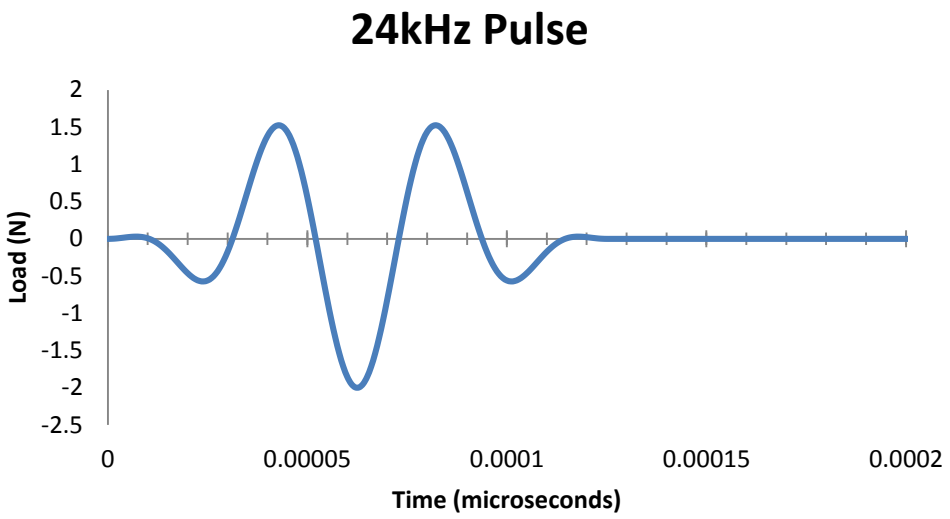


Figure 6-12: Input signal used for the numerical models

This transmitting pulse was used as input signal for all numerical models. A mesh sensitivity study was necessary to ensure the robustness and reliability of the numerical results. The model was produced using polar coordinates and mesh. This set up allowed for an easier implementation of the polar orthotropic material properties.

As mentioned above, a polar mesh was used in this study, as it simplifies the process of applying polar orthotropic material properties to the model. It also eases the process of defining the hole inside the model to represent the damage. Three different meshes were used for the investigation, each of which had the same geometry. This study refers to the meshes by the number of angles that were used, i.e. Mesh 128, Mesh 256 and Mesh 512.

A denser mesh does produce more accurate results, however, it is more computationally expensive. A convergence tests were undertaken on the three meshes to determine which mesh to use during the modelling procedure.

From the graph it can be seen that Mesh 256 and Mesh 512 provide similar results to a TOF value of 84 microseconds. The pattern produced by Mesh 128, however, shows a different pattern. Since the computational resources required to simulate Mesh 512 are too time consuming, an alternative must considered. Mesh 256 is more computationally feasible and produces results that are nearly identical to Mesh 512. Hence, from the convergence study it was concluded that Mesh 256 will be used for the computations in this study.

## 6.4 Results and Discussion

### 6.4.1 Damage Detection – Longitudinal

Figure 6-13 shows the influence of the reduction of the specimen diameter on the P-wave velocity in longitudinal direction. In the first case, the cross-section was reduced in one dimension only and the maximum reduction of the wave velocity was 4% when the cross section was reduced to 10% of its original size. For the second case, where the specimen's cross-section was reduced in two dimensions, the wave velocity with the maximum reduction, which equals a size of the original cross-section of only 1%, is 6.5% lower compared the original wave velocity.

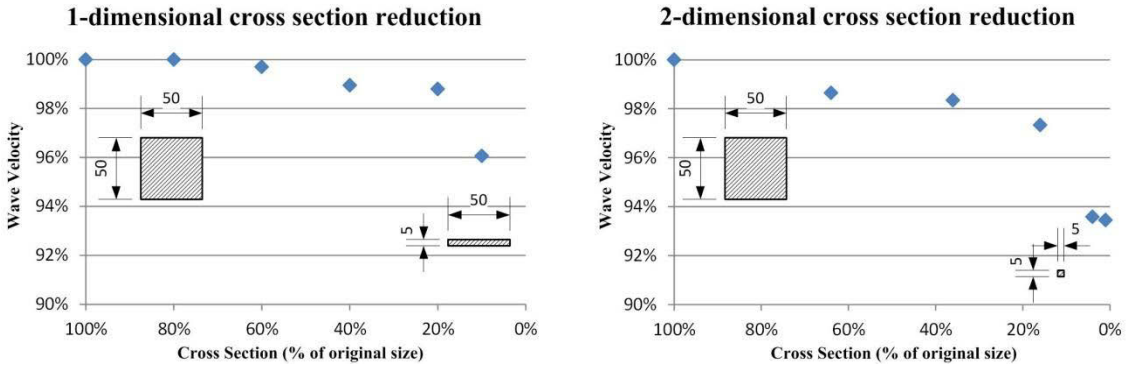


Figure 6-13: Reduction of the wave velocity as a function of the reduction of the specimen cross-section

Bucur (1984) tested spruce specimens with a length of 300 mm and a cross-section of 100/100 mm for the P-wave velocity in longitudinal direction with a frequency of 1 MHz. The cross-section was reduced in one dimension to a plate with a cross-section of 100/7 mm. The researcher's results showed a reduction of the wave velocity of about 8.5% from the original to the minimum cross-section. However, the wave velocity reduced continuously and became almost constant the smaller the cross-section.

For the results obtained from the one-dimensional cross-section reduction tests in this study, the velocity was almost constant for the first three measurements and again when the cross-section was reduced for the fourth and fifth time. The biggest drop in wave velocity, however, occurred with the last reduction of the cross-section to 5 mm which was 10% of the initial specimen thickness. This trend can also be observed for the specimen whose cross-section was reduced in both dimensions, however, with the wave velocity starting to decrease already after the first cross-section reduction. For the last two

measurements with cross-sections of 10/10 mm and 5/5 mm, respectively, the wave velocities are almost constant which is in agreement with the results obtained by Bucur (1984).

However, the reduction of the wave velocity is small compared to other factors, e.g. damage type and moisture, which also have an influence on the propagation velocity of the wave.

### 6.4.2 Damage Detection – Transversal

#### 6.4.2.1 Influence of Cracks

For the Spotted Gum specimen with dimensions of 85/50/50 mm and annual growth rings aligned approximately at a 45° angle, the TOF was first measured as a whole, before it was cut in half, and then tested with an increasing gap between the two specimen halves.

Figure 6-14 shows the decreasing wave velocity with increasing gap size. The two measurements with no gap (crack width is 0 mm) present the TOF measurements of i) the intact specimen (maximum wave velocity) and ii) the specimen cut in half with both halves pressed together with no visible gap in between. For the second case, the velocity decreased by 4% compared to the maximum velocity. After this point, the wave velocity decreases with an increasing air gap.

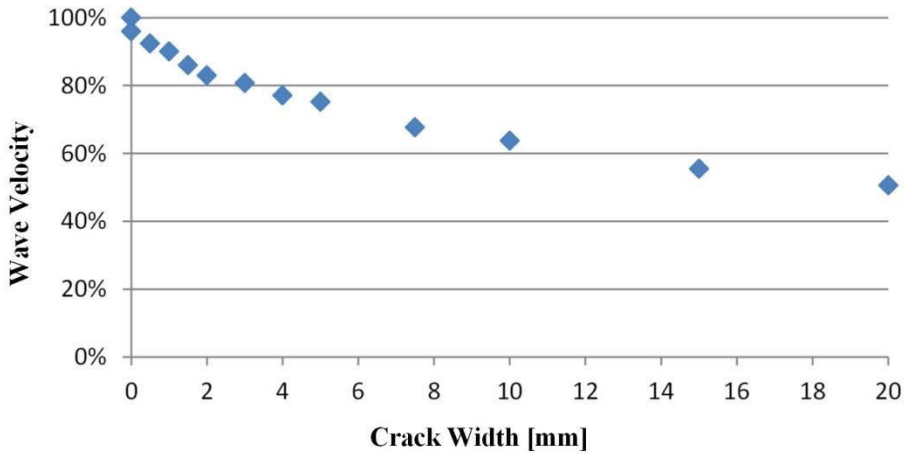


Figure 6-14: Influence of the crack width on the wave velocity

The wave velocities result from the velocity and distance travelled through the specimen added to the velocity and distance travelled through the air gap at 343 m/s. With an

increasing gap width, the attenuation increased to a point where the arriving signal was too weak to exactly determine the time of the wave arrival. This happened after a 20 mm gap width. All measurements were taken with a voltage setting of 500 V, a gain of 100x and an impulse length of 20 µs, the same settings used for all non-destructive tests.

#### 6.4.2.2 Small Clear Specimens

The results obtained from the tests on the octagonal small clear specimen (see chapter 6.3.3) are presented in this section. Figure 6-15 presents the determined TOF measurements with increasing damage size for the measurements taken directly across the specimen (i.e. paths 1-5, 2-6, 3-7 and 4-8 according to Figure 6-8). Since the tested specimen was glued together from smaller pieces, (aligned in radial and tangential direction) the TOFs were not the same in both directions or at the 45 degrees direction. However, with increasing damage size, the influence of the direction of wave propagation became smaller. The trend shows a nearly linear increase in the wave velocity.

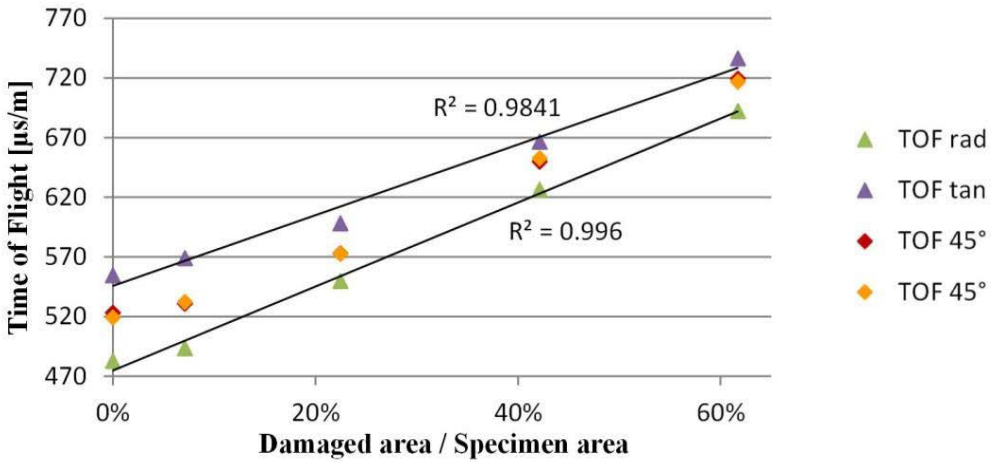


Figure 6-15: Increasing TOF across the specimen as a function of increased damaged area

The TOF increases by 43% in radial, 33% in tangential direction and 38% at a 45° angle. From the tests on the influence of cracks, it became evident that ultrasonic waves cannot bypass a gap larger than approximately 20 mm with the used equipment and settings. From these tests and from the fact that the ultrasonic wave velocity in air is slower than in the tested specimen, it can be concluded that the measured TOF is from the wave propagating around the specimen and not through the damage as illustrated in Figure 6-17.

In order to compare the influence of the damage to the wave velocity measurements not only across the specimen but also between all sensor locations, the measured times of the same paths (i.e. paths 1-2, 2-3, 3-4, … and 1-3, 2-4, 3-5, … and 1-4, 2-5, 3-6, … according to Figure 6-8) were combined and averaged. The results are shown in Figure 6-16 with 1 corner presenting the shortest measured distances across one corner, 2 corners presenting the measurements across two corners, and so on.

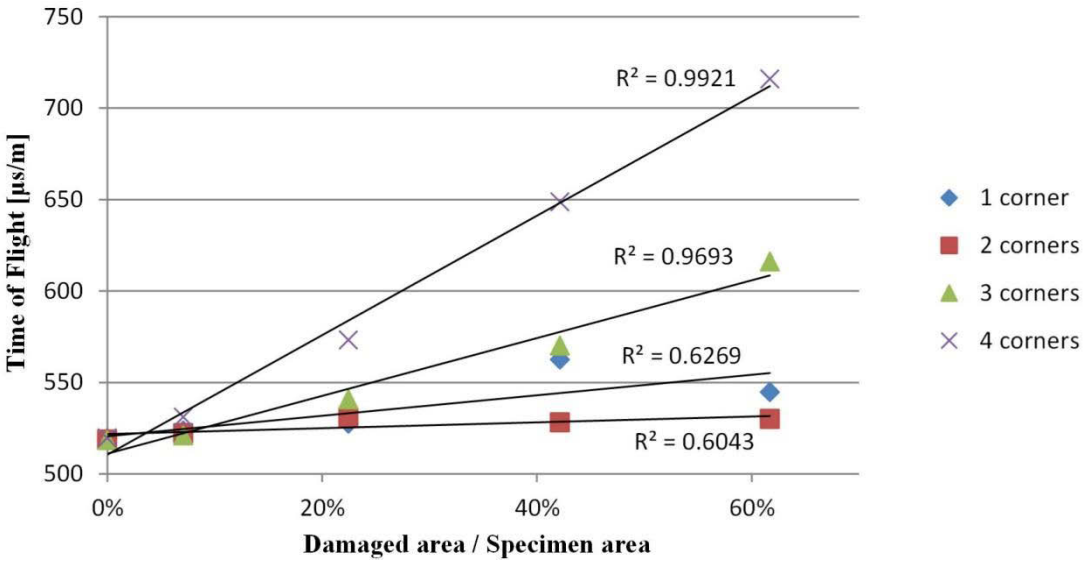


Figure 6-16: Combined and averaged time of flight measurements between all sensor locations

As already shown in Figure 6-15, the measurements across 4 corners have a high linear correlation with an R squared value of over 99%. Also the TOF measurements across 3 corners still have a high linear correlation with 97%. For the measurements across two and one corner, the values drop which is due to the fact that the travelled distances between the sensors get shorter and the transducers were placed manually and therefore contain inaccuracy. From the graph, it can also be seen that for the measurements across 1 and 2 corners, the influence of the damage is virtually negligible. Hence, for ultrasonic wave testing, these measurements should not be taken into account for calculating the damage size.

#### 6.4.2.3 Numerical Results

In order to correctly simulate the experimental testing, a study had to be conducted that investigates if the impulse of the experimental transducers, which had a diameter of 50 mm, were sent and received from the centre or the edge of the transducers.

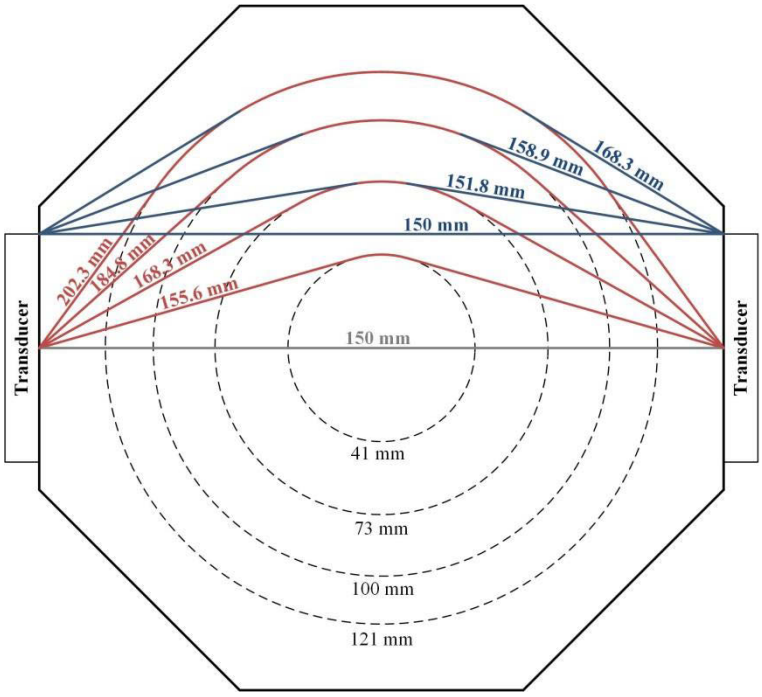


Figure 6-17: Shortest travelling distance from centre to centre and edge to edge of the transducers

Figure 6-17 presents the actual distances travelled by the ultrasonic wave from transducer centre to centre (red lines) and edge to edge (blue lines) for each damage case. A comparison of the TOFs calculated using the measured distances - centre to centre and edge to edge - (calculated lines), to the experimentally determined TOF values (triangle and diamond symbols) is presented in Figure 6-18.

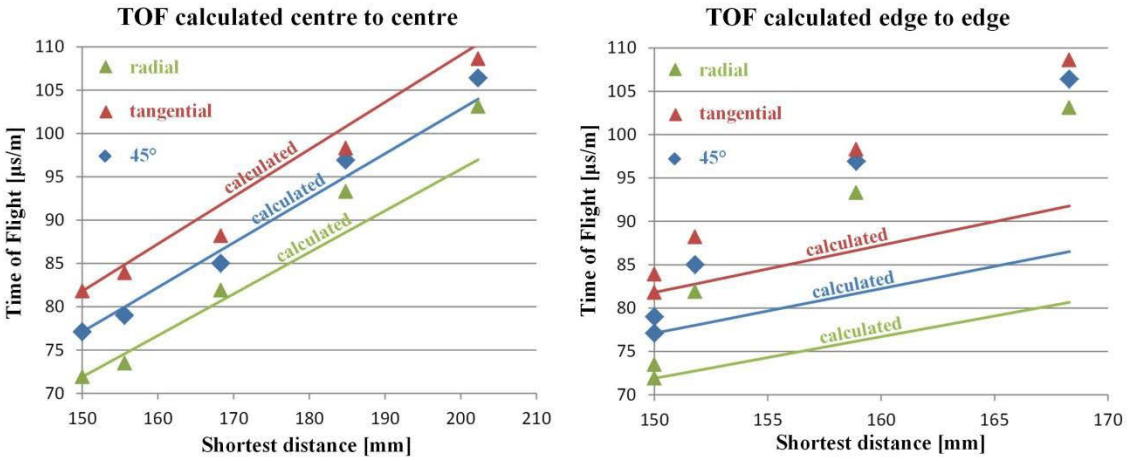


Figure 6-18: Comparison of experimentally measured TOFs against TOFs calculated from centre to centre and edge to edge of transducers

It can be seen that the experimental data corresponds much better to the centre to centre case, than the edge to edge case. While for the edge to edge case, the calculated times much too fast; for the centre to centre case, the measured TOFs are slightly faster in

tangential direction and slightly slower in radial direction in comparison to the calculated times while in 45 degree direction the experimental data almost matches the calculated values. From these results, it was concluded to use the centre to centre case for the numerical modelling of the wave sending location and the wave receiving location.

Table 6-1: Comparison of experimental and numerical TOFs

| **TOF's with different hole diameters** [µs] | | | | | |
|---|---|---|---|---|---|
| | ***Solid*** | ***41 mm*** | ***73 mm*** | ***100 mm*** | ***121 mm*** |
| Experimental | 81.8 | 83.9 | 88.2 | 98.3 | 108.6 |
| Numerical | 85 | 88 | 94 | 104 | 120 |
| Difference | 3% | 3% | 5% | 6% | 12% |

To gain a deeper understanding of how ultrasonic stress waves propagate through the cross-section of damaged timber pole specimen, a numerical analysis focusing on stress distribution was undertaken. The particular focus of this analysis was to understand how the stress wave propagation interacts with the damage void in the centre of the pole specimen. In addition, this investigation was used to verify the findings from the experimental damage detection study. Figure 6-19 displays the obtained numerical stress wave plots showing the stress distribution across the damaged pole section at different times of the stress wave propagation. It is noted that the vertical direction represents the material properties that are perpendicular to the grains and the horizontal direction represents the material properties that are parallel to the grains.

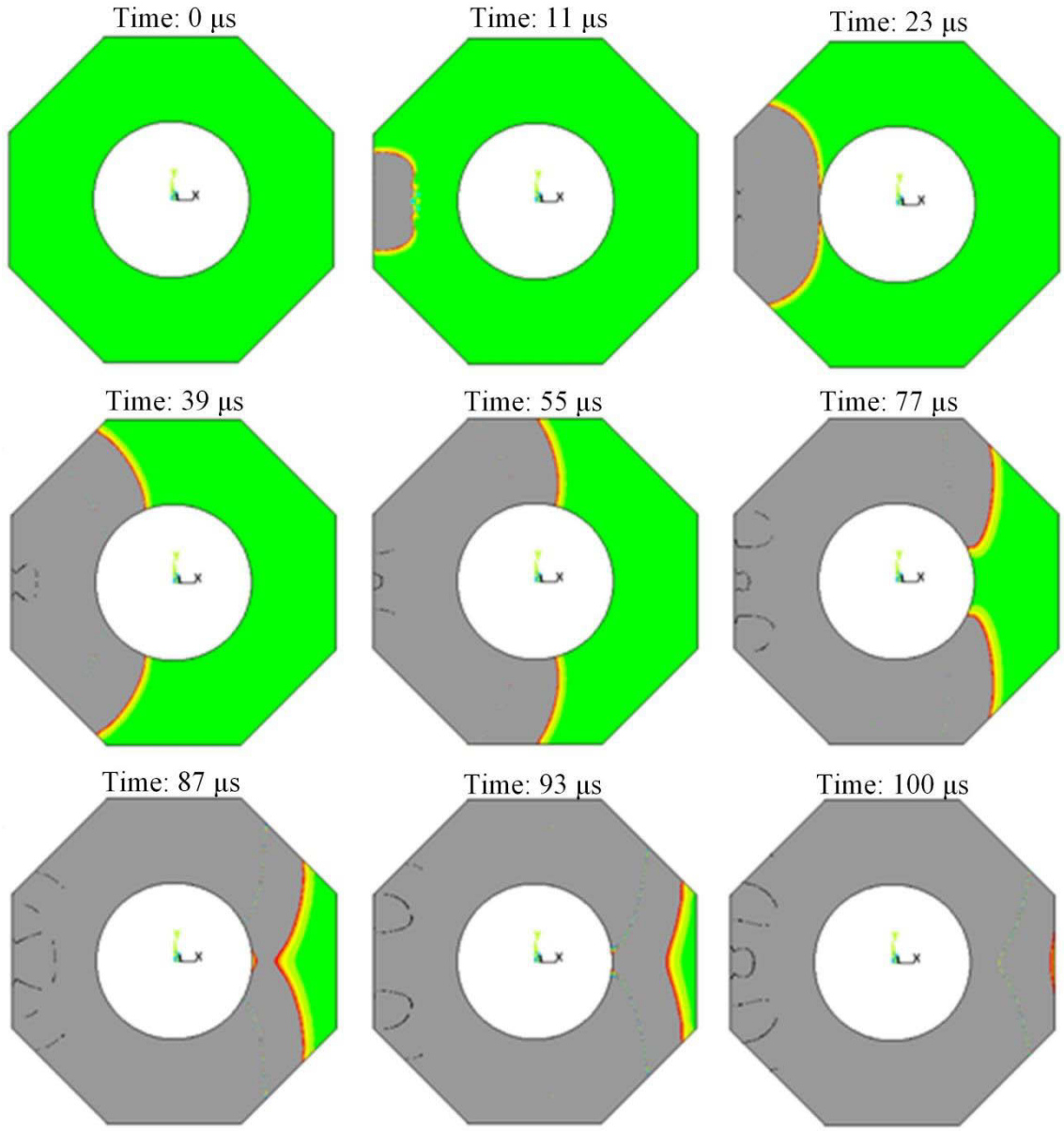


Figure 6-19: Numerical simulation of propagating ultrasonic wave (grey) through specimen cross-section (green) at different times

The initial impulse is applied to the model with a wide wave front. This is because the MOE in the vertical direction of the model is higher than the horizontal direction of the model due to the orientation of the grains. As the wave front reaches the holes, it separates into two wave fronts facing the direction that is defined by the edge that is adjacent to the edge where the pulse was applied and the circular hole. The wave front changes direction again after it reaches the next edge. At the next edge, the two wave fronts meet and appear to split towards the left and the right. The wave travelling to the right proceeds to the receiving transducer thus measuring the TOF.

#### 6.4.2.4 Simulating Rot

These tests were performed to investigate if rot damage, which is most difficult to identify, can be simulated by filling a void with sawdust in dry and wet condition. These tests were conducted on the specimen with the largest hole and the transducers located in opposite locations (i.e. 1–5, 2–6, 3–7, 4–8) - it is easiest to locate a big rotten area compared to only a small one. In order for the rot damage to have an influence on the TOF, the wave would need to propagate faster through the rot from the sending to the receiving transducer than around the artificially damaged area. The speed of sound in water is approximately 1484 m/s at 20° Celsius and therefore slower as in radial and tangential direction of the tested species where it lies between 1760 m/s and 2095 m/s.

The dry sawdust (MC≈12%) was not expected to make a difference in the TOF measurements since its compressed density was only approximately 200 kg/m$^3$ and therefore still comprised a lot of air. The compressed wet sawdust, however, had a density of about 800 kg/m$^3$ and was therefore four times denser than the dry sawdust but still less dense than the intact wood. Therefore, for both cases, the sawdust did not make a difference on the TOF. In a last test, the void was filled with only water, and as expected the wave was fester travelling through the water than around the damage. The shortest distance around the damage was 202 mm (see Figure 6-17) in comparison to the shortest, direct distance of 150 mm and therefore around 35% longer. The wave velocity in solid wood, however, is merely around 20% faster than the one in water and the wave travelling through water therefore arrived first at the receiving transducer.

The density of actual rot in poles is unknown, but based on these tests it can be assumed that rot does have an influence on the TOF. The wave velocities in radial but especially also in tangential direction of the two tested species are very fast (faster than the speed of sound in water) and even very wet rot would be detected if the wood structure gets affected by the rot.

#### 6.4.2.5 Pole Sections

The procedure of measuring the TOF on the cross-sectional pole sections was the same as performed on the small clear specimen. In Figure 6-20 the results from the undamaged specimen and both damage cases are shown. The figures a) show the TOF as they were measured based on the distance between the centre of the transducers while in fig-

ures b) the TOF for the undamaged specimen were adjusted to the same value to display the increasing TOF with increasing damage size. For the sake of uniformity the measurement locations were denominated using the same notation (i.e. 1 corner, 2 corners, …) even though the specimens were round and not octagonal. The degrees in brackets indicate the angle between the sending and receiving transducer faces.

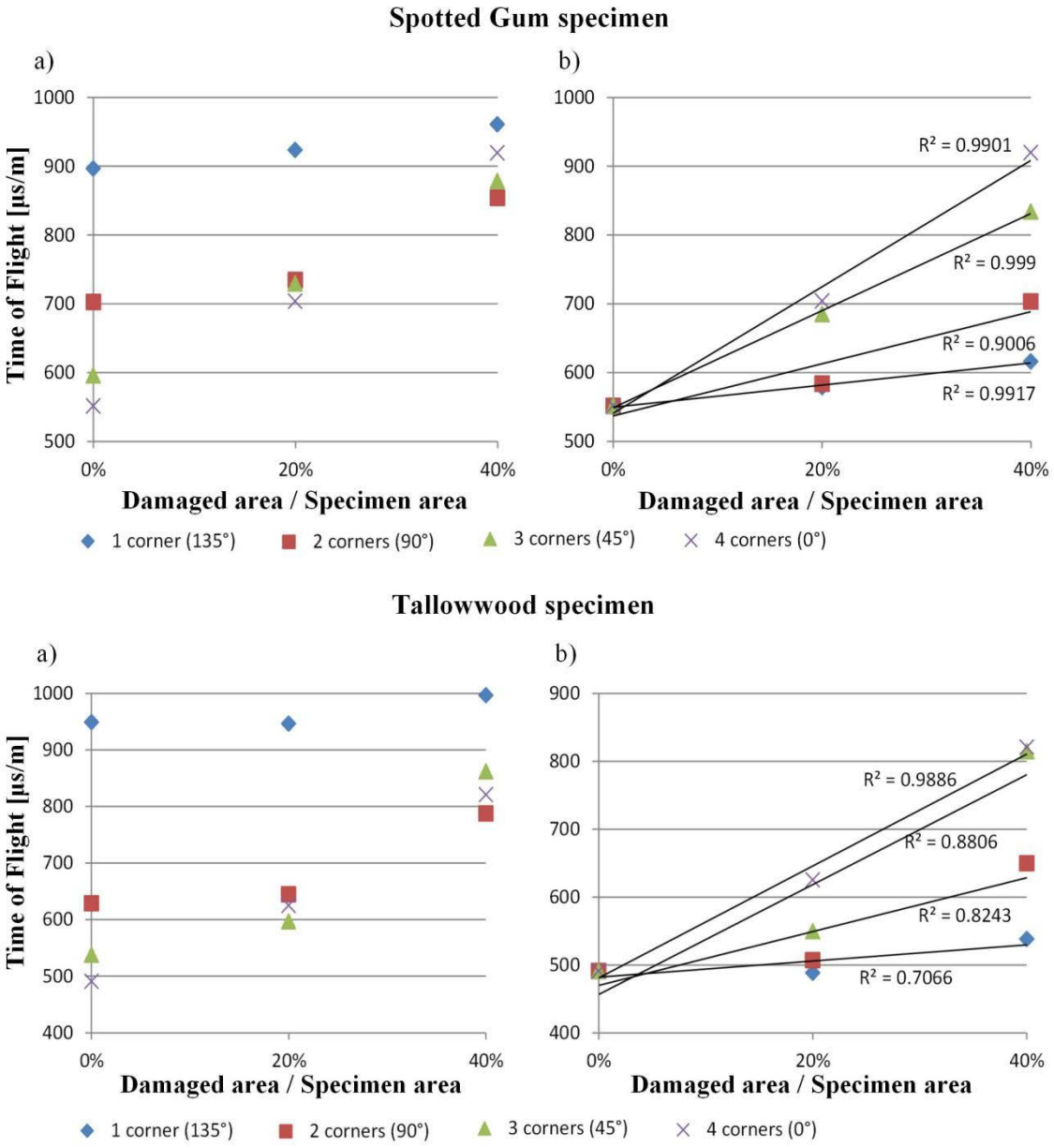


Figure 6-20: Combined and averaged TOF measurements of Spotted Gum and Tallowwood specimen between all sensor locations a) original data and b) with adjusted TOFs

The linearity of the TOFs measured on the Spotted Gum specimen is higher in comparison to the TOFs measured on the Tallowwood specimen and also higher than the results obtained from the small clear specimen. This is surprising since the Spotted Gum pole disc showed heavier cracking than the Tallowwood disc as shown in Figure 6-21. The

behaviour regarding the increasing TOF with increasing damage size was the same however. For all specimens, the TOF across the specimen increased the most while the TOF to the neighbouring measurement points show the smallest increase. In general, the increase of the TOF in the cross-sectional pole sections was bigger than in the small clear specimens.

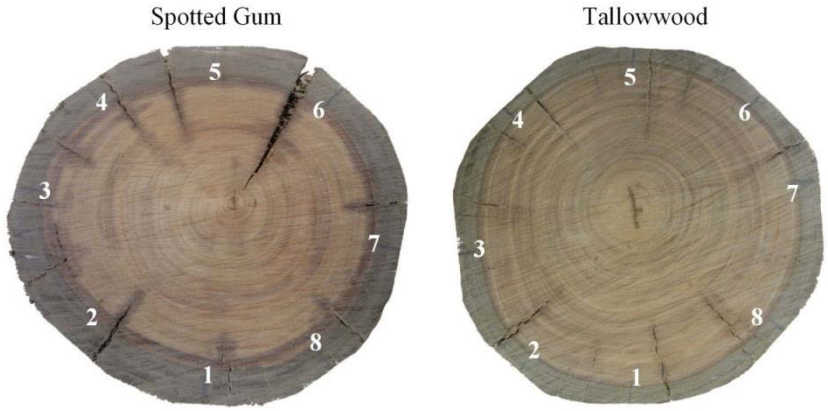


Figure 6-21: Cross-sectional pole disc specimens used for the TOF measurements in undamaged state indicating the measurement locations

The increase between the initial TOF measurement on the undamaged specimen and the TOF with the biggest damage are listed in Table 6-2. Except for the measurements across one corner, the TOF of the pole discs increase more than the ones of the small clear specimen.

Table 6-2: Increase of the TOF between undamaged and maximum damage specimen

| **TOF increase** | | | | |
|---|---|---|---|---|
| ***Specimen*** | ***1 corner*** | ***2 corners*** | ***3 corners*** | ***4 corners*** |
| Spotted Gum (pole disc) | 7.2% | 21.6% | 47.4% | 66.7% |
| Tallowwood (pole disc) | 5.0% | 25.2% | 60.2% | 67.2% |
| Spotted Gum (small clear) | 4.9% | 2.2% | 18.8% | 37.8% |

The reason for the larger increase of the TOFs of the pole discs are the inherited cracks which slow down the wave and attenuate its energy making it impossible for the wave to travel through too wide gaps. The higher variation in TOF is generally beneficial for detecting internal damage. Determining the exact arrival of the wave becomes more challenging, however. The first arriving wave may be travelling through the cracks, losing a lot of its energy, while a slower wave may be arriving containing more energy. Since for these tests the wave arrival was determined manually, always the very first

wave arrival was chosen for determining the TOF. However, if the TOFs were determined automatically, these waves may be missed if the signal to noise ratio becomes too big.

A further observation was made when calculating and comparing the dynamic MOEs of the different damage cases. While the single MOE values are not very meaningful when calculating the average MOEs of all measurements, (28 for each damage case) the averages of the damaged specimens roughly decreased by the percentage of the damaged area. Table 6-3 presents these proportions.

Table 6-3: Decreasing averaged MOE values with increasing damage size

| **Averaged MOE values** | | | |
|---|---|---|---|
| ***Specimen*** | ***0% damage*** | ***20% damage*** | ***40% damage*** |
| Spotted Gum (pole disc) | 100% (2395 N/mm$^2$) | 80% (1916 N/mm$^2$) | 62% (1480 N/mm$^2$) |
| Tallowwood (pole disc) | 100% (2874 N/mm$^2$) | 83% (2400 N/mm$^2$) | 57% (1625 N/mm$^2$) |

When taking the undamaged specimen as 100%, the averaged MOE values decreased by 20% for Spotted Gum and 17% for Tallowwood at a damaged area of 20%. For the 40% damaged area, the MOEs decreased by 38% for Spotted Gum and 43% for Tallowwood compared to the sound pole discs. The relationships are quite close for both specimens despite the fact that the Spotted Gum disc had significantly larger cracks compared to the Tallowwood disc. For the small clear specimen, these relationships did not match since the TOF did not decrease as much due to the missing cracks. To verify these finding, a future study should be conducted on further test specimens.

### 6.4.3 Acoustic Tomography

From the TOF measurements, a tomographic image can be generated to illustrate the internal conditions of a testing specimen and to estimate the size of any damage such as a void or hole. To facilitate the tomographic imaging, numerical simulations were performed using the following sensor arrangement according to the experimental tests.

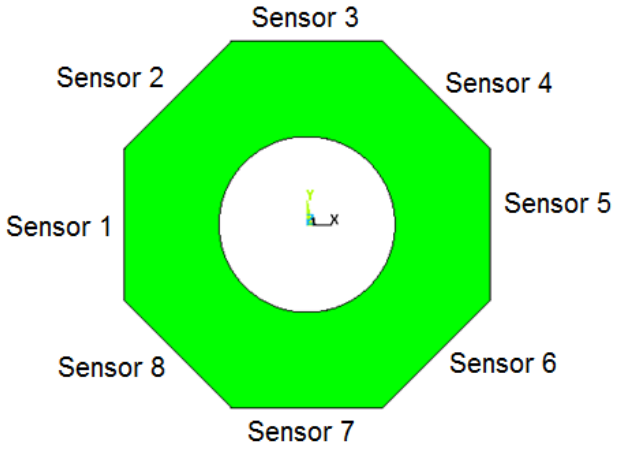


Figure 6-22: Numerical setup and sensor arrangement according to experimental tests

At each sensor location, the displacements and corresponding velocities were recorded to determine the TOF values for each wave travel path. From the numerical simulation, the relationship between the TOF readings and the size of the hole could be established for each sensor. The results of this relationship are shown in Table 6-4.

Table 6-4: Relationships between the sending transducers (sensor 1) and receiving transducer

| **Relationships** | | |
|---|---|---|
| ***Sensors*** | ***Relationship*** | $R^2$ |
| 2 and 8 | y = -14.375x + 391.88 | 0.0718 |
| 3 and 7 | y = 30.455x - 1419.2 | 0.8866 |
| 4 and 6 | y = 5.8965x - 366.98 | 0.9563 |
| 5 | y = 3.5271x – 270.19 | 0.8881 |

Using this relationship, an algorithm was produced that calculates the size of the hole based on the TOF measurements and that generates a graphical representation of the readings. The following TOF measurements from the experimental tests were supplied to the algorithm: Sensor 2 and 8, 23 µs; Sensor 3 and 7, 49 µs; Sensors 4 and 6, 75 µs and Sensor 5, 94 µs.

This information in combination with the relationship between the size of the hole and the TOF values was used to generate the tomographic image displayed in Figure 6-23. The red areas represent the presence of timber material and the blue areas represent the hole in the material. All other colours in between red and blue represent the uncertainty between the presence of the material and the hole.

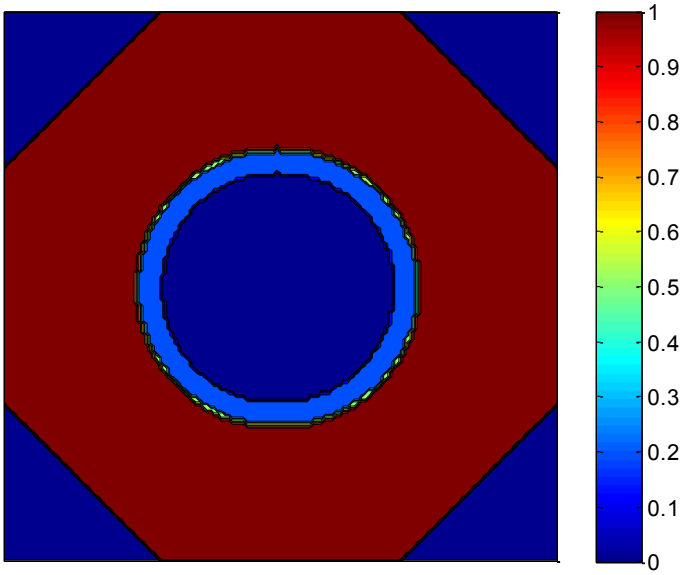


Figure 6-23: Tomographic image resulting from the experimentally measured TOF

For this case with an exactly round hole, the tomographic image represents the real case very accurately.

## 6.5 Conclusions

For the two tested eucalyptus species, the ultrasonic-based damage detection method produced reliable and reproducible results. The fact that ultrasonic waves travel very fast through healthy material of these high density woods helps to produce more reliable results as they have been reported by other researchers for woods with lower ultrasonic velocities.

Due to the fact that the velocity of intact timber material compared to voids (air) is larger by a factor of approximately 5.6 (using the average measured radial and tangential velocities from both species of approximately 1900 m/s versus the speed of sound in air of approximately 340 m/s), makes identifying voids easier. In the presented research work, also the tests conducted with simulated rot produced accurate results since the ultrasonic wave travelled much faster around the damaged area rather than through it. Since the rot damage simulated in this research consisted of sawdust mixed with water, it cannot be concluded that rot, as it actually occurs in utility poles in service, has the same properties and influence on the wave propagation velocity. For this reason, tests on real pole sections with rot damage must be conducted to confirm the experimental

laboratory results.

It must also be noted that internal damage has a smaller influence on the remaining strength of a pole compared to external damage, since the heavy stresses from bending occur on the outside fibres of the pole. Therefore, internal damage only becomes significant from a certain size onwards, which makes the damage detection easier, since large-size damage has a greater influence on the wave velocity and will therefore be detected easier.

# 7 SYNTHESIS

## 7.1 Discussion

In this thesis, thorough investigations have been conducted in order to develop a novel non-destructive testing methods based on ultrasonic waves for the material characterisation and damage detection of in-situ eucalyptus utility poles. Such research has not been carried out for high density woods such as the two investigated eucalyptus species, i.e. Spotted Gum and Tallowwood.

Ultrasonic tests have many advantages over static tests such as the non-destructive nature of the tests, the easier and less time consuming testing approach and the more cost effective application. Static tests, however, produce more reliable results and are therefore needed to qualify and calibrate ultrasonic testing. Once the ultrasonic tests are calibrated, their advantages clearly predominate and the fact that ultrasonic tests can be carried out in the field make them the first choice for in-situ material characterization.

The aim of the conducted tests was twofold: firstly, the pole's material properties can be characterised non-destructively in contrast to static testing and empirical values, and secondly, the TOF approach is capable of identifying internal damage based on wave velocities. However, the presented methods rely on static values for calibration and will become more accurate and robust with the testing and analysis of a larger number of poles.

### 7.1.1 Static Results

For the static tests, recommendations of the testing procedure for the 4-point bending test in radial and tangential direction and for the Poisson's ratio tests were made and additional practical testing advices for further material tests were provided.

The comparison of the bending, compression and tensile tests for determining the MOE showed that all methods produce similar results. Especially the bending and compression values matched very well for both species. Since the results were so close and the compression test requires smaller specimens and is easier to carry out, it can be considered as standard test for the determination of MOE values. For the remaining material properties (tensile strength, compression strength, bending strength and Poisson's ratios), reference values were determined where no literature values were available before. Where literature values were available, the obtained results corresponded well to those values.

The fact that material testing of timber always implies uncertainties due to its inhomogeneous and orthotropic characteristics and the lack of standards for certain tests makes it a challenging task compared to steel or concrete testing. Missing data for material properties of Spotted Gum and Tallowwood in the radial and tangential direction made testing indispensable.

The tension tests in radial and tangential direction were not conducted within the framework of these tests but would complete the testing comparison of MOEs of all values. To fully complete the investigation on all elastic properties, the Poisson's ratio and the shear modulus should be investigated.

### 7.1.2 Ultrasonic Results

The conducted ultrasonic tests were i) material tests that were compared against static testing in order to calibrate them for material characterization, and ii) damage detection tests. Both sets of tests were based on the TOF method. Factors were calculated which can be used to adjust the ultrasonic results to the static results. Furthermore, the influence of the moisture content of the timber and the grain angle were investigated. For the moisture content study, a linear behaviour of the wave velocity as a function of the moisture content was found, as previously shown by researchers for other woods. For

the influence of the grain angle, several available formulas were compared against the experimental results with the Hankinson formula delivering the most accurate results. The trigonometric exponents which complemented the formula to exactly match the experimental case were determined and can be used as an accurate adjustment if the grain angle is an essential feature, for example for poles with strong spiral growth.
For the two tested eucalyptus species, the ultrasonic damage detection method produced reliable and reproducible results. The fact that ultrasonic waves travel very fast through healthy material of these high density woods helps to produce more reliable results as they have been reported by other researchers for woods with lower ultrasonic velocities.

The damage detection tests yielded very accurate and repeatable results which were visualized using tomographic imaging. The fact that the ultrasonic wave velocity in the two investigated high density eucalyptus species in transversal direction was very high in comparison with other timber species made the detection of internal voids more reliable. This, however, was only proven for the experimental case under laboratory conditions and needs to be further verified for in-situ tests. Rot was simulated using wet compressed sawdust which did not have an influence on the reliability of the tests. However, in-situ test must be conducted to reveal if the method also yields reliable results under real field conditions.

## 7.2 Conclusions and Outlook

The findings from this thesis have to be understood as part of the entire research project on the determination of the remaining strength of utility poles in New South Wales, Australia, which has been conducted at the Centre of Built Infrastructure Research at the Faculty of Engineering and Information Technology at the University of Technology, Sydney in conjunction with Ausgrid as industrial partner. This research project involved three PhD and one Master student working on four different aspects of the project.

The research work conducted for the master thesis focuses on the practical experimental investigations which produced material property values used not only as a basis for the ultrasonic tests but also for comprehensive orthotropic numerical modelling and analyt-

ical work conducted by other project members. The static as well as ultrasonic testing results build a basis for further testing to be conducted in the field on in-service timber poles which reached the end of their service life. Those tests are aimed at providing further important information of damage cases and serve the aim of building a data base for ultrasonic testing.

For the remaining eucalyptus species that are frequently used for utility poles, similar material tests need to be conducted to provide benchmark data where no literature values are available.

The aims set for this research were greatly achieved and are the basis for continuing field tests with the aim of developing a commercial damage detection device for the determination of the remaining strength of timber utility poles.

# 8 BIBLIOGRAPHY

(U.S.) Forest Products Laboratory. (2010). *Wood Handbook: Wood as an Engineering Material*. The Service.

Armstrong, J. P. (1991). Comparison of three equations for predicting stress wave velocity as a function of grain angle. *Wood and Fiber Science*.

Astley, R. J., Stol, K. A., & Harrington, J. J. (1998). Modelling the elastic properties of softwood. *Holz als Roh- und Werkstoff*, *56*(1), 43–50

Baar, J., Tippner, J., & Gryc, V. (2011). The influence of wood density on longitudinal wave velocity determined by the ultrasound method in comparison to the resonance longitudinal method. *European Journal of Wood and Wood Products*, *70*(5), 767–769.

Baskaran, G. (2007). Simulation of the TOFD technique using the finite element method. *Insight*, *49*(11), 641–646.

Bergander, A., & Salmen, L. (2000). Variations in transverse fibre wall properties: relations between elastic properties and structure. *Holzforschung*, *54*, 654 – 660.

Bertholf, L. D. (1965). *Use of Elementary Stress Wave Theory for Prediction of Dynamic Strain in Wood*. Technical Extension Service, Washington State University.

Bodig, J., & Goodman, J. R. (1973). Prediction of Elastic Parameters for Wood. *Wood Science*, *5*(4), 249–264.

Bodig, J., & Jayne, B. A. (1982). *Mechanics of Wood and Wood Composites*. New York: Van Nostrand Reinhold Company Inc.

Bolza, E., & Kloot, N. H. (1963). The Mechanical Properies of 174 Australian Timbers. Melbourne.

Bootle, K. R. (2005). *Wood in Australia; Types, Properties and Uses* (2nd ed.). McGraw-Hill Australia.

Bucur, V. (1984). *Ondes ultrasonores dans le bois. Caractérisation mécanique et qualité de certaines essences de bois*. Institut Supérieur des Matériaux, St Ouen, Paris.

Bucur, V. (2005). Ultrasonic techniques for nondestructive testing of standing trees. *Ultrasonics*, *43*(4), 237–9. Bucur, V. (2006). *Acoustics of Wood*. (T. E. Timell & R. Wimmer, Eds.) (2nd ed.). Berlin.

Bucur, V., & Archer, R. R. (1984). Elastic constants for wood by an ultrasonic method. *Wood Science and Technology*, *18*(4), 255–265.

Bucur, V., & Chivers, R. C. (1991). Acoustic Properties and Anisotropie of Some Australian Wood Species. *Acoustica*, *75*, 69–74.

Bucur, V., & Feeney, F. (1992). Attenuation of ultrasound in solid wood. *Ultrasonics*, *30*(2), 76–81.

Burgert, I. (2000). *Die mechanische Bedeutung der Holzstrahlen im Lebenden Baum: Dissertation*. I. Burgert.

Burmester, A. (1965). Zusammenhang zwischen Schallgeschwindigkeit und morphologischen, physikalischen und mechanischen Eigenschaften von Holz. *European Journal of Wood and Wood Products*, *23*(6), 227–236.

Carrasco, E. V. M., & Junior, A. P. A. (2003). Avaliação Não Destrutiva de Propriedades Mecânicas de Madeiras Através de Ultra - Som – Fundamentos Físicos e Resultados Experimentais. *Engenharia Civil*, *17*, 43–57.

Cave, I. D., & Walker, J. C. F. (1994). Stiffness of wood in fast-grown plantation softwoods: The influence of microfibril angle. *Forest Products Journal*, *44*(5), 43–48.

Comino, E., Socco, V., Martinis, R., Nicolotti, G., & Sambuelli, L. (2000). Ultrasonic tomography for wood decay diagnosis. In *International Symposium on Tlant Health in Urban Horticulture* (p. 279). Braunschweig Germany.

Dackermann, U., Crews, K., Kasal, B., Li, J., Riggio, M., Rinn, F., & Tannert, T. (2013). In situ assessment of structural timber using stress-wave measurements. *Materials and Structures*.

De Oliveira, F. G. R., Candian, M., Lucchette, F. F., Luis Salgon, J., & Sales, A. (2005). A technical note on the relationship between ultrasonic velocity and moisture content of Brazilian hardwood (Goupia glabra). *Building and Environment*, *40*(2), 297–300.

De Oliveira, F. G. R., & Sales, A. (2006). Relationship between density and ultrasonic velocity in Brazilian tropical woods. *Bioresource Technology*, *97*(18), 2443–2446.

Dill-Langer, G., Bernauer, W., & Aicher, S. (2006). Inspection of glue-lines of glued-laminated timber by means of ultrasonic testing. In *Symposium on Nondestructive Testing of Wood* (pp. 47–60).

Divós, F., & Szalai, L. (2002). Tree evaluation by acoustic tomography. In *Proceedings of the 13th Internatinal symposium on nondestructive testing of wood* (pp. 251–256). Berkeley.

Donaldson, L. (2008). Microfibril angle: Measurement, variation and relationships - A review. *IAWA journal*, *29*(4), 345–386.

Eidg. Forschungsanstalt WSL. (2012). *Holzfäulen: Braunfäule, Weissfäule und Moderfäule*.

Farrell, R., Innes, T., & Nolan, G. (2008). *Sorting plantation Eucalyptus nitens logs with acoustic wave velocity* (Vol. 61).

Fengel, D., & Wegener, G. (1983). *Wood: chemistry, ultrastructure, reactions*. De Gruyter.

Forest Research Institute NZ. (1976). *Forest and Timber Insects in New Zealand*. Forest Research Institute, New Zealand Forest Service.

Franke, B., Müller, A., Vogel, M., & Tannert, T. (2012). *Holzfeuchte-Langzeitmessung: Langzeitmessung der Holzfeuchte und Dimensionsänderung an Brücken aus blockverleimtem Brettschichtholz*. Biel, Switzerland.

Gamper, A., Dietsch, P., & Merk, M. (2012). *Gebäudeklima – Langzeitmessung zur Bestimmung der Auswirkungen auf Feuchtegradienten in Holzbauteilen*. Stuttgart.

Gautschi, G. (2002). *Piezoelectric Sensorics: Force, Strain, Pressure, Acceleration and Acoustic Emission Sensors, Materials and Amplifiers*. Springer.

Gerhards, C. C. (1982). Longitudinal Stress Waves for Lumber Stress Grading: Factors Affecting Applications. *Forest Products Journal*, *32*(2), 20–25.

Gilbert, E. A., & Smiley, E. T. (2004). Picus Sonic Tomography for the quantification of decay in white oak (Quercus Alba) and hickory (Carya Spp.), 277–281.

Grabner, M., Müller, U., Gierlinger, N., & Wimmer, R. (2005). Effects of heartwood extractives on mechanical properties of larch. *IAWA journal*, *26*(2), 211–220.

Graff, K. F. (1975). *Wave Motion in Elastic Solids*. Dover Publications.

Green, D. W., Winandy, J. E., & Kretschmann, D. E. (2010). *Wood Handbook - Wood as an Engineering Material*. Madison, Wisconsin: Forest Products Laboratory, Madison, Wisconsin.

Hankinson, R. L. (1921). Investigation of Crushing Strength of Spruce at Varying Angles of Grain. *Air Service Information Circular*, *259*.

Hearmon, R. F. S. (1948). *The elasticity of wood and plywood*. London: H.M.S.O.

Hearmon, R. F. S. (1961). *An introduction to applied anisotropic elasticity*. Oxford: Oxford University Press.

Hearmon, R. F. S. (1965). The Assessment of Wood Properties by Vibrations and High Frequency Acoustic Waves. In *Symposium on Nondestructive Testing of Wood* (pp. 49–66). Pullman, WA: Washington State University.

Hudson, J. A. (1993). *Comprehensive Rock Engineering: Principles, Practice and Projects*. Oxford: Pergamon Press.

Ilic, J. (2003). Dynamic MOE of 55 species using small wood beams. *Holz als Roh- und Werkstoff*, *61*, 167–172.

Ilic, J., Scientific, C., & (Australia), I. R. O. (1991). *Csiro Atlas of Hardwoods*. Springer.

Jones, R. M. (1975). Mechanics of composite materials. *Scripta Book Company*.

Kabir, M. F. (2001). Prediction of Ultrasonic Properties from Grain Angle. *Journal of the Institute of Wood Science*, *15*(5), 235–246.

Keunecke, D., Sonderegger, W., Pereteanu, K., Lüthi, T., & Niemz, P. (2006). Determination of Young's and shear moduli of common yew and Norway spruce by means of ultrasonic waves. *Wood Science and Technology*, *41*(4), 309–327.

Kim, K. Y. (1986). A note on the Hankinson formula. *Wood and Fiber Science*, *18*(2), 345–348.

Kohlhauser, C., & Hellmich, C. (2012). Poisson's ratios in isotropic, transversely isotropic, and orthotropic materials by means of combined ultrasonic-mechanical testing of normal stiffnesses: Application to metals and wood. *European Journal of Mechanics A/Solids*, *33*, 82–98.

Kollmann, F. F. P., & Cote, W. A. J. (1968). *Principles of Wood Science and Technology* (p. pp. 326). New York: Springer-Verlag Inc.

Kollmann, F. F. P., & Krech, H. (1960). Dynamische Messung der elastischen Holzeigenschaften und der Dämpfung Ein Beitrag zur zerstörungsfreien Werkstoffprüfung. *Holz als Roh- und Werkstoff*, *18*(2), 41–54.

Krautkrämer, J., & Krautkrämer, H. (1983). *Ultrasonic testing of materials*. Springer-Verlag.

Lin, C.-J., Kao, Y.-C., Lin, T.-T., Tsai, M.-J., Wang, S.-Y., Lin, L.-D., … Chan, M.-H. (2008). Application of an ultrasonic tomographic technique for detecting defects in standing trees. *International Biodeterioration & Biodegradation*, *62*(4), 434–441.

Martinis, R., Socco, V., Sambuelli, L., Schmitt, O., & Bucur, V. (2004). Tomographie ultrasonore pour les arbres sur pied. *Ann. Forest Sci.*, *61*(2), 157–162.

Mattheck, C. G., & Bethge, K. A. (1993). Detection of decay in trees with the metriguard stress wave timer. *Journal of Abroriculture*, *19*(6), 374–378.

Mishiro, A. (1996a). Effect of density on ultrasonic velocity in wood. *Mokuzai Gakkaishi*, *42*(9), 887–894.

Mishiro, A. (1996b). Effects of Grain and Ring Angles on Ultrasonic Velocity in Wood. *Mokuzai Gakkaishi*, *42*(2), 211–215.

Nguyen, M., Foliente, G., & Wang, X. (2004). State of the practice & challenges in Non- destructive evaluation of utility poles in service. *Key Engineering Materials*, *270-273*.

Niemz, P. (1993). *Physik des Holzes und der Holzwerkstoffe*. DRW-Verlag.

Niemz, P., Kucera, L., & Bernatowicz, G. (1999). Untersuchungen zum Einfluss des Faserwinkels auf die Ausbreitungsgeschwindigkeit von Schallwellen in Holz. *Holz als Roh- und Werkstoff*, *57*.

Niemz, P., & Ozyhar, T. (2011). *Ermittlung elastomechanischer Kennwerte von Rotbuchenholz*. Zurich.

Niklas, K. J. (1997). Mechanical Properties of Black Locust ( Robinia pseudoacacia L .) Wood . Size- and Age-dependent Variations in Sap- and Heartwood. *Annals of Botany*, *79*, 265–272.

Nzokou, P., & Kamdem, D. (2004). Influence of Wood Extractives on Moisture Sorption and Wettability of Red Oak (Quercus Rubra), Black Cherry (Prunus Serotina), and Red Pine (Pinus Resinosa). *Wood and Fiber Science*, *36*(4), 483–492.

Payton, R. G. (2003). WAVE FRONTS IN WOOD. *Mechanics & Applied Mathematics*, *56*, 527–546.

Pellerin, R. F., De Groot, R. C., & Esenther, G. R. (1985). Nondestructive stress wave measurements of decay and termite attack on experimental wood units. In *Proceedings of the 5th nondestructive testing of wood symposium* (pp. 319–353). Pullman, WA.

Pellerin, R. F., & Ross, R. J. (2002). *Nondestructive Evaluation of Wood*. *Forest products journal* (p. 210). Forest Products Society.

Ross, R. J. (1991). *Nondestructive Evaluation of Wood: Past, Present and Future*. Plenum Press.

Ross, R. J., & Pellerin, R. F. (1994). *Nondestructive testing for assessing wood members in structures: a review*. U.S. Dept. of Agriculture, Forest Service, Forest Products Laboratory.

Ross, R. J., Pellerin, R. F., Volny, N., Salsig, W. W., & Falk, R. H. (1999). *Inspection of timber bridges using stress wave timing nondestructive evaluation tools: a guide for use and interpretation* (p. 15). Madison, WI.

Ross, R. J., Pellerin, R. F., Volny, N., Slasig, W. W., & Falk, R. H. (2000). Stress Wave Timing Nondestructive Evaluation Tools for Instecting Historic Structures: A Guide for Use and Interpretation. *Forest Products Laboratory, Madison*. Madison, WI.

Royer, D., & Dieulesaint, E. (2000). *Elastic Waves in Solids I: Free and Guided Propagation*. Springer.

Saint-Venant, B. (1856). Sur la distribution d'elasticite autour de chaque point d'un solide ou d'un milieu de contexture quelconque. *Jounal de Mathematiques Pures et Appliquees*, *8*, 257–561.

Sakai, H., Minamisawa, A., & Takagi, K. (1990). Effect of moisture content on ultrasonic velocity and attenuation in woods. *Ultrasonics*, *28*(6), 382–385.

Sanabria, S. J., Neuenschwander, J., Niemz, P., & Sennhauser, U. (2010). Structural health monitoring of glued laminated timber with a novel air-coupled ultrasound method. In *World Conference on Timber Engineering*.

Sandoz, J.-L. (1989). Grading of construction timber by ultrasound. *Wood Science and Technology*, *23*, 95–108.

Sandoz, J.-L. (1993). Moisture content and temperature effect on ultrasound timber grading. *Wood Science and Technology*, *27*, 373–380.

Scheer, C. (1986a). *Holzbau-Taschenbuch 8. Auflage, Band 1*. Berlin: Architektur techn. Wissenschaften.

Scheer, C. (1986b). *Holzbau-Taschenbuch 8. Auflage, Band 1*. Berlin: Architektur techn. Wissenschaften.

Schneckenberger, J. E. (1991). Comparison of three equations for predicting stress wave velocity as a function of grain angle. *Wood and Fiber Science*, *1*, 32–43.

Schneider, M. H., Phillips, J. G., Tingley, D. A., & Brebner, K. I. (1990). Mechanical properties of polymer impregnated sugar maple. *Forest Products Journal*, *40*(1), 37–41.

Schubert, S., Gsell, D., Niemz, P., & Dual, J. (2005). Numerical simulation of elastic wave propagation in the radial-tangential plane of wooden trunks with and without fungal decay. In *3rd Workshop "NDT in Progress."* Prag.

Schwarze, F. (2007). Wood Decay under the Microscope. *Fungal Biology Reviews*, *21*(4), 133–170.

Siau, J. F. (1984). *Transport processes in wood*. Springer-Verlag.

Smulski, S. (1991). Relationship of stress wave-and static bending-determined properties of four northeastern hardwoods. *Wood and Fiber Science*, *23*(1), 44–57.

Stein, S. (2003). *An Introduction to Seismology, Earthquakes, and Earth Structure*. Malden: Blackwell Publishing Ltd.

Subhani, M., Li, J., Gravenkamp, H., & Samali, B. (2013). Effect of elastic modulus and Poisson's ratio on guided wave dispersion using transversely isotropic material modelling. *Advanced Materials Research*, *778*, 303–311.

Tallavo, F. J., Pandey, M. D., & Cascante, G. (2012). Probabilistic characterization of ultrasonic wave propagation in wood poles. *Canadian Journal of Civil Engineering*, *39*(4), 484–493.

Tanasoiu, V., Miclea, C., & Tanasoiu, C. (2002). Non-destructive Testing Techniques and Piezoelectric Ultra-Sonics Transducers for Wood and Built in Wooden Structures. *Journal of Optoelectronics and Advanced Materials*, *4*.

Team of Authors. (2003). Holzlexikon. In *Holzlexikon*. DRW-Verlag Leinfelden-Echterdingen.

Tomikawa, Y. I., Arita, K., & Yamada, H. (1990). Nondestructive inspection of a wooden pole using ultrasonic computed tomography. *IEEE Transactions UFFC*, *33*(4), 354–358.

Wagenführ, R. (2007). *Holzatlas*. Hanser Fachbuchverlag.

Wang, H. (2004). *Theoretical evaluation of embedded plate-like and solid cylindrical concrete structures with guided waves*. Northwestern University, Evanston, IL, USA.

Wang, X., Pilon, C., Brashaw, B. K., Ross, R. J., & Pellerin, R. F. (2004). *Assessment of Decay in Standing Timber Using Stress Wave Timing Nondestructive Evaluation Tools*. U.S. Dept. of Agriculture, Forest Service, Forest Products Laboratory.

Wang, X., Ross, R. J., & Carter, P. (2007). Acoustic evaluation of wood quality in standing trees, Part 1 - Acoustic wave bahavior. *WOOD AND FIBER SCIENCE*, *39*, 28–38.

Wangaard, F. (1950). *The Mechanical Properties of Wood*. New York: John Wiley & Sons, Inc.

Wasley, R. J. (1973). *Stress wave propagation in solids*. New York: Marcel Dekker.

**Standards**

ASTM International. (2004). ASTM E132 – 04 - Standard Test Method for Poisson's Ratio at Room Temperature.

ASTM International. (2008). Standard Test Method for Laboratory Determination of Pulse Velocities and Ultrasonic Elastic Constants of Rock.

ASTM International. (2009). ASTM D143 – 09 - Standard Test Methods for Small Clear Specimens of Timber.

Ausgrid. (2011). Network Standard NS 145, Pole Inspection and Treatment Procedures.

Australian Standard. (2005). 5604 - Timber — Natural durability ratings.

Australian Standard. (2012). 1604.1 - Specification for preservative treatment, Part 1: Sawn and round timber.

Australian/New Zealand Standard. (1997). 1080.1 - Timber — Methods of Test, Method 1 : Moisture content.

Australian/New Zealand Standard. (2000a). 2078 - Timber - Classification into strength groups.

Australian/New Zealand Standard. (2000b). 1080.3 - Timber — Methods of test, Method 3 : Density.

Australian/New Zealand Standard. (2010). 4063.1 - Characterization of structural timber, Part 1 : Test methods.

Deutsche Norm. (1976). DIN 52185 - Bestimmung der Druckfestigkeit parallel zur Faser.

Deutsche Norm. (1977). DIN 52180 - Prüfung von Holz, Probenahme. Berlin.

Deutsche Norm. (1978). DIN 52186 - Biegeversuch.

Deutsche Norm. (1979a). DIN 52192 - Druckversuch quer zur Faserrichtung.

Deutsche Norm. (1979b). DIN 52188 - Bestimmung der Zugfestigkeit parallel zur Faser.

# INDICES

## Index of Figures

# Index of Tables

# Index of Equations

# 9 APPENDICES

## APPENDICES

# 9.1 Appendix A

Static material testing specimens

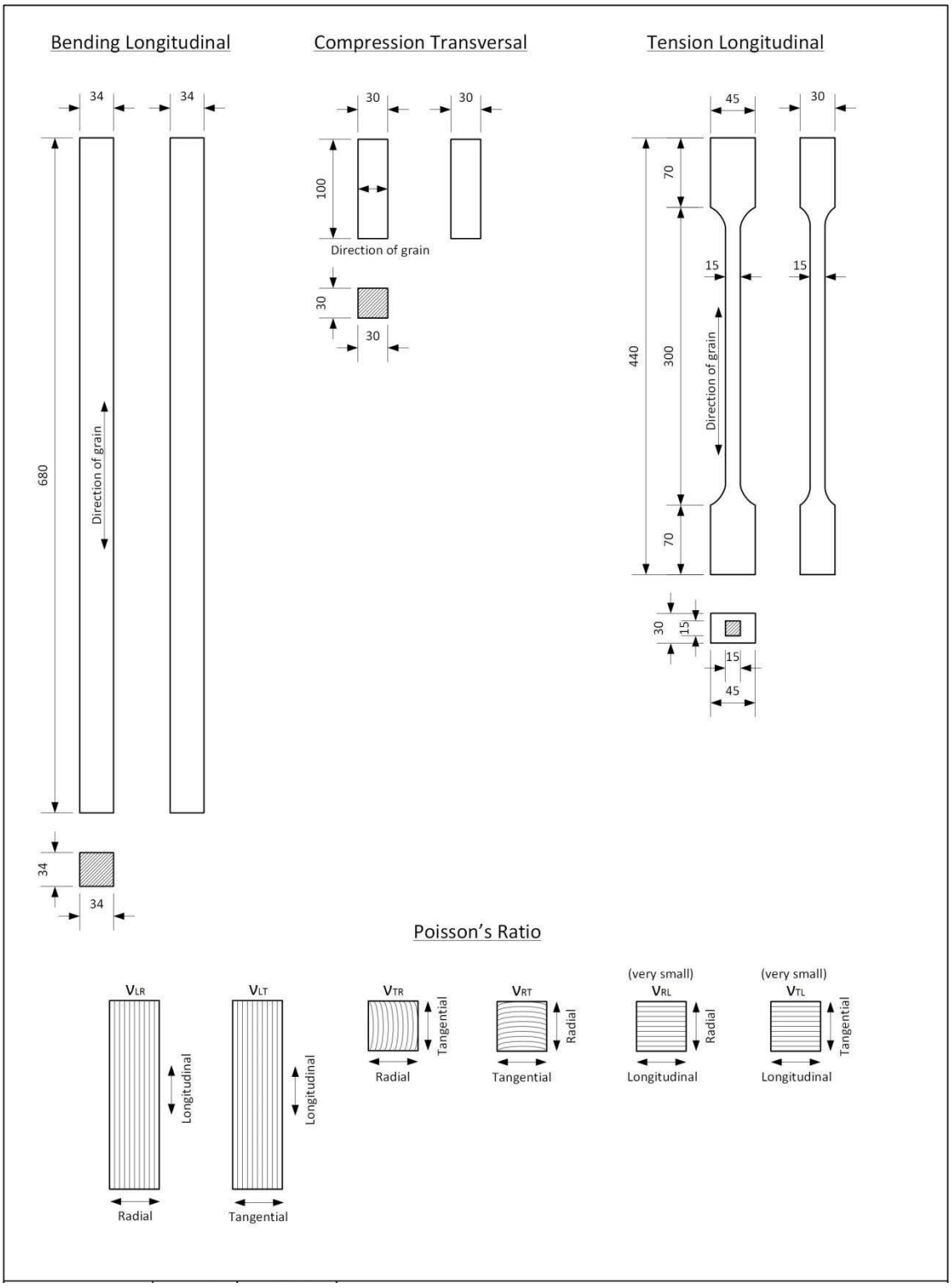

## 9.2 Appendix B

These graphs are complementing the graphs in Figure 5-13 on page 93 and are showing the influence of the wood moisture content on the P-wave and S-wave velocities. FSP is indicating the fibre saturation point and WS is indicating the fully water saturated state

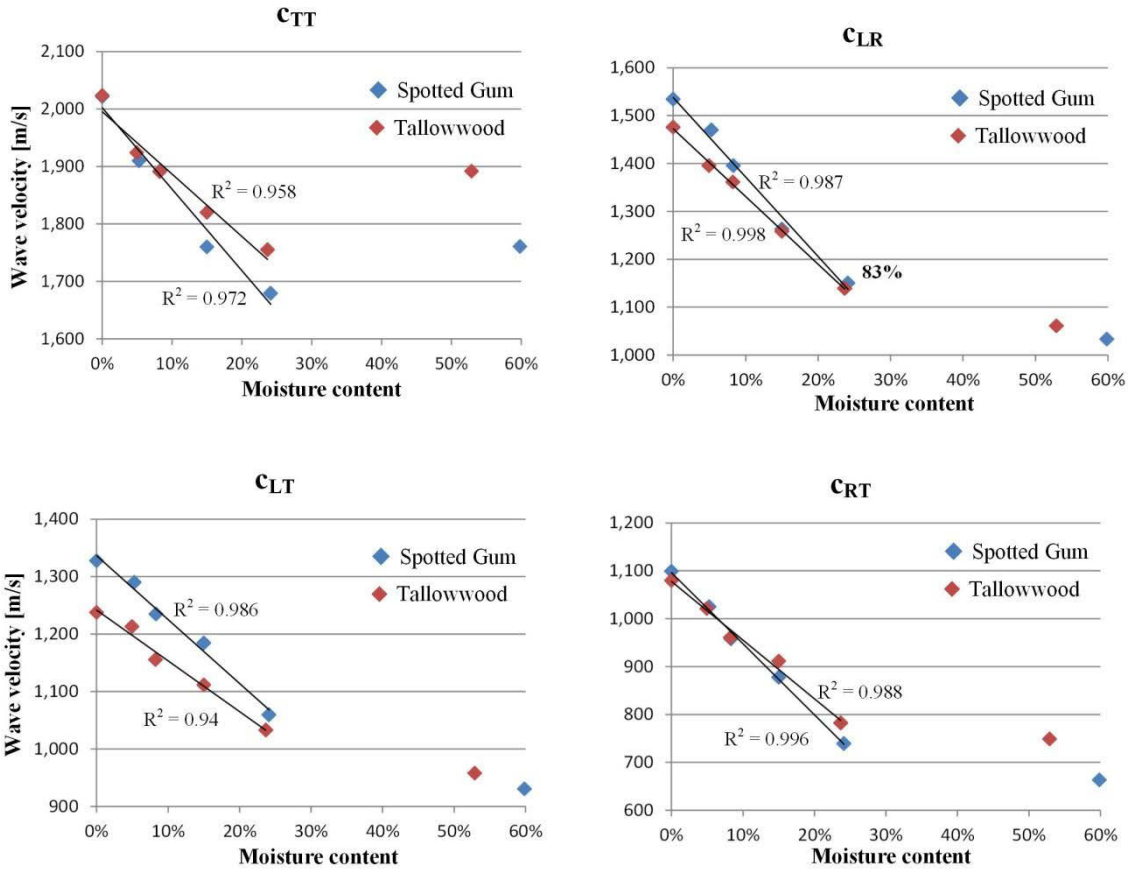

## 9.3 Appendix C

In order to display how stress waves propagate through the model, the waterfall chart can be drawn. This chart consists of all nodes between the transmitting sensor and the receiving sensor. The figure below shows the case with a 41 mm and 73 mm hole.